Towards an All-Polymer Biosensor for Early Alzheimer's Disease

Christiansen, Nikolaj Ormstrup

Publication date:
2013

Document Version
Publisher's PDF, also known as Version of record

DTU Nanotech
Department of Micro- and Nanotechnology

Ph.D. Thesis

Towards an All-Polymer Biosensor for Early Alzheimer's Disease

Nikolaj Ormstrup Christiansen

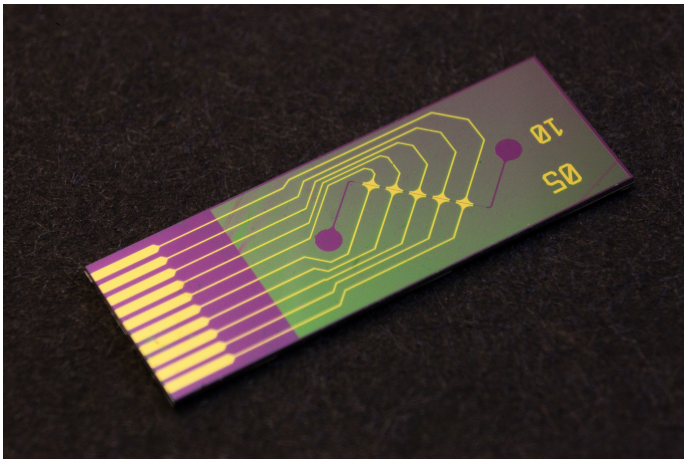

Supervisors:
Asc. Prof. Noemi Rozlosnik, DTU Nanotech
Dr. Med. & Scient. Niels Heegaard, Statens Serum Institut

November 4th 2013

"I may not have gone where I intended to go,
but I think I have ended up where I needed to be."
Douglas Adams

Abstract

Alzheimer's disease (AD) is quickly evolving into one of the biggest and most costly health issues in Europe and the United States. AD is a protein misfolding disease, caused by accumulation of abnormally folded β-amyloid and tau protein in the brain. The build-up of protein is believed to degenerate the brain tissue literally shrinking the brain. This slowly destroys function of these parts of the brain. It has been discovered that the concentration of Aβ_{42} in cerebrospinal fluid (CSF) is a biomarker for this disease. It is therefor of great interest to develop quick and low cost methods for measuring this.
Lab-on-a-chip biosensors are one of the fastest growing technologies for in vitro diagnostics. The combination of microfluidics and biosensing offers exciting possibilities for producing extremely sensitive and low cost applications for medicine and diagnostics.

This thesis include studies on self-assembly of peptide structures. An investigation into the fibrillation of Aβ_{42} was conducted with the purpose of using in vitro formed fibrils for pre-concentrating Aβ_{42}. Diphenylalanine (phe-phe) has previously been described as the key recognition motif of the amyloid fibrillation. This thesis also presents a thorough study of the physical and chemical properties of self-assembled Tert-butoxycarbonyl-Phe-Phe-OH peptide structures.

Conductive polymer nanowires has recently been suggested as an alterneative to silicon nanowire. In this work we have demonstrated a rapid fabrication of polymerized p-toluenesulfonate doped poly(3,4-ethylenedioxythiophene) (PEDOT:TsO) nanowires. The PEDOT:TsO nanowires are demonstrated to be promising temperature sensors. We also show that the nanowires can be gated with a backgating potential, which is a requirement for using it as a biosensor. The nanowires were also shown to be able to measure changes in larger biological samples as cells. This shows a promise for utilizing the PEDOT:TsO nanowires as Aβ_{42} biosensors.

A prototype for a lab-on-a-chip system consisting of a double assay sorting channel and a electrochemical impedance spectroscopy coulter counter were developed. It was shown that the coulter counter could measure a polystyrene bead concentration with 97% accuracy.

Resumé

Alzheimers sygdom (AD) er hurtigt ved at udvikle sig til et af de største og dyreste sundhedsproblemer i Europa og USA. AD er en protein misfoldnings sygdom forårsaget ved en ophobning a unormalt foldet Beta-Amyloid og Tau protein i hjernen. Ophobningen af protein menes at degenerere hjernevæv og bogstaveligt talt få hjernen til at skrumpe. Hvilket langsomt ødelægger funktionerne i disse dele af hjernen. Det er blevet observeret at koncentrationen af AB42 i rygmarvsvæske er en biomarkør for sygdommen. Det er derfor utrolig interessant at udvikle en hurtig og billig metode for at måle dette.
Lab-on-a-Chip biosensorer er en af de hurtigst udviklende teknologier ti l in vitro diagnostik. Kombinationen af mikrofluid og biosensing giver nogle fantastisk muligheder for at producere ekstremt sensitive og billige applikationer for medicin og diagnostik.

Denne afhandling omfatter undersøgelser af self-assembly af peptid stucture. Fibrillering af AB42 blev undersøgt for at bruge in vitro formerede fibriller til at præ-koncentrere AB42. Diphenylalanin (phe - phe) er tidligere blevet beskrevet som "the key recognition motif" for amyloid fibrillering. Denne afhandling præsenterer et grundigt studie af de fysiske og kemiske egenskaber af self-assembled Tert-butoxycarbonyl-Phe-Phe-OH peptide strukturer.

Elektrisk ledende polymer nanowires er blevet foreslået som et alternativ til silicium nanowires. I denne afhandling demonstrerer vi en hurtig fabrication af polymeriseret p -toluensulfonat doped poly (3,4- ethylenedioxythiophene) (PEDOT : TSO) nanowires. Vi demonstrerer at PEDOT:TsO nanowires er lovede temperatur sensorer. Vi demonstrere også at de kan blive gated ved hjælp af et backgating potentiale, hvilket er et krav for at kunne dem som biosensorer. Vi viser også at de er i stand til at måle ændringer i biologiske prøver som f.eks. celler. Dette giver løfter om at de også kan bruges til at måle på AB42.

Der er også blevet udviklet en prototype på et lab-on-a-chip system, som består af en dobbelt assay sorterings kanal og en elektrokemisk Coulter tæller. Vi viser at tælleren kunne måle en koncentration af polystyrene beads med 97% nøjagtighed.

Preface

This thesis has been written to document the work I've done in the PolyMeDiag group at DTU Nanotech over the last three years. It has been submitted in order to meet the requirements for obtaining the academic degree of Doctor of Philosophy, Ph.D..
The work in this thesis has been carried out under the supervision of Noemi Rozlosnik in the period June 1st 2010 to November 4th 2013.

Kongens Lyngby, November 4th 2013

Nikolaj Ormstrup Christiansen

DTU Nanotech - Department of Micro- and Nanotechnology
Technical University of Denmark
DTU - Building 424
DK-2800 Kongens Lyngby
Denmark

Acknowledgements

Throughout the last three years of work there have been a lot of very skilled and helpful persons who have help me out. Without these persons these results and this would never have existed. First I'll like to thank my supervisor Noemi Rozlosnik for giving me this chance to do science in a very interesting field and to allowing free reins to explore a lot of different idea both fruitful and bad.

I would also like to thank my colleges in the PolyMeDiag group for a good working environment. Especially Johannes Daprá for all his help with understanding the wonders and mysteries of PEDOT, for exchanging and discussing a large range of fun and interesting idea, also all the ones we'll never have time to try, and for co-supervising a number of students together. Another special thanks goes to Katrine Kiilerich-Pedersen for all our, mostly non-work related, discussions and coffee breaks. They were always a nice procrastination. And also thanks for the work we did together on the cell measurements.

Lotte Nielsen was a great help with setting up and explaining the HPLC system and MALDI-ToF experiments. The personal at Danchip who helped with cleanroom work should also be mentioned. Especially Helle Vendelbo Jensen for dicing all my chips over the last three years and Conny Hougaard for training in certain cleanroom processes and taking good care of all my students. Thanks to all the students that has been involved in this work during the last three years; Dmitri Kozine and Dashne Tofiq on their work with purifying and fibrillating Aβ_{42}, Alexander Leirvåg for his very good work on PEDOT thin films and patterning experiments, Sofie Rahbek and Astrid Engberg for their work on functionalizing Topas®and polysterene beads and testing the sorting channel with Aβ_{40}, Anders Olin and Alexander Neergaard Olesen for fabricating and testing the coulter counter. I found that it demands a lot of work and planning to supervise students on their bachelor and master projects, it was however als overy rewarding both in terms of results, but mostly as a great experience that taught me a lot too.

A major thanks goes to Simon Levinsen and Karsten Brandt Andersen for also sticking around DTU these past three years as well as the six years before that. It is always nice to have someone to complain to when the experiments are not working. Thanks to Karsten for all our work together. We might have set a record for efficient work to an article. And thanks to Simon for all the lunches we had and all the Sandwich biscuits in the office.

Finally I'd like to thank Julie and Naja for making it worth going home every night instead of lingering in the labs. And to Julie for taking care of everything at home these last couple of months where I had to linger in the labs.

-Nikolaj O. Christiansen

Contents

List of Abbreviations

AD	Alzheimer's Disease
Aβ	Amyloid β
Aβ_{42}	Amyloid β42
Aβ_{40}	Amyloid β40
NTF	Neuro Fibrillar Tangles
CSF	Cerebrospinal Fluid
APP	Amyloid Precursor Protein
LOC	Lab-on-a-Chip
POC	Point-of-care
μTAS	Microscale Total Analysis system
MEMS	Micro Electro-Mechanical Systems
DARPA	Defence Advanced Research Projects Agency
PhD	Philosophiae doctor
Phe-Phe	Diphenylalanine
RNA	Ribonucleic acid
DNA	Deoxyribonucleic acid
FET	Field Effect Transistor
Bio-FET	Bio-Field Effect Transistor
PSS	Polystyrene Sulfonate
PEDOT	Poly(3,4-ethylenedioxythiophene)
TsO	Iron (III)Tosylate
RIE	Reactive Ion Etch
EIS	Electrochemical Impedance Spectroscopy
UV-Vis	Ultraviolet visible spectroscopy
ThT	Thioflavin T
MS	Mass Spectroscopy
Maldi-TOF	Matrix-Assisted Laser Desorption/Ionization-Time of Flight
AFM	Atomic Force Microscopy
FPLC	Fast Protein Liquid Chromatography
HPLC	High-Performance Liquid Chromatography
RI	Refractive Index
UV	Ultraviolet
PBS	Phosphate Buffered Saline
BOC	Tertibutoxycarbonyl
HFP	1,1,1,3,3,3-Hexafluoro-2-propanol
FIB	Focussed Ion Beam
SEM	Scanning Electron Microscopy

FD	Force Distance
PVD	Physical Vapor Deposition
C-AFM	Conductive Atomic Force Microscopy
TEM	Transmission Electron Microscopy
FF	Diphenylalanine
EDOT	3,4-Ethylenedioxythiophene
LPNE	Lithographically Patterned Nanowire Electroposition
SCE	Saturated Calomel Electrode
DPN	Dip-Pen Nanolithography
PNT	Peptide Nanotubes

Chapter 1

Introduction and Motivation

1.1 The Basics of Alzheimer's Disease

Alzheimer's Disease (AD) was first reported in 1907 by Alois Alzheimers.[1] Through post-mortem autopsy of a dement women he observed two alterations in her brain. The two alterations are still the known as the pathonomic features of the disease today. Alzheimer described a "peculiar substance" occurring as extracellular deposits in the brain. In the 1980's it was discovered that this plaque consisted of amyloid-β (Aβ) peptide,[2] An illustration of an Aβ plaque on a neuron can be seen on figure 1.1 (A). The other alteration was described as neurofirillary tangles (NFTs), again it wasn't until the 1980's that it was discovered that the NFTs were aggregates of tau protein.[3] The plaque and NFTs are not the only significant pathological changes related to AD, there is a large range of different structural and functional alterations present it has recently been suggested that (Aβ) oligomers might also be neuro toxic. However, the combined effect of all these pathological changes is severe neuronal and synaptic dysfunction. AD also leads to a severe shrinking of the brain,[4] figure 1.1 (B).

1.2 Effects on Society

Alzheimer's disease (AD) is a protein misfolding disease, caused by accumulation of abnormally folded beta-amyloid and tau protein in the brain. The build-up of protein is believed to degenerate the brain tissue literally shrinking the brain. This slowly destroys function of these parts of the brain. The symptoms of AD include loss of memory, decreased langues skills and incapability of solving logical problems. AD is fatal and as of now incurable. The life expectancy of a person with AD is on average 7-10 years where more than half is often spend in nursing homes or with great need for caretaking. The disease most often occurs after the age of 60, however, in rare cases the patients shows symptoms as early as their late 30's.[6] Alzheimer's disease is the sixth most common cause of death in the United States and also the only disease on that top ten that cannot be prevented, cured or even slowed down.[5]
In 2006 it was belied that there was 26.6 million sufferers from AD worldwide.[7] In Den-

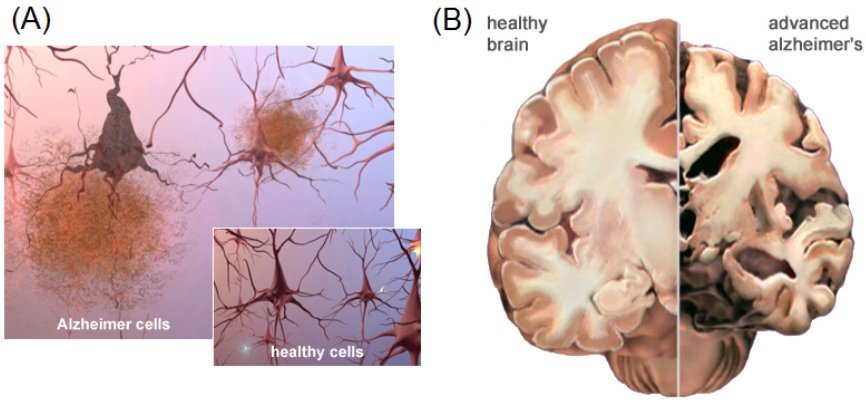

Figure 1.1: *(A) illustrates neuron cell attacked by amyloid β plaque. The insert shows how the same cell look without the plaque. (B) Illustrates the shrinkage of a brain with Alzheimer's disease compared with a healthy brain. The figure is modified from the Alzheimer's Association.*[5]

mark alone approximately 50.000 patients suffers from the disease. The occurrence of AD increases with age. With the demographic development in the world where the population of people over 60 increases dramatically it indicates that the number of AD patients could explode over the next 50 years. It's believed that in Denmark alone the number of AD patients will have risen to 93.000 in 2040.[8]
The disease is becoming an ever increasing societal problem. As the general population grows older it is becoming important to stay in the working force until an older age. Few people beyond very mild Alzheimer will be able to contribute to society. On the contrary will they demand societies help instead. In Denmark the state is in 2011 using approximately 9-15 billion DKK on dementia patients a year.[8] In the United States the the total bill for Alzheimer patients will total 183 billion dollars this year and unless something changes the bill will increase to 1.1 trillion dollars by 2050.[5] It is obvious that treatment of AD has and will have an increasing value in the coming years. The knowledge on AD is still very limited and there is no way to regenerate damaged brain tissue. Today's researchers are mainly working on preventing or slowing down the disease by e.g. hindering the formation of excess protein in the brain. However, it is very difficult to diagnose the disease early enough to have test subjects to monitor to see if the medical approaches are working. Hence, a earlier diagnose can lead to better research and maybe slowing or preventing the illness before it has too influential or fatal consequences for the patients. Approximately half to two thirds of the cost of AD is due to care taking of the patients. With an expected lifetime of less than ten years it is seen that slowing the disease for just three years will bring an enormous economical benefits as well as personal for the patient.

1.3 Diagnosing Alzheimer's Disease

Diagnosing AD is very difficult and is largely based upon clinical assessments and interviews with the patients. The only definitive diagnosis of AD today is still post mortem autopsy. For studying the disease to understand its development, find ways to slow it down or even cure it, it is necessary to discover patients at an earlier state. The study of the development of AD is hindered by the fact that patient classifications relies on clinical diagnosis, which due to the unclear ways of diagnosing is uncertain. This gives a large uncertainty in the obtained data. Due to these challenges an identification of biomarkers for AD would allow for a less invasive and more accurate diagnosis in the antemortem period. Which again could lead to better studies of the disease and possible treatments. The amyloid plaques mainly consist of Aβ peptides of 39-43 amino acids[9] where Aβ42 is found to be the most dominant. Because of this many groups has investigated Aβ42 and other Aβ species as possible biomarkers. It was found that the concentration of Aβ42 decreases in cerebro spinal fluid (CSF) in AD patients.[10–15]

1.3.1 Amyloid β

Amyloid Beta (Aβ) is a peptide consisting of between 36-43 amino acids. In essence Aβ is a cleavage product of a large transmembrane protein, Amyloid Precursor Protein (APP). APP can be cleaved by the proteolytic enzymes α-, β- and γ-secretase. The cleavage is done by the α-secretase prevents Aβ formation Aβ and instead forms the neuroprotective sAPPα fragment. Aβ is formed through a sequential cleavage by first β- and the γ-secretases which cleaves within the transmembrane region of APP.[16] The most common Aβ is Aβ_{40} and Aβ_{42} where the former is the most common the later, however, is more fibrillogenic and thus more related to diseases.
Aβ_{42} is present in monomeric form after cleavage from APP.[17] Depending on the conditions e.g. temperature, concentration and pH the monomers start to form low-molecular-weight (LMW) oligomers (dimer, trimers and 8-mers). These β-sheet rich oligomers forms small aggregates known as pre-aggregates for proto-fibrils which can can lead to form higher ordered aggregates known as amyloid fibrils. Amyloid fibrils refer to elongated protein aggregates with long and relatively straight morphologies and cross-β sheets.[17] The formation of amyloid fibrils involve a structural re-arrangement of the native state of the protein into β-sheet rich fibrillar conformation. β-sheets provides a scaffold that favors protein assembly as the edge strands of β-sheets are unstable and can grow by interacting with other β-sheets.[17]
Aβ fibrils are not uniquely determined by the amino acid sequence. They are also dependent on the specific growth conditions. It has been discovered that amyloid fibril growth is seeded by smaller aggregate or small fibrils.[18] The mechanism by which the amyloid fibril formation is initiated *in vivo* are still being investigated. However, it is very likely that once the initial seeds are formed the fibrils grow by elongation due to monomer additions .[19,20] The presence of seeds speeds up to fibrillation process. It is e.g. well known that the addition of seeds to a monomer population can reduce or completely remove the lag time of the spontaneous fibrillation.[19,21] The fibrillation pathway is sketched in figure 1.2

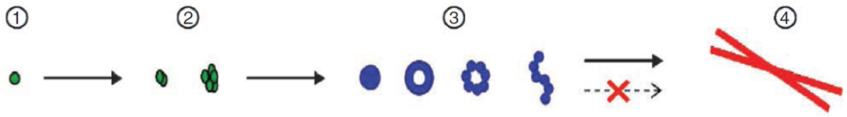

Figure 1.2: *Aβfibrillation pathway. 1) Aβin monomeric form. under the right conditions they can aggregate into small aggregates 2) The small aggregates can vary from LMW molecules to highly ordered structures such as protofibrils and Aβ-derived diffusible ligands (ADDLs). 3) These aggregates can be on one of two pathways; either to fibril formation where they disappear upon fibril formation or to a non-fibril formation (the two paths are depicted by the solid and dashed arrow respectively.). The figure is adapted from Jan et al. 2010*[22]

1.4 Lab-on-a-Chip

Lab-on-a-chip (LOC) systems is usually referred to as devices that can integrate one or multiple functions on a small chip, which would otherwise have been carried out in a laboratory. The first works on LOC were done more than 30 years ago. Terry et al. 1979[23] fabricated a gas chromatograph using standard silicon processing known from micro electronics. The miniaturized chromatograph results proved to be comparable to standard equipment.[24] During the last 20 years LOC systems has been linked especially to microfluidics and micro-scale total analysis systems (μTAS).[25]
One of the original driving forces for LOC and microfluidics was the success of microelectronics and microelectronicmechanical (MEMS). The original hope of microfluidics was that the standard silicon processing techniques would be directly applicable to microfluidics and LOC.[24,26]
The field received a boost in the 1990's when the μTAS systems showed promise for genomics applications e.g. DNA sequencing.[26] The first μTAS system were presented by Manz et al. 1990.[27] Another increased interest in the whole LOC research came from the United States military, Defence Advanced Research Projects Agency (DARPA).[26] They saw LOC as possible counte technology to chemical and biological weapons.

Despite the fact that the LOC technology has been a research topic for over 30 years and has received a high amount of both attention and financing there are surprisingly few LOC-based devices on the market.[28] So the question is will the technological breakthrough come and why is it worth to keep investing in it?. The answer is that the possible advantages are simply too great to pass up.[26] The LOC systems aims at miniaturizing and automating laboratory protocols for use both in laboratories and outside.[24,28] The advantages of down scaling the laboratory equipment into microscale include better control of reactions, less manual handling, greater possibility for automation and parallelization and the portability coming with the size.[25] The small size also lead to a smaller consumption of reagents and allows for small samples sizes.[24] The biological reactions at microscale are

also faster due to the smaller diffusion lengths.[24,25,28]

1.5 Aim of the Project

To approach a possible treatment of Alzheimer's disease it is important to be able to diagnose patients at an earlier stage of the disease. This is important to both study the disease and for being able to test possible drug candidates. It is widely believed that the path to treat Alzheimer's disease will be to slow it down or even stop it's development at an early stage. It has also been suggested that Aβ_{42} in cerebrospinal fluid can be a viable biomarker for Alzheimer's disease.

The aim of this project is to investigate a range of methods for lab-on-a-chip systems for measuring the concentration of Aβ_{42} in solution. This project mainly investigates two types of conductive polymer based transducers for biosensors.

The project also explores the possibility for speeding up up the fibrillation process of Aβ_{42} to facilitated a possible pre-concentration and increase a possible transducer response.

During this work a thorough investigation of the physical properties of self-assembled diphenylalanine (phe-phe) structures was carried out. These structures have previously been considered as the core recognition molecule of Alzheimer's disease[29] and to have remarkable physical properties.[29–31] The investigations of these peptides served as an introduction to handling short amino acid sequences. Initial investigations didn't fit the published literature, which led to a side project on characterizing the self-assembled Phe-Phe spheres.

1.6 Outline of Thesis

Chapter 1: Introduction and Motivation This chapter gives an introduction to Alheimer's disease and what it means to society. It also describes Aβas a possible biomarker for Alzheimer's disease and states the aim of this work.

Chapter 2: Introduction to Biosensors This chapter gives an introduction to the fundamentals of a biosensor. It gives an overview of the most common transducers and biorecognition molecules. It also gives a short introduction the theory behind the biosensors used in the work.

Chapter 3: Induced Fibrillation of Aβ_{42} This chapter covers the initial experiments of handling Aβ_{42} and investigates the possibility of having an fast controlled fibrillation. It shows how to obtain a pure Aβ_{42} monomer solution and examines the kinetics of Aβ_{42} fibrillation.

Chapter 4: Characterization of Peptide Spheres The work described in this chapter is a side project to the overall aim of this thesis. Boc-Phe-Phe-OH have previously been reported to have remarkable physical properties. This chapter describes an in depth physical characterization of the Boc-Phe-Phe-OH peptide spheres.

Chapter 5: Sandwich Assay Analyser This chapter describes a lab-on-chip system based on a EIS coulter counter detecting a polystyrene bead concentration. This is combined with a sorting device using an antibody double assay for the biological specificity.

Chapter 6: PEDOT Nanowire Review This chapter is a review of previously published articles on PEDOT Nanowires. It focusses on the fabrication, characterization and applications.

Chapter 7: Fabrication of PEDOT Thin Films and PEDOT wires This chapter examines the fabrication of PEDOT thin films and the possibility of fabricating PEDOT nanowires using a stamping technique.

Chapter 8: PEDOT Nanowire by Self-Assembled Peptides. This chapter shows a novel fabrication method for PEDOT nanowires using Phe-Phe tubes as etch masks. It is also shown that the PEDOT nanowires are sensitive sensors for temperature measurements.

Chapter 9: Cellular Studies This chapter covers another small side project. The PEDOT nanowires are shown to have a potential for being used for single cell measurements.

Chapter 2

Introduction to Biosensors

The concept of biosensors is a major research area. A biosensor is a device that can selectively detect/sense a biological target analyte. The biosensor need to distinguish the target analyte from other elements in the sample. This is a highly demanding task as biological samples are often very complex entities. To solve this rather complex task biosensors utilizes bioreceptors from nature, such as antibodies, nucleic acid and enzymes, which have a strong specificity towards certain target analytes.[32–34] A biosensor consists of a bioreceptor that provides the selectivity, a transducer which translates the biological event into a readout and an interface that connects the two. Biosensors can be divided into two subcategories; labeled and label free. If the analyte can be detected directly from interaction of between the analyte and bioreceptor it is called label free. This is, however, not always possible, some biosensors rely on a second molecule (label) to provide or enhance the output. These are the labeled biosensors.

2.1 Bioreceptors

Beside grouping biosensors into labeled and label free sensors they are also grouped according to the type of bioreceptor. There is a broad selection of bioreceptors including enzymes, antibodies, nucleic acids, cells. This thesis includes work with antibodies and nucleic acids. These will be explained further in this section.

Antibodies Antibodies are Y-shaped proteins formed as an immune response to foreign objects (antigen), e.g. a virus, in the body. An antigen-specific antibody has a very high specificity. The antibody antigen interaction can be explained with an analogue to a key and lock where the form of the key enables it to open the lock. The antigen-specific antibody fits its antigen in an equally specific way. This unique property have proved immensely important for their role in biosensors where only the specific analyte of interest fits the antibody binding site.[35] As the field of biosensors has evolved antibodies has become a common bioreceptor[36–39]

Aptamers Aptamers are rapidly gaining interest as an alternative to antibodies due to their ability to bind a wide range of targets with high specificity. Aptamers are peptides or olionucleotides (RNA or single stranded DNA). The affinity of aptamer towards a target molecule is mainly owed to the stabilization of secondary structural motifs in the presence of the right target. Typical motifs are hairpins, duplexes, loops, G-quadruplexes, bulges, junctions and internal loops.[40] While showing similar affinity and specificity towards the target analyte as antibodies, aptamers have a higher resistance to environmental influence such as temperature or harsh chemical conditions because they do not denature irreversibly in these conditions.[41] The aptamers also have an almost unlimited shelf life, if kept under sterile conditions. Aptamers are produced in-vitro which has a number of advantages compared to the in-vivo based origin of antibodies. The target range is not limited to immunogenic compounds, but can target a wide range of small and large molecules, virusses, bacteria, whole cells and even single ions, as well as toxins. The in-vitro selection of aptamers also excludes batch to batch variations and reduces the costs and time.[42] The smaller size of aptamers compared to antibodies also prove some advantages as some analytical methods, such as impedimetric sensors and field effect transistors are most sensitive when the binding event takes place within the Debye screening length. The Debye screening length is determined by the ion concentration in the electrolyte surrounding the electrodes; for biological relevant solutions this is in the range of 5-10 nm.

2.2 Transducer

The transducer element of the biosensor translates the analyte-bioreceptor interaction into a measurable signal. There is a wide range of different transduction methods from which the most frequent is listed here.

- **Optical Detection** utilizes light as the measured parameter. The biosensor can be based on either fluorescence or optical diffraction. Fluorescence can be measured either by native fluorescence directly from a target analyte or by adding a label molecule. Diffraction sensing is applied in e.g. enhanced Raman spectroscopy and surface plasmon resonance.

- **Resonant Biosensors** is e.g. quartz crystal microbalances (QCM) or cantilever based sensors, which are oscillating in certain modes. The interaction of an analyte to the surface of the cantilever results in change of oscillating modes which can be detected.

- **Calorimetric Biosensors** are temperature sensitive. When an analyte reacts with a bioreceptor on the surface of the calorimetric biosensor the reaction heat is measured. The total amount of heat that is absorbed or produced is proportional to molar enthalpy and total number of molecules in the solution.

- **Electrochemical Biosensors** are a broad term. The basic principle for this class is the the chemical reaction between the bioreceptor and analyte produce a change

in ions or electrons which can be measured either as a change in potential or conductance. The biosensors presented in this thesis belongs to this group and is explained further in section 2.2.1

- **Biological Field Effect Transistor (FET)** Field effect transistors, in which the gate region has been modified with an enzyme or antibody, can also detect very low concentrations of various analytes as the binding of the analyte to the gate region of the FET cause a change in the drain-source current

2.2.1 Electrochemical Impedance Spectroscopy

Electrochemical Impedance Spectroscopy (EIS) is a very sophisticated and powerful characterization technique which provides the specific impedance output for an applied frequency domain.[43,44] Impedance is the complex definition of a given systems ability to resist an electrical current with an alternating potential (AC). The direct current (DC) equivalent is known as electrical resistance which can be described by Ohm's law:

$$U = R \cdot I \Rightarrow R = \frac{U}{I} \tag{2.1}$$

where U is the electrical potential of the circuit, I is the current in the circuit and R is the total resistance of the circuit. Extending to alternating current (AC), the ability of the circuit to resist the electrical current in a given circuit is given by the electrical impedance Z. This is a complex number consisting of the real part Z_r which gives the resistance and the imaginary part Z_i called the reactance. The relation between the AC potential $U(\omega)$, the AC current $I(\omega)$ and the impedance $Z(\omega)$ is given by:

$$Z(\omega) = \frac{U(\omega)}{I(\omega)} = Z_r + Z_i \tag{2.2}$$

The magnitude $|Z|$ and phase $\angle Z$ is given by:

$$|Z| = \sqrt{Z_r^2 + Z_i^2} \tag{2.3}$$

$$\angle Z = \theta = tan^{-1}\left(\frac{Z_i}{Z_r}\right) \tag{2.4}$$

EIS is measured by applying an AC potential across an electrochemical cell and measuring the crossing current. The applied potential can be written as:

$$E_t = E_0 \cdot Sin(\omega t) \tag{2.5}$$

where E_t is the potential at time t, E_0 is the amplitude of the signal and ω is the radial frequency ($\omega = 2\pi f$, where f is the applied frequency). The responding current can be written as:

$$I_t = I_0 \cdot Sin(\omega t + \phi) \tag{2.6}$$

where I_t is the corresponding current at time t, I_0 is the amplitude and ϕ is the phase angle depending on the impedance of the system. Going back, the impedance $Z(\omega)$ can be written as:

$$Z(\omega) = \frac{E_0 \cdot Sin(\omega t)}{I_0 \cdot Sin(\omega t + \phi)} = Z_0 \frac{Sin(\omega t)}{Sin(\omega t + \phi)} \tag{2.7}$$

from this it can be seen that the impedance can be expressed in terms of the magnitude Z_0 and phase shift ϕ.[43] For mathematical purposes this can also be written with complex notation:

$$Z = Z_r + jZ_i \tag{2.8}$$

There are two common ways of presenting EIS data; the Nyquist plot and the Bode plot, see figure 2.1. The Nyquist plot represents the data as Z_i versus Z_r with each point on the plot corresponding to a different frequency with the frequency increasing from right to left. The Bode plot represents the data as the absolute impedance $|Z|$ as function of frequency f. The high interest in EIS stems from the fact that the measured data can be fitted to an equivalent electrical circuit. This creates a fantastic opportunity for interpretation of the data. Most data can be fitted by relatively simple circuits consisting of capacitors, inductors and ohmic resistors.[43] The most common circuit is the Randles' circuit which can be seen in figure 2.1 (A). The Randles circuit consists of a resitsor R_1 in series with a parallel circuit of a capacitor C in parallel with a resistor R_2 and a Warburg resistance W. R_1 is dependent on the properties of the solution and the geometry of the electrodes. R_2 corresponds to the charge transfer resistance between the solution and electrodes. C is the double layer capacitance stemming from the interface between the electrodes and solution. W is contributes to the impedimetric spectrum at low frequencies and comes from the mass transfer between the solution and the electrode surface.[43,45] From this it can be seen that it is possible to use EIS to measure or characterize many different interactions in a chemical cell. Biological interactions on the surface, e.g. binding of a target analyte to an antibody or aptamer induce a large change in the double layer capacitance (C) whereas interactions in the solution, e.g. a bead passing the electrodes, will give a change in the R_1.

2.2.2 BioFET

Field Effect Transistors (FET) has long been the most prolific part of the electronics industry. In recent years there has been carried out a lot of work on making nanowire based FETs. This has let to the possibility of electrochemical gating of nano wires for use in biosensors, so-called bioFETs. The bioFETs has shown an extremely high sensitivity, down to measuring single molecules.[46] The origin of this high sensitivity stems from the high surface to volume ratio on the nano scale, as the conductance of the nanowire is intrinsic (volume dependent) whereas the analyte interaction is extrinsic (surface dependent). When an analyte with a given charge binds to the surface of the nanowire, within the Debye screening length from the surface, it introduces an electrical field into

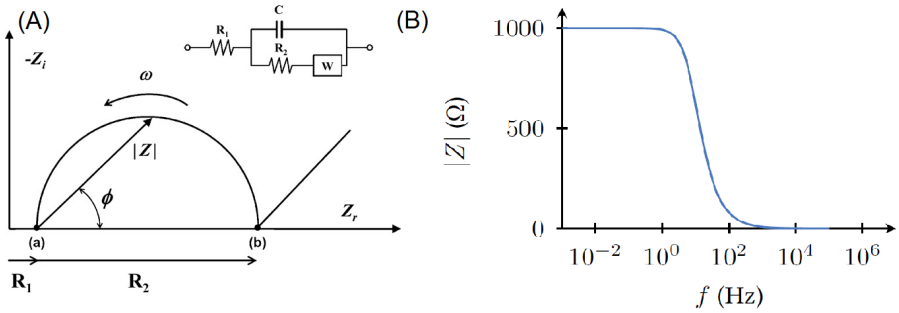

Figure 2.1: *(A) Example of a Nyquist plot and the corresponding equivalent circuit. Figure is modified from Bonanni et. al. 2010.*[43] *(B) Example of a Bode plot*

the nanowire. This field pertubes the charges carriers inside the wire, this is illustrated in Figure 2.2 . The conductivity σ and conductance G can be found from:

$$\sigma = \mu n e \tag{2.9}$$

$$G = \sigma A / L \tag{2.10}$$

where μ is the mobility, n is the charge density, e is the electron charge, A is the cross

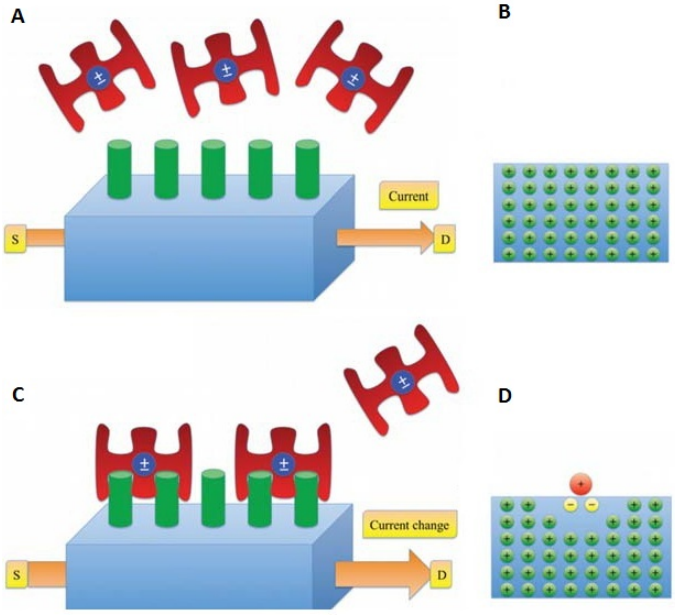

Figure 2.2: *Illustration of a bioFET. A shows a nanowire with incoming charged analytes. B shows a uniform charge density in a cross section of the nanowire. C shows two charged analytes have bound to the nanowire, which pertubes the charge density inside the nanowire as illustrated in D. The figure is modified from De Vico et al. 2011*[47]

sectional area and L is the length of the wire. Considering an ideal crystaline nanowire the conductance is seen to be proportional to the charge density. In a normal FET the charge density is pertubed by applying a potential to the gate electrode. The bioFET is gated when a charged analyte binds to the nanowire, this perturbs the charge density. The gating of a theoretical nanowire bioFET was investigated by De Vico et al.[47] The model considers a cylindrical nanowire between a source and drain, with a oxide layer on the surface of the wire and a bio functionalized layer containing the recognition molecule and analyte. They found that the conductance change could be quantified to:

$$\frac{\Delta G}{G_0} = -\frac{2}{Rep_0}\Gamma(\Gamma_l\sigma_b + \sigma_s) \tag{2.11}$$

where R is the radius of the nanowire, p_0 is the hole density, e is the elementary charge, Γ is a dimensionless function quantifying the sensitivity of the nanowire and Γ_l is a dimensionless function quantifying σ_s. Γ and Γ_l are found numerically from the computational model. When the incident of the charged analyte binding to the nanowire the additional charge σ_b changes the charge density σ_s in the vicinity of the nanowire surface. The new electrical field close to the surface pertubes the charge-carrier density n_0 in the nanowire by Δn. This change ultimately changes the conductance G_0 by ΔG. The effect of the analyte on the conductance of the nanowire is dependent on the Wire radius R, the buffer's Debye length λ_D and the nanowire's Thomas-Fermi length λ_{TF}. λ_{TF} is a charge screening length into the wire. From eq. 2.11 it is seen that the sensitivity of the nanowire is depending on the radius of the nanowire. This stems from the fact that the influence of the surface charges only penetrates into the nanowire with the fine length of λ_{TF} as well as the surface to volume ratio. Whereas the radius and λ_{TF} is limiting the sensitivity inside the wire the Debye length λ_D is important outside the wire. λ_D is the length of ionic screening from the surface. It is dependent on the ionic concentration of the solution. The position of the analyte on the surface is therefore important. This is mainly determined by the position of the binding site and size of the bioreceptor.

2.3 Introduction to Conductive Polymers

The scope of this work have been to design and fabricate all-polymer lab-on-a-chip systems. The transducers used throughout this work has been based on a conducting polymers, poly(3,4,ethylenedioxythiophene)(PEDOT). PEDOT has been extensively investigated and exploited at the department of DTU nanotech.[48–53]

The conductivity of electrical conducting polymers stems from having backbones with a conjugated system of π-bonds. The π-bonds originates from chemical double and triple bonds, e.g. between carbon atoms in orbital interactions. Considering one of the simplest conducting polymers, polyacetylene, the $2s$ and two $2p$ orbitals hybridize into a sp^2 orbital. The remaining p_z stands perpendicular to the sp^2 orbital, see figure 2.3. Overlapping sp^2 orbitals form σ-bonds whereas the p_z orbitals close to each other form π-bonds. For a long polymer chain the electrons in the p_z orbitals can be considered de-localized over all p_z orbitals with an even distance between carbon atoms. This means the electrons has a very high mobility and basically creates 1-dimensional metal. However, this doesn't happen in reality due to Peierls distortion, which gives rise to alternating bond lengths. This gives conjugating polymers a periodic change in the distance between carbon bonds. From the Blochs theorem it is found that such a periodicity gives rise to a band gap in the polymer. for PEDOT the band gap between the valence band and conducting band is about 1.6 - 1.7eV.[54] Conjugated polymers needs to be doped with ions to become conducting. In a polymer the doping refers to a charge on the backbone. Analogue to a p-doped semi conductor an oxidized conjugated polymer contains de-localized holes, which functions as charge carriers along the π-bonds. The extra charge carriers need to be stabilized by anions.

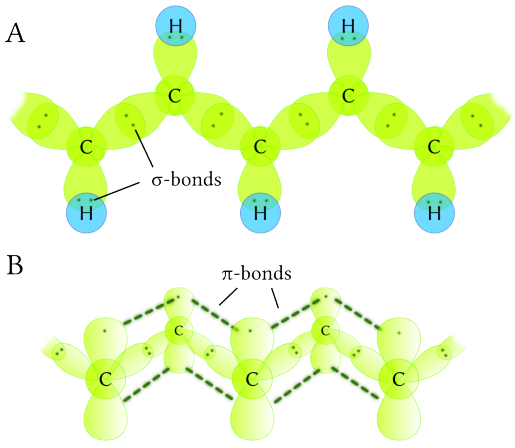

Figure 2.3: *Hybridised sp^2 orbitals overlap with each other and s orbitals from hydrogen atoms to form σ-bonds (A) Neighbouring p_z orbitals form π-bonds, allowing high electron mobility (B), Figure adapted from Daprá 2013*[55]

2.3.1 Poly(3,4-ethylenedioxythiophene) (PEDOT)

Poly(3,4-ethylenedioxythiophene) (PEDOT), figure 2.4, is a polythiophene that was developed by Bayer AG research laboratory in the late 1980's and ha become one of the most interesting conductive polymers for practical applications.[56] PEDOT has some exciting properties; it has low oxidation potential and in the oxidized state exhibits a high stability and high conductivity.[57] In the oxidized state PEDOT thin films has a light blue color and turns transparent during reduction. PEDOT can be produced from 3,4-ethylenedioxythiophene (EDOT) by either electrochemical polymerization or oxidative chemistry.[58] PEDOT can be doped to increase the conductivity. The most commonly used dopant is poly(styrene) sulfonate (PSS), which is a high molecular molecule. The size of the PSS allows it to be somewhat physically trapped inside the PEDOT making it more stabile. Smaller dopants like tosylate can diffuse more easily out of the PEDOT and can be exchanged with other ions in the surrounding environment.[56] This material is promising for biosensor systems as it combines high stability in its oxidized state withe high conductivity and compatibility with aqueous electrolytes.[57,59] PEDOT als oshows a high stability against biological reducing agents due to its ordered molecular structure.[60]

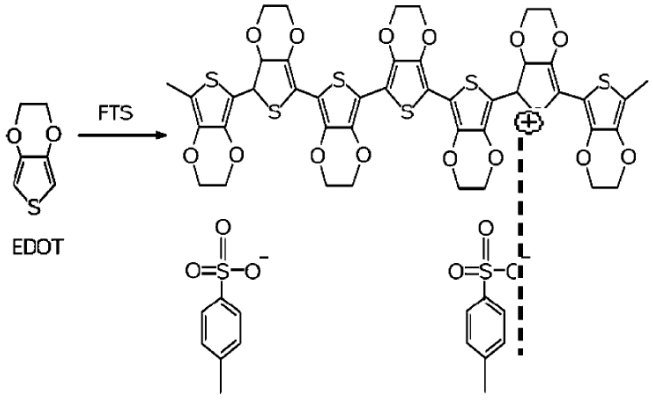

Figure 2.4: *The chmical structure of PEDOT, adapted from Rozlosnik 2009*[56]

Chapter 3

Induced Fibrillation of Aβ_{42}

The aim of this thesis was to explore different methods for the detection of Aβ_{42}. One approach was that to induce an artificial fibrillation of Aβ_{42} by seeding would help in the detection. Therefore the kinetics of Aβ_{42} fibrillation was investigated. By having the Aβ_{42} monomer population represented as fibrils it could be possible to pre-concentrate the sample using microfluidic size separation techniques. The large size of the fibril compared to the monomers would also increase a possible transducer output. Our group has previously presented a powerful all-polymer bio-sensor based on Electrical Impedance Spectroscopy (EIS). It's believed that fibrils situated on the surface of this device would give a significant output.

EIS measures a change in the double layer capacitance when a molecule is situated on top of the measuring electrodes. A large aggregate like amyloid fibrils has an advantage over small molecules such as the monomeric form of the Amyloid Beta peptides. The size and charge of the fibril induces a larger change in the double layer capacitance than the monomeric peptides. The size of the peptides also makes it possible to facilitate an microfluidic based up-concentration of the fibrils.

Amyloid fibrils are not present in native cerebrospinal fluid but are formed at the neurons during the build up of plaque. There has been numerous reports on inducing fibrillation using seeds of fibrils.[18,19,61] This chapter describes our work with investigating the formation of amyloid fibrils and artificially inducing the fibrillation process.

To obtain results that can be used to determine if artificial seeding of Aβ_{42} monomers into fibrils can be controlled in a way which we can use there is a range of pre-requirements that need to be fulfilled;

- It is necessary to obtain a uniform population of monomers without or as few minor aggregates as possible. The minor aggregates would act as seeds themselves blurring the results of the experiment.

- Finding a method to determine the concentration of Aβ_{42} in monomeric form before fibrillation.

- Finding a method for observing the ongoing fibrillation and verifying the fibrillation.

3.1 Materials and Equipment

The chemicals used in these experiments were all bought from Sigma Aldrich® except for the peptides which was purchased from Covance®.

3.1.1 Thioflavin T

Thioflavin T (ThT) is a benzothiazole dye that exhibits an enhanced fluorescence upon binding to cross-β sheets. The morphology of amyloid fibrils has made ThT a commonly used mean for diagnosing amyloid fibrils both in vivo and in vitro.[62,63] ThT in aquarius solutions shows a low fluorescence signal with an excitation and emission maxima at 350 nm and 440 nm respectively. However, when bound to cross-β the ThT fluoresces strongly with an excitation and emission maxima at 440 nm and 490 nm. From this shift in fluorescence it is easy to follow the formation of fibrils as an increasing amount of cross-β will give an increasing fluorescent signal.

3.1.2 UV-Spectrophotometer

UV-Spectrophotometer - ultraviolet-visible spectrophotometry (UV-Vis) refers to absorption spectroscopy in the ultraviolet-visible spectral region. In this region of the electromagnetic spectrum, molecules undergo electronic transition (electrons are excited to a higher energy level) when absorbing the UV-light. The Lambert-Beer Law states that the absorbance of a solution is directly proportional to the concentration of the absorbing species and the path length of light through the solution.

$$A = c \cdot \epsilon \cdot l \tag{3.1}$$

where, A is the measured absorption, l is the length of the light pathway through the sample and ϵ is the extinction coefficient and c is the concentration. ϵ is defining how strongly a substance absorbs light at a given wavelength per molar concentration.
In biochemistry the extinction coefficient of a protein at 280 nm is almost exclusively based on the number of aromatic residues and can therefore be deduced from the amino sequence. Another characteristic wavelength for proteins is 220 nm. Proteins show a high absorption at this wavelength due to the chemical bond s between the carboxyl groups and amino groups of the neighboring amino acid. Getting a response at 220 nm thereby indicate that the measured sample is a peptide or protein. The extinction coefficient of Aβ_{42} at 280 nm is 1490 nm.[22]

3.1.3 MALDI-TOF

MALDI-TOF is a mass spectroscopy (MS) based analytical method for characterizing for example proteins[64] The MALDI (Matrix Assisted Laser Desorption/Ionization) is a soft ionization technique. That allows materials that usually tends to be fragile and fragment,

i.e. proteins, when ionized, to be ionized. The sample is placed on a matrix element, which absorbs the laser energy while transferring ions to the sample which in turn is ionized. The ionized proteins leaves the matrix in a gaseous state. These are then accelerated in an high electrical field towards detector. The ions are separated due to the time it takes the to cover the distance from the matrix to the detector. This is known as the Time of Flight (TOF). Ion with the same charge are emitted at the same time from the matrix. The velocity is dependent on the mass of the ion. By detecting every impact of the ions on the detector it is possible to create a fingerprint of the sample protein.

3.1.4 AFM

Atomic force microscopy (AFM) utilizes on the principle of a small tip being moved across a surface. The tip detects holes or protrusions on the surface through interactions with the surface forces. The size of the tip is very important for the resolution of the AFM, the ideal tip ends in a single atom. If the tip is close enough to the surface it interacts through the surface forces. These forces are normally in the range of 1 nN but can be as low as tenths of pN The most used interaction force is the Van der Waals force. However, this is not the only one; other forces such as capillary forces and electrostatic forces are present too. In this thesis, for simplicity, only the Van der Waals forces are considered. The tip is positioned on a cantilever, which detects according to the surface forces. By measuring this de ection it is possible to get a read out of the surface topography. The AFM used in this work was a XE-150 PSIA.

3.1.5 FPLC

Fast Protein Liquid Chromatography is a technique used for separating different structures like proteins from complex mixtures. Liquid Chromatography is a term which refers to all chromatographic methods with a liquid mobile phase. FPLC is a type of liquid chromatography where the velocity of the buffer is held constant. The sample is loaded into an injection loop. Through an injection valve the sample is then run through a column where the separation takes place. The actual separation method depends on the specific column and can based on size exclusion, charge distribution, hydrophobicity, reverse-phase or bio-recognition i.e. antibodies. After passing through the column the sample passes one or two flow cells which measures the concentration of the passing sample over time. Finally the separated fractions can be collected.
In this work a system with a Superdex 75 HR 10/30 column and both an UV- and Refractive index (RI) flow cells was used. The specific column has previously been reported to separate Aβ_{40} and Aβ_{42}.[22] The separation method used is Size-Exclusion Chromatography (SEC). The column is packed with a porous gel that allows small particles to enter the pores whereas larger particles will pass by. The extra pathway through the pores will slow down the smaller particles creating a separation.

3.2 Experimental Procedure

Lyophilized 98% purified $A\beta_{42}$ peptide was dissolved in 6M guanidine hydrochloride (GndCl) at 1 mg per ml. The solution is mixed in an ultra sonic bath for 30 s and is carefully visually inspected to ensure the liquid is clear and the peptide has been dissolved. During experiments it was found that it is preferable adding GndCl to the lyophilized peptide rather than adding the lyophilized peptide to the GndCl solution. It was observed that the later had a higher tendency to produce unwanted protofibrils. This could be due to a very high local concentration when adding the peptide. $A\beta_{42}$ aggregates very fast at room temperature. To avoid a large formation of protofibrils the sample is kept on ice at all times. The dissolved peptide then centrifuged at $16.000g$ for 10 min at 4°C whereafter the supernatant was carefully collected. This was done to limit the amount of aggregated being injected into the FPLC.

The supernatant was then injected into the FPLC using a 1 ml sample loop. The column had been equillibrated with PBS buffer over night. Due to the easy aggregation of the $A\beta_{42}$ the best conditions for performing the FPLC would be to have the equipment placed in a cooled room at 4°C. This option was however not available so the running buffer on the FPLC was cooled down with ice before use and the column was placed in a cooled water bath during experiments. Using a flow rate of $\approx$0.5 ml min^{-1} (the system was a little bit inconsistent.) the sample was run on the column. The eluent was expected at $\approx$30 min and was collected after being observed on the UV- and RI-signals. The concentration of the purified peptide solution was measured using UV-spectrophotomer with wavelengths of 220 nm and 280 nm. The UV-source was turned on 15-20 min before use to obtain a stabile output. First 1 ml blank sample (PBS) was loaded into a quartz cuvette and measured as a reference, then 1 ml of the peptide solution is loaded into another quartz cuvette. The concentration can be found from the Beer-Lambert law see equation 3.1. The peptide solution was then mixed with PBS to a final concentration of 10 μM.

To form fibrils the $A\beta_{42}$ is incubated at 37°C for between 15 and 70 hours. To study the kinetics of the fibrillation 20 μM ThT is mixed with $A\beta_{42}$ solution. The ThT solution is prepared by dissolving 0.32 mg of ThT in 10 ml of Milli-Q water giving a concentration of 100 μM. The solution is then filtered using a 0.22 μm PES syringe filter. The ThT solution was then mixed into the $A\beta_{42}$ solution to a final concentration of 20 μM. A platereader (Victor$^3_{\text{TM}}$, Perkin Elmer$^{\text{TM}}$) was used to monitor the fibril formation. 250 μl sample was placed into a series of well in a 96 microwell plate (Nunc$^{\text{TM}}$). As controls a couple of blank samples of pure PBS and PBS with 20 μM ThT was also added to the well plate. Finally the well plate was sealed with a lid to avoid evaporation. The well plate was then inserted into the platereader which heated the sample to 37°C and measured the fluorescent output once per hour for 70 hours.

For testing the hypothesis of increasing the fibrillation process rate by seeding, a $A\beta_{42}$ solution was prepared as described before. The solution was the incubated at 37° C for 70

hours in a water bath. The fibrillated solution was then sonicated using a stick sonicator at 50% pulses for 30 s. The sonicated solution was then diluted 1:5 with PBS to make the final seeding solution. A new Aβsolution was prepared and 200 μl was added to each micro well and mixed with 50 μl of the seeding solution. The well was then inserted into the platereader and measured as described previously.

3.3 Results and Discussion

3.3.1 Calibration of FPLC

The FPLC purification of Aβ_{42} was expected to give a pure monomer eluent after $\approx$ 30 min. However, on some of the initial runs we also observed a minor peak around 26 min this peak is expected to be minor aggregates as e.g. protofibrils. To ensure that the collected eluent is the Aβmonomers the FPLC system was calibrated using a standard kit of proteins containing; Phenylalanine, Cytochrome C, Myoglobin and Ovalbumin. Figure 3.1 shows the results of the calibration with the K_{av}-value over the logarithm of the molecular weight. K_{av} is the partition coefficient which is given as:

$$K_{av} = \frac{V_e - V_v}{V_{tot-V_v}} \tag{3.2}$$

where V_e is eluent volume, V_v is the column void and V_{tot} is the total volume.[65] It is observed that the experimental value is relatively close to the expected value. The small difference can be caused by the error of reading the exact elution volume or instability of the exact flow rate.

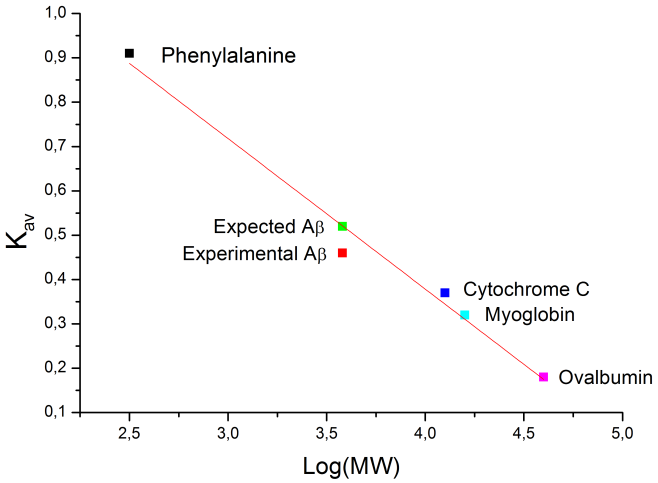

Figure 3.1: *Calibration of the Superdex 75 column on the FPLC system.*

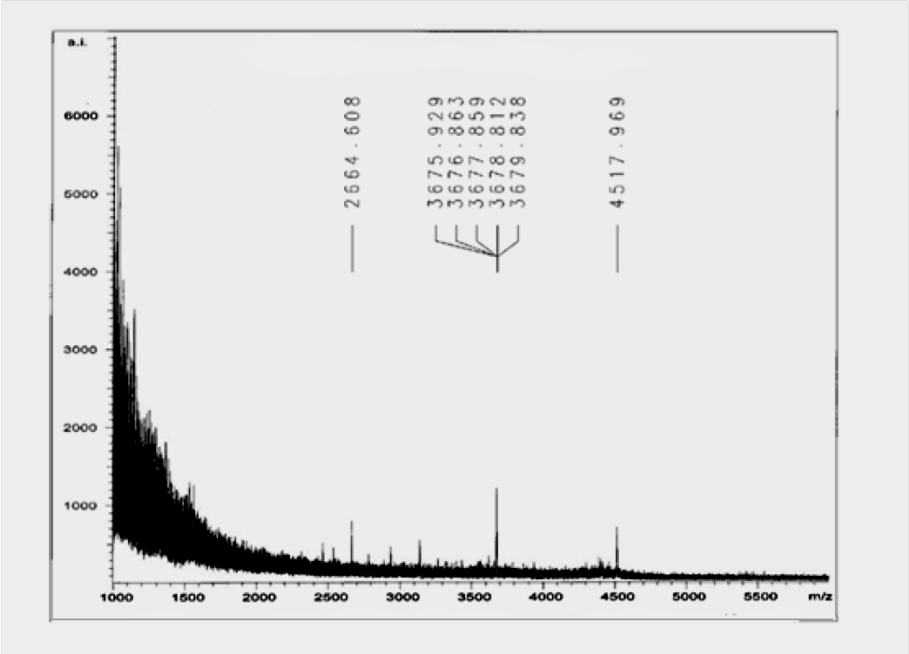

Figure 3.2: *MS-spectra of the collected eluent from the FPLC. It is observed that there is a distinct peak at 4518.0 m/z, which fits with an expected value for* $A\beta_{42}$

3.3.2 MS on Eluent

To ensure that the eluent corresponded to $A\beta_{42}$ and was not artifact due to the GndCl or PBS a MS-spectrum was found by MALDI-TOS. Figure 3.2 shows the obtained MS-spectra. The spectra shows three distinct peaks and a variety of minor peaks. The distinct peaks corresponds to a mass-to-charge ratio (m/z) of 2664.6, $\approx$ 3677.9 and 4515.0. The last peak fits well with the expected value for $A\beta_{42}$.[66] The other peaks could also indicate $A\beta_{42}$, 3677.9 however, could also refer to $A\beta_{33}$. The acquired protein used in this experiment was 95% purified, which means the extra peaks could be from impurities in the original peptide. A control sample was made by collecting an eluent after the expected $A\beta_{42}$. This sample showed no distinct peaks in the MS-spectra.

3.3.3 Fibrillation of $A\beta_{42}$

Comparing the results of the FPLC and MALDI-TOF to previously published results[22,66] it can be concluded that the eluent after 30 min is the $A\beta_{42}$ monomer. The investigation of the fibrillation rate was carried out by mixing the monomer with ThT and incubate them in the platereader for between 40-70 hours. Figure 3.4 shows the fibrillation of the $A\beta_{42}$ as the intensity of ThT over time. It is seen that the intensity increase steeply over the first 10 hours and then ease off. This means the monomers fibrillate into mature fibrils over this time span allowing. These results fits with previously published results.[67,68] The fibrillation was verified further by AFM, several formations of fibrils was observed, see

figure 3.3.

The nucleated polymerization process can be divided into three phases; The first is a relatively slow nucleation lag phase where thermodynamical unfavorable interactions begins the formation of nuclei or seeds. The second is the elongation where additional monomers lead to a formation of higher order aggregates e.g. fibrils. The third is a steady state phase where there is a equilibrium between the monomers in solution and the fibrils.[69] It has previously been published that the initial lag phase can significantly reduced by the addition of seeds.[70] To investigate this a small amount of seeding solution was prepared and mixed with the standard Aβ_{42} solution before incubation in the platereader. Figure 3.5 shows the intensity of the ThT over the incubation time for one sample containing 200 μl Aβ_{42} solution and 50 μl seeding solution (magenta), two samples of 250 μl Aβ_{42} (red and blue) solution and a blank sample only containing 250 μl PBS (black). It can be seen that the fibrillation follows the same rate for both the seeded and un-seeded solutions. The amplitude of the intensity for the seeded solution is higher than for the un-seeded solution. This could be caused by extra amount of added seeds, which will also react with the ThT. The lack of increased fibrillation rate could be due to a variety of things. It is possible that the temperature of the Aβ_{42} solution have been too high at times during the experiments. This could have caused a formation of small aggregates to form before the intended incubation. This could in turn mean that a small seeding is already taking place, which again means that there won't be seen a difference when adding seeds.
Handling of Aβ_{42} is a general problem in these experiments. During experiments it was observed that the peptide has a high tendency to stick surfaces which created a risk that not all of the peptide is transferred between experimental steps. The Aβ_{42} starts the initial fibrillation quickly if heated above 4° C or kept in high concentrations. The tendency to stick and fibrillate means that for every transfer of the Aβ_{42} solution there is an increased risk of early fibrillation and reduced concentration of Aβ_{42}.

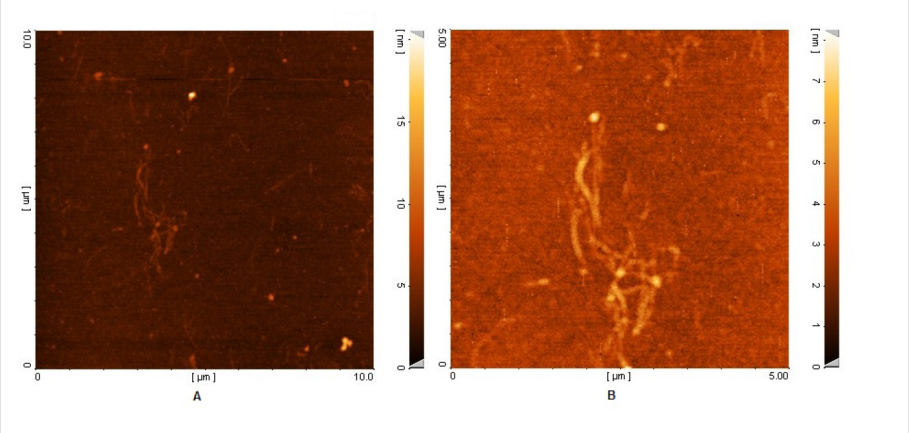

Figure 3.3: *AFM scan on an incubated sample. A formation of fibrils is clearly seen on figure (A). (B) is a close up of the fibril formation.*

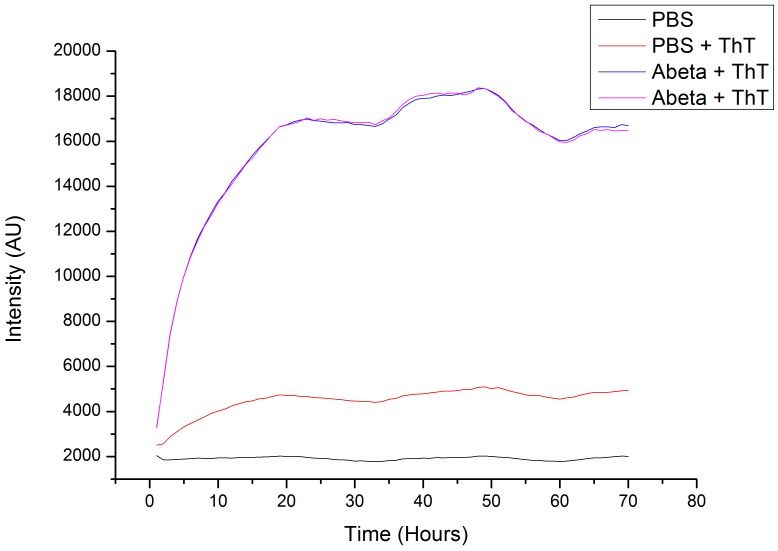

Figure 3.4: *The fibrillation of $A\beta_{42}$ is observed from the fluorescence output of the ThT. The black line is pure PBS. The red line is PBS and ThT. The blue and magenta lines are the $A\beta_{42}$ solution with ThT*

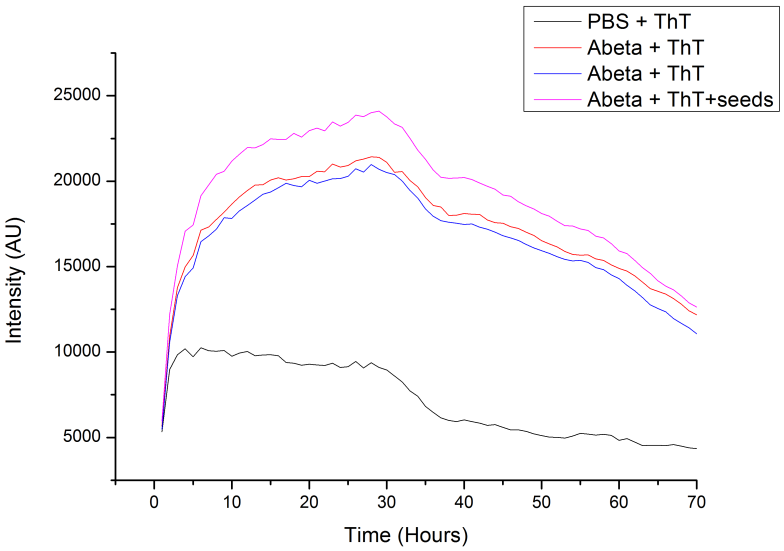

Figure 3.5: *The fibrillation follows the same trend for both the un-seeded and seeded solutions. The magenta line is the seeded solution. The red and blue lines are the un-seeded solution and the black line is pure PBS.*

3.4 Conclusion

The initial gain that was obtained from this work was the knowledge on how to handle Aβ_{42} to avoid unwanted fibrillation. The very sticky nature of the Aβ_{42} indicates that there could be lost a small amount of peptide when transferring samples between containers e.g. Eppendorf tubes. There was obtained uniform population of monomeric Aβ_{42} using FPLC and it was shown that this could be fibrillated by incubation. From the experiments carried out in this work the seeding of Aβ_{42} does not decrease the lag phase of the fibrillation significantly. This could be explained by several theories and would need to be examined further to conclude finally.
The experimental phase of this work experienced a time consumable setback. We had successfully showed that we could make controlled purification of Aβ_{42} monomers and fibrillation using a 95% purified Aβ_{42} batch from Covance®. Upon receiving a new batch of Aβ_{42}, the new range of experiments did not show the expected ThT intensity profile for fibrillation, indication that the Aβ_{42} didn't fibrillate. After a range of experiments a new sample was acquired from the manufacturer which did not show any fibrillation either. This was initially believed to be caused by instrumental or experimental errors. This caused us to test the equipment thoroughly. We were however not able to find any obvious issues with neither the equipment nor the procedure. Finally a range of experiments were carried out at Statens Serum Institut and at COBIS (Copenhagen Bio Science Park) using our peptide. From these experiments it was concluded that the lack of fibrillation was due to the quality of the peptide. After a number of conversations with the producent of the Aβ_{42} peptide, Covance®, they agreed to replace the previously bought 95% pure peptide with a new batch of 98%. This readily solved the problem and made it possible to make the seeding experiments. The whole process however took three months of work without progress. Due to this delay and to the imposed time frame of this PhD it was decided to not pursue the detection of Aβ_{42} through fibrillation further. Even though the experiments in this chapter is not concluding enough as to confirm if it is a plausible path to investigate.

Chapter 4

Characterization of Peptide Spheres

4.1 Introduction

Diphenylalanine (FF) has previously been presented as the key recognition molecule for AD.[29] It is suggested that the FF plays a significant role in the process of amyloid fibril formation.[29] Do to previous knowledge working with these peptide structures it was decided to investigate them further as an introduction to handling peptides and understanding the kinetics of self-assembling peptide structures e.g. peptide tubes[71,72] and peptide spheres.[31] The FF tubes has previously been reported to be insoluble in most liquids[73] which could support the motif claim as amyloid fibrils are also insoluble. It has however been shown that the FF tubes are in fact soluble in most liquids including water. The initial studies led to a side project investigating the physical and chemical properties of FF peptide spheres.

Biological nanostructures have outstanding properties that inspire researchers to employ them in bionanotechnological applications.[74,75] Molecular self-assembly is a spontaneous process that plays a key role in biological systems. This natural process has attracted an increasing interest in nanotechnology and inspired the fabrication of new materials through a bottom-up approach. Several building blocks that are able to self-organize into defined nanostructures are available in nature.
An example of such a substance is the short aromatic dipeptide known as diphenylalanine (FF). This compound is able to rapidly self-assemble into nanotubes, nanofibers or nanoparticles under mild conditions.[76,77] The nanostructures it forms have been characterized and some of their properties have paved the way to significant applications,[71,77–82] such as for instance the nanotubes obtained from the diphenylalanine peptide. These structures present a remarkable stiffness and can be easily functionalized with a long list of functional molecules such as enzymes, quantum dots and magnetic particles.[83] Thanks to these biological self-assembled nanostructures, biosensing devices for detection of compounds of biomedical relevance have been reported as well as new clean-room fabrication

methods.[72,84–89] It is expected that new applications using the diphenylalanine peptide and its analogs will be developed in fields such as biomedicine, bioelectronics, and biomaterials.[77,82] Tert-butoxycarbonyl-Phe-Phe-OH (Boc-Phe-Phe-OH) peptide is a member of the aromatic diphenylalanine peptide family and it can self-assemble into spherical nanoparticles or tubular nanostructures depending on the conditions of the synthesis.[30] Recently, this substance was highlighted as one of the stiffest organic materials reported - even stiffer than Kevlar and steel.[78,90] As a consequence, it has been suggested that it be employed in the fabrication of medical implants and materials for aviation or space applications.[90] The mechanical properties of Boc-Phe-Phe-OH nanoparticles were studied using Atomic Force Microscopy (AFM). Based on an indentation-type study combined with finite element simulations and the assumption that the nanoparticles were spheres containing a cavity, values of 885 Nm^{-1} for the stiffness and 275 GPa for the Young modulus were determined. However, a previous investigation carried out in our laboratory on the structural characterization of this type of biological nanoparticles demonstrated with electrostatic force microscopy that the particles are in fact solid.[80] This could have an influence on the previously reported values of the stiffness and the Young modulus for these Boc-Phe-Phe-OH nanoparticles.[78]

The present study has involved a structural analysis of the Boc-Phe-Phe-OH nanoparticles using focused ion beam (FIB) milling to cut them, followed by imaging of their interior in order to confirm our previous results that they are indeed solid entities without cavities. AFM was then used to determine the Young modulus of the particles using two different systems. Additionally, the conductivity of these particles as well as their stability in various solutions was also evaluated.

Based on the obtained results, a Young modulus between 20 and 30 MPa was calculated. These results are approximately 10,000 times lower than the value previously reported. Additionally, we proved that the Boc-Phe-Phe-OH nanoparticles are non-conductive solid structures and that they are soluble in water and phosphate buffer. The present investigation has clarified the properties of these biological nanostructures for possible applications in the reinforcement and the fabrication of new materials.

4.2 Materials and Methods

4.2.1 Samples Preparation

The Boc-Phe-Phe-OH particles were fabricated by preparing a 100-mg/mL stock solution in 1,1,1,3,3,3-hexafluoro-2-propanol (HFP) at room temperature. Aliquots of the peptide stock solution were dissolved in 50% ethanol to a final concentration of 5 mg/ml.

4.2.2 Stability Experiments

The stability of the Boc-Phe-Phe-OH particles in solution was examined by adding a 10-μl drops of the peptide solution to a microwell plate and drying them under vacuum conditions at room temperature. To test the stability, 1 ml of solvent was added to the wells on top of the dried peptide particles after which high-performance liquid chromatography

(HPLC) and mass spectroscopy (MS) analyses were performed. Small samples (10 μl) of the fresh solution added to the peptide particles were collected at different times after the addition to the wells. MS determinations of the peptide particles were performed using turbo ion ® spray MS (QSTAR ®,-i-Q-TOF tandem mass spectrometer, PE Sciex, Toronto, Canada) connected in series to an HPLC system from Perkin Elmer (Boston, USA).
The collected samples, having an increasing contact time with the biological particles, were serially injected into the system via the LC autosampler. The mass spectrometer was set to positive ion mode with a needle voltage of +5500 V and the quadrupole system was set to scan m/z 200-1000 in TOF-MS mode, whereas a range of m/z 50-1000 was chosen for the product ion mode (i.e., MS/MS). The MS data was analyzed using the software Analyst, QS (PE Sciex, Toronto, Canada).

4.2.3 Young's Modulus Measurements

The Young modulus measurements were carried out on both mica and silicon substrates. The silicon surface was cleaned using water followed by ethanol and water again and dried using a nitrogen flow. In both cases, a 3-μl droplet of the peptide solution was placed on the substrate and dried under vacuum conditions at room temperature.
A gold grid pattern was prepared on a silicon substrate using standard cleanroom processes, in order to locate the particles for the AFM measurements. Initially, a topography image was obtained in tapping mode, after which the AFM tip was moved to the center of a peptide particle where the indentation was made. The sample was imaged with a Scanning Electron Microscope (SEM) (Zeiss - Supra 40 VP) and later with Atomic Force Microscopy (AFM) under ambient conditions using an XE150 system (Park Systems, Korea) in contact mode with a silicon cantilever (Cont-Al, Budget Sensors, spring constant: 0.2 N/m). The employed AFM tip had a pyramidal shape with a tip radius of 25 nm (Budget Sensors, Tap300Al-G). Using the grid, all AFM measurements were carried out on the same area, which had already been imaged with SEM. Only areas containing peptide particles (located by SEM) were imaged by AFM with a scan size of 10 x 10 μm and a scanning rate of 0.1 μm/s. Force-distance (FD) curves were also measured for each peptide particle.
A parallel measurement was conducted by Casper Hyttel Clausen at the University of California, Berkeley, where the samples were prepared on mica. The measurements were performed with a Brucker Catalyst Bioscope mounted on a Zeiss Observer 1 using a Brucker SCM-PICW with a spring constant of 0.1 N/m and a scanning rate of 0.033 μm/s. Also in this case, the AFM tip had a pyramidal shape with a tip radius of 25 nm.

The Young modulus can be calculated with the Hertz model when one knows the spring constant of the cantilever and by using the indention of the particle and the deflection of the cantilever. The Hertz model has previously been used to calculate the Young modulus of both biological and non-biological nanostructures[91–103]assuming small indentations, and it was also used in this work.

4.2.4 Focus ion Beam Experiment for Structural Characterization

A 2-μl droplet of the peptide solution was deposited on a silicon substrate and dried under vacuum conditions at room temperature. The sample was then placed in a dual beam microscope (QUANTA 3D LIFT-OUT, FEI Company). Two detached Boc-Phe-Phe-OH particles were located using SEM. Half of the peptide particles were then removed through focused ion beam milling (FIB) with a beam power of 10 nA. By tilting the stage in the dual beam microscope it was possible to obtain SEM images of the cross-section of the remaining particles. For the close-up imaging of the peptide nanoparticles 30 kV, a current of 91 pA, a working distance of 14.9 mm and tilt angle of 52 degrees were used.

4.2.5 Conductivity Experiment

Conductive AFM measurements were carried out to investigate the conductivity of the Boc-Phe-Phe-OH particles. A 3-μl droplet was placed on a freshly cleaned gold substrate and dried under vacuum conditions at room temperature. The gold surface, 100 nm, was deposited using physical vapor deposition (PVD) on top of a 10-nm Ti layer used to increase the gold adhesion. To ensure the electrical connection between the particles and the gold surface, the substrate was cleaned first with milliQ water, and then with ethanol and finally plasma-treated for 30 s before the peptide solution droplet was placed on its surface. The AFM experiments were performed with a PSIA XE-150 AFM mounted with a Cr/Pt coated cantilever (ContE-Al, Budget Sensors). The current through the AFM tip and sample was measured using an inverting current amplifier and one of the analogue-digital converter inputs of the AFM controller. The output of the current amplifier was a voltage, which was proportional to the current. In this way, the current map was obtained parallel to the topographic image. The zero level of the system was calibrated by performing a measurement on clean glass.

4.3 Results and Discussion

The aim of this study was to investigate the structural and electrical properties of Boc-Phe-Phe-OH nanoparticles and their stability in organic solvents by measuring their size, Young modulus, electrical conductivity and solubility in liquids. Initially, the size distribution of the Boc-Phe-Phe-OH particles was measured by analyzing 514 particles on the SEM images. The diameter of the particles varied from 120 nm to 1500 nm (figure 4.1). The measured size distribution was in a good agreement with the previously reported data measured on these types of biological structures.[31,76,78]

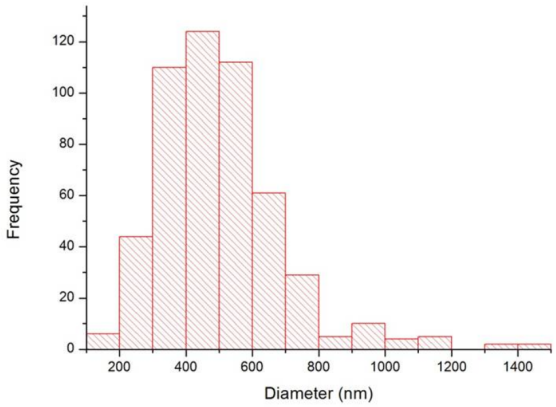

Figure 4.1: *Size distribution of Boc-Phe-Phe-OH particles as determined from SEM images*

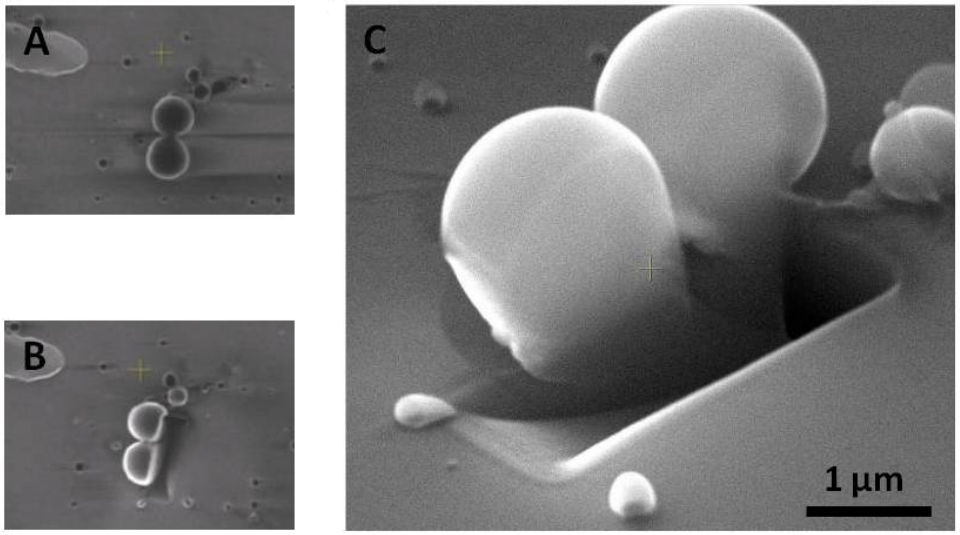

Figure 4.2: *SEM images of Boc-Phe-Phe-OH particles on a silicon substrate. A: Two nanoparticles prior to FIB milling. B: A rectangular section of the particles after FIB milling. C: Cross-sectional image of the particles.*

4.3.1 Focus Ion Beam Experiment for Structural Characterization

We have previously presented results, obtained from transmission electron microscopy (TEM) and electron force microscopy (EFM) measurements, that strongly indicate that the Boc-Phe-Phe-OH particles are solid rather than hollow materials.[80] To validate these results, two Boc-Phe-Phe-OH nanoparticles were cut in half by FIB milling. By tilting the sample stage 52 degrees, an angled SEM image could be taken of the cross section of the milled Boc-Phe-Phe-OH particles (figure 4.2). The cross section did not show any indications of a cavity inside the particles, which appeared as solid entities.

4.3.2 Young's Modulus

Boc-Phe-Phe-OH particles have previously been described to have remarkable mechanical properties with metallic-like point stiffness and a Young modulus of 275 GPa.[78,90] This would make the Boc-Phe-Phe-OH particles one of the hardest biological materials known [20]. The previously reported Young modulus has been determined from on point stiffness measurements carried out by AFM, followed by Young modulus calculations through modeling the Boc-Phe-Phe-OH particles with different sized cavities inside. However, since we have found no indications that the Boc-Phe-Phe-OH particles contain cavities, a renewed investigation of the Young modulus was carried out.
In this work, the Young modulus of the Boc-Phe-Phe-OH particles was determined by means of indentation measurements performed with AFM. To verify the results, two independent sets of measurements were conducted: one at the Technical University of Denmark (DTU) and the other at University of California, Berkeley (USA). To ensure that the substrate did not influence the results, the two measurements were performed on both silicon and mica substrates.
The first set of measurements was carried out on a grid-patterned silicon substrate in order to locate the areas with Boc-Phe-Phe-OH nanoparticles using SEM. This way, only those areas were imaged with AFM. The second set of measurements was conducted with a Brucker Catalyst Bioscope mounted on a Zeiss Observer 1. Samples were prepared on mica, and a Brucker SCM-PICW cantilever with a spring contact of 0.1 N/m was used. The data obtained by AFM was then inserted in the Hertz model. This model has been previously employed to calculate the Young modulus of biological samples.[91–98,104–107]
The first set of measurements using 42 peptide particles deposited on a silicon surface gave a mean value for the Young modulus of E $\approx$ 20 MPa (stand. dev. 1.4x10^{-7}). In the second set of measurements, 121 Boc-Phe-Phe-OH particles were measured on a mica surface and led to a mean Young modulus of E $\approx$ 30 MPa (stand. dev. 6.7x10^{-8}). The distribution of the Young modulus of the Boc-Phe-Phe-OH nanoparticles deposited on mica and silicon surfaces is presented in Figure 4.3.
The values found here are approximately 10.000 times lower than the previously reported values.[78] To further validate the results presented here some of the measured nanoparticles were topography imaged again after the force-distance measurements. Figure 4.4 shows the nanoparticle with a small cavity in the center from the AFM tip. The cantilevers with relatively low stiffness used here should not be capable of inducing this kind of cavities if in fact the nanoparticles are stiffer than steel. There can be numerous explanations to why the two results differ so much. In the work done by Adler-Abramovich and colleagues they assume that the nanoparticles are hollow spheres with a cavity up to 40% of the total volume. The measured stiffness of the nanoparticles were then related to Young's modulus through finite element simulations. However this work concludes that the nanoparticles are in fact solid entities. Assuming a cavity would give a higher Young's modulus than is the case. Another explanation could be miss aligning of the AFM tip before conducting the force-distance measurements. If the measurements in the previously published work has been conducted by an automatic system it could have given rise to incorrect measurements. In this case a large topography scan is conducted and the position of the

nanoparticles is stored. The automated system then produces the force-distance measurements on the designated coordinates. There can however be drift in the x-y plane of the AFM over time. This could lead to not measuring centered on the nanoparticles. This could have led to measurements being conducted on the surface rather than on the actual nanoparticles. In our measurements the force-distance measurement were done directly after the topography scan thereby ensuring the placement of the measurement on top of the nanoparticles.

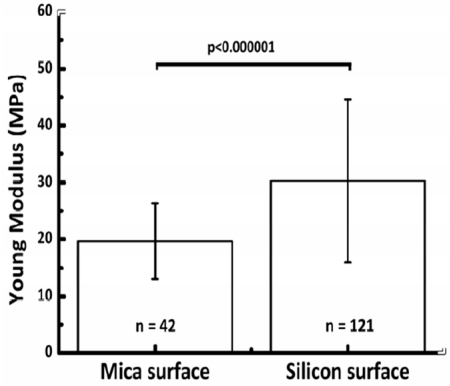

Figure 4.3: *Distribution of the Young modulus of the Boc-Phe-Phe-OH nanoparticles deposited on mica and silicon surfaces.*

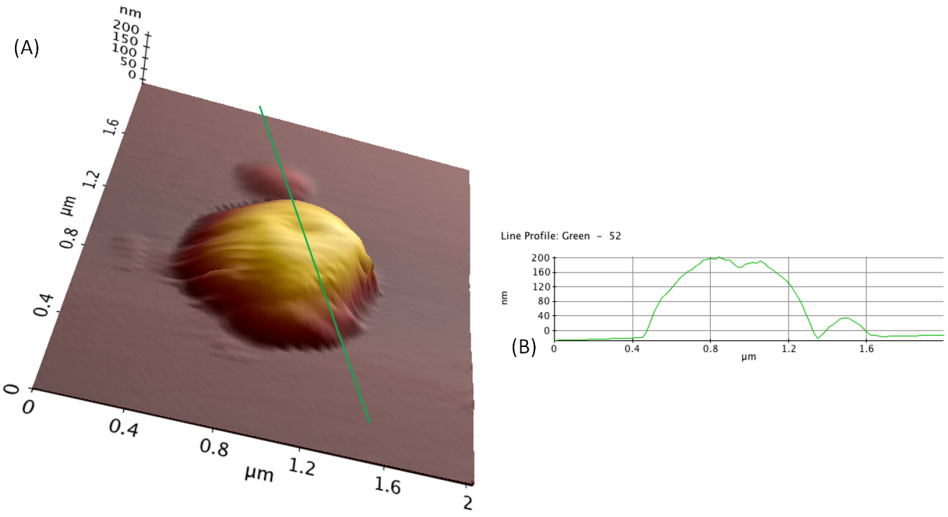

Figure 4.4: *(A) Shows a 3D topography image of the peptide sphere after a force-distance measurement. It is seen that the measurement has produced a cavity in the sphere. (B) shows the line trace highlighted in (A). The cavity is clearly seen in the middle of the peptide.*

4.3.3 Electrical conductivity Measurements

Self-assembled peptide nanostructures have previously been used for the development of biosensing platforms aimed to detect compounds such as metal ions, cancer cells and glucose, among other substances.[85,87,108,109] Nanofibers formed using diphenylalanine were presented as biological structures possessing semiconducting properties.[110] These previous results motivated us to investigate the conductivity of the Boc-Phe-Phe-OH particles using a setup with a conductive AFM tip.
During scanning of a gold surface containing Boc-Phe-Phe-OH particles, a topographical image (figure 4.5 (A)) and a conductivity map (figure 4.4 (B)) were obtained. The current map demonstrated that the current was below 5 pA (which is the noise level of the current measuring circuit) at the positions where the peptide particles were located on the topography map. This fact indicated that the particles were nonconducting, as expected for these types of biological nanostructures.

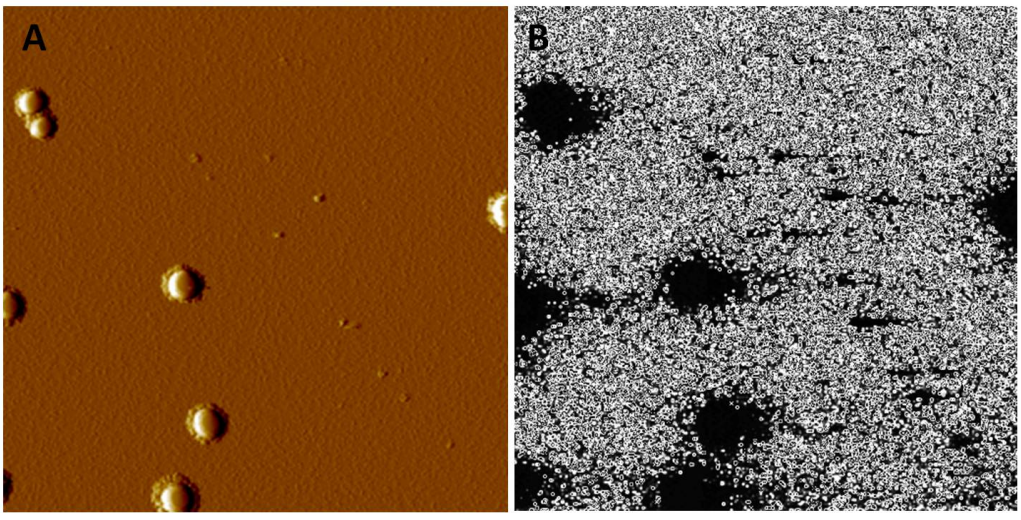

Figure 4.5: *AFM imaging and electrical conductivity measurements of Boc-Phe-Phe-OH nanoparticles on a gold substrate. A: Topography map B: Current map (the black parts indicate ¡ 5 pA current).*

4.3.4 Stability in Liquids

It has been suggested that nanostructures fabricated using the FF peptide and their analogs could play a key role in bionanotechnological applications[75,82] because of their particular properties such as facile synthesis under mild conditions, easy chemical decoration, and non-toxicity for certain cell lines. One of the proposed applications involves using the nanoparticles as cargo vehicles for drug-delivery purposes. The requirement for such an application is that the biological structure is stable in water-based solutions in order to deliver the drug compound to the desired location.[77,82]
Additionally, certain manipulation methods, such as sorting, dielectrophoresis, and microfluidic applications also require the immersion of the particles in liquids.[79,111,112]
Previous studies have dealt with the solubility of FF nanotubes and nanofibers in organic solvents and buffers.[71,113] It was found that while FF nanofibers could withstand the immersion into various solutions without structural changes, FF nanotubes were rapidly dissolved. In order to evaluate the stability of our Boc- Phe-Phe-OH particles in water-based solutions and in organic solvents, we thus carried out a similar investigation.
As described in the experimental section, Boc-Phe-Phe-OH particles were immersed in water, phosphate buffer, acetone and ethanol and aliquots of these solutions were taken at different times: 1, 5, 10, 15, 30, 60, 120, 180, and 240 min. These aliquots were then measured using HPLC-MS in order to determine the concentration of the peptide in the solution. If the Boc-Phe-Phe-OH particles were soluble at these solutions, the height of the corresponding peaks in the chromatographic analysis should increase with the immersion time.
From this analysis, it was found that the Boc-Phe-Phe-OH particles dissolved within one min after being immersed into the solutions. Figure 5 shows the chromatographic results for the solubility of Boc-Phe-Phe-OH particles in water for different immersion times. The peak corresponding to the Boc-Phe-Phe-OH peptide appeared already after immersion for one minute, and then slightly increased until saturation. Similar results were obtained with phosphate buffer, ethanol and acetone (data not shown). This indicates that these types of biological nanoparticles need to be modified in order to improve their stability in solvents.
Even though our results suggest that Boc-Phe-Phe-OH nanoparticles cannot be used as reinforcement in applications where they will be in contact with organic solvents, the properties of these structures could open new possibilities in applications such as check-valves in lab-on-chip systems by tuning their solubility in liquids. This way, the peptide nanoparticles will dissolve slowly and will allow the liquid to pass between two reservoirs once it is completely dissolved. Such a change in solubility has already been demonstrated in the case of diphenylalanine self-assembled peptide nanotubes by altering the synthesis parameters.[71]

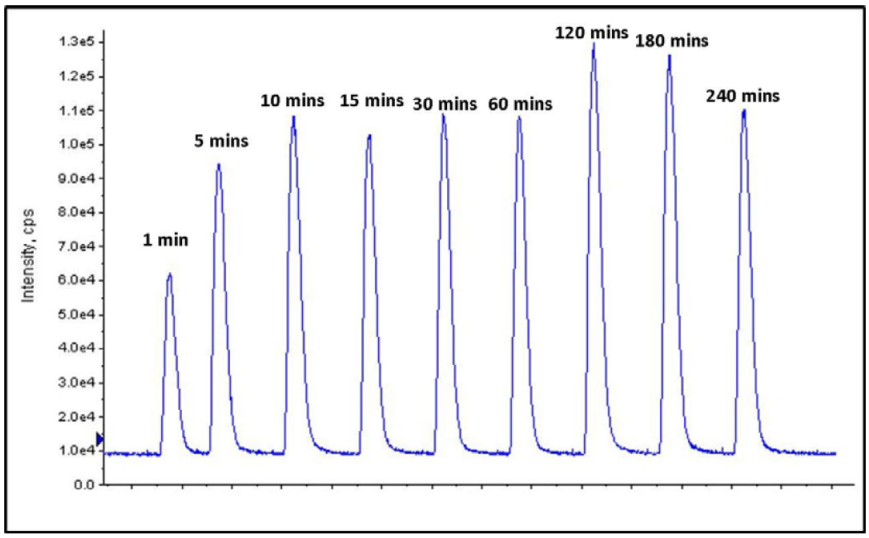

Figure 4.6: *A representative HPLC/MS measurement performed to assess the solubility of Boc-Phe- Phe-OH particles in water. The horizontal axis shows the actual time of the measurement, and not the immersion time. The immersion times are indicated at the peak tops.*

4.4 Conclusion

This article has described the structural and electrical characterization of Boc-Phe- Phe-OH peptide nanoparticles and their stability in organic solvents. The obtained results indicate that Boc-Phe-Phe-OH particles are nonconductive, solid structures that rapidly dissolve in solutions such as water, phosphate buffer and ethanol. Additionally, the Young modulus of these peptide nanoparticles was found to be between 20 and 30 MPa (as measured by AFM). This is approximately 10,000 times lower than the previously reported value.[78]

Chapter 5

Sandwich Assay Analyser

This chapter focusses on designing a lab-on-a-chip system for determining the concentration of Aβ. A possible design is a microsystem consisting of a sortingchamber and a subsequent electrochemical coulter counter. Due to the complications of handling Aβ_{42} it was chosen to test this design using Aβ_{40} as it is less sticky and less likely to fibrillate. Polystyrene beads are coated by antibodies for Aβ_{40} which then will bind specifically to the peptide. The beads are then sent through the sorting chamber; a long channel coated by another type of antibody for Aβ_{40}. The two different kinds of antibodies used during this project both bind specifically to Aβ_{40}: β Amyloid, 17-24 (4G8) Monoclonal Antibody, Purified (4G8) and Beta Amyloid, 1-16 (6E10) Monoclonal Antibody, from now on called 4G8 and 6E10, respectively. The double specificity of antibodies increases the credibility of the system considering the detection of the right peptide; Aβ_{40}. Initially the beads labeled with 6E10 is mixed with the cerebrospinal fluid (CSF) leaving the Aβ_{40} monomer to bind to the antibodies on the beads. This will leave a number of beads with and without attached Aβ_{40}. The sample fluid with the beads are then injected into the Lap-on-a-chip system. The beads with attached Aβ_{40} can bind to the channel surface labeled with 4G8 leaving the beads without A$\beta$to pass through. The beads without Aβ_{40} will be counted in a coulter counter. The coulter counter is based on Electrochemical Impedance Spectroscopy (EIS) between two measuring electrodes and an exciting electrode. When a bead passes between the electrodes it perturbs the electrical field and changes the impedance between the electrodes. From knowing the starting concentration of beads and measuring the concentration after the sorting channel it is possible to find the number of beads bound in the channel which in turn can be related to the Aβ_{40} concentration. The electrodes will ideally be fabricated in PEDOT:TsO. This work however focusses more on a prototype for a prove of concept. This means that platinum electrodes were chosen as they are better characterized.

Initially the sorting will be done at steady state, leaving the beads time to sediment and bind in the channel before flushing the unbound beads through the coulter counter. However, for future work it is of interest to do the sorting at a continuous flow rate. At this point the system is designed to only measure the bead concentration after the sorting

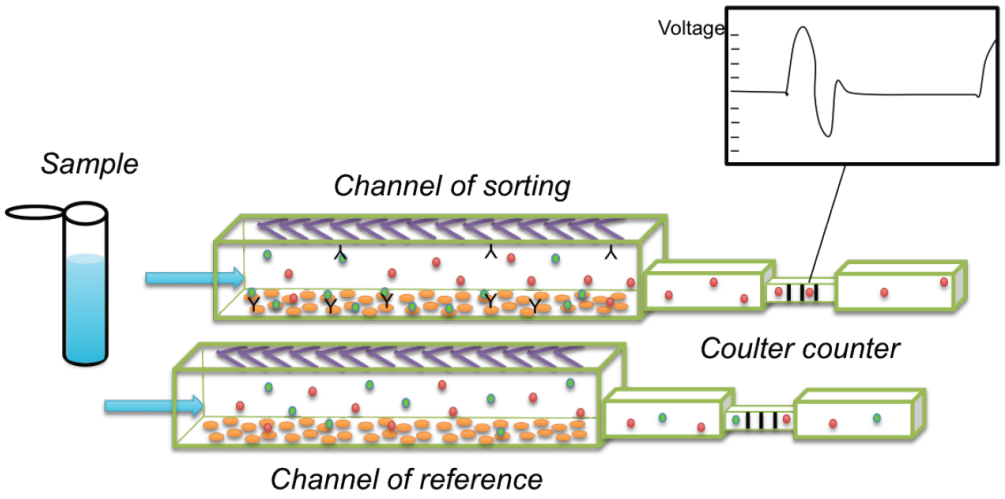

Figure 5.1: *An illustration of the entire lab-on-a-chip system. It is a dual channel system with sorting channel and a control channel both connecting to an EIS based coulter counter.*

channel as the initial concentration can be controlled. However, to minimize the error of beads getting lost during the injection it might be of interest to have two coulter counters; one before the sorting chamber and one after. There is a risk that an amount of beads without Aβ_{40} will stick in the sorting channel due to sedimentation or adsorption of the antibody coating to the channel surface. To remove this effect it would be important to have a dual channel system where the other channel is un-coated as control. An illustration of the whole lab-on-a-chip system can be seen in figure 5.1

5.1 Impedance System

5.1.1 System Model without Bead

The impedance system used as coulter counter is essentially measuring the impedance in a channel between two electrodes. The impedance changes with the presence of a bead which alters the conductivity between the electrodes.
The proposed electrical circuit of the system without a bead present is illustrated in figure 5.2. In the interface between the electrolyte and electrodes there is an electrical double layer of charges with opposite polarities. This stems from the ions just inside the electrodes and the ions of opposite charge in the electrolyte. This double layer gives rice to a capacitance at the surface known as a double layer capacitance C_{dl}. The electrolyte between the two electrodes is modeled as an capacitor C_m and a resistor C_m in parallel. The parasitic capacitance represents the dielectric property of the channel wall in relation to the two electrodes.[114] The double layer capacitance can be calculated by:

$$C_{dl} = \frac{A\epsilon}{\lambda_D} \tag{5.1}$$

where A is the area of the electrode, ϵ is the dielectric constant of the electrolyte and λ_D is the Debye length. The capacitance C_m and resistor R_m of the electrolyte is given by:

$$C_m = \frac{\epsilon A}{L} \tag{5.2}$$

$$R_m = \frac{L}{\sigma h w} \tag{5.3}$$

where L is the distance spanning from the start of one electrode to the end of the second electrode, σ is the conductivity of the electrolyte, h and w is the height and width of the channel. The total impedance of the system can be obtained from:

$$Z_1 = \left(\left((\frac{1}{R_m} + j\omega C_m)^{-1} + \frac{2}{j\omega C_{dl}} \right)^{-1} + j\omega C_p \right)^{-1} \tag{5.4}$$

To design an optimized system it is necessary to maximize the contribution stemming from R_m and C_m. Figure 5.3 shows a bode plot of Z_1 plotted against the frequency $F = \omega/2\pi$. For plotting following values were chosen; $w = 30\mu$m, $h = 30\mu$m, $L = 25\mu$m, $A = 300\mu$m, $C_{dl} = 354$ pF, $R_m = 20.8$ kΩ, $C_m = 7.08$ fF and $C_p = 1$ pF. C_p is estimated as being equivalent to previously published data.[114] By changing the parameters it can be observed how the impedance changes in relation to the frequency. For example, if the width of the electrodes is halved, then C_{dl} is halved and influence the impedance only at the lower frequencies as shown by the green dotted line. From figure 5.3 it is clear the the region between the two vertical lines are dominated by $R - m$ as there is no frequency dependence. This is the expected frequency range in which to measure to optimize the system fully.

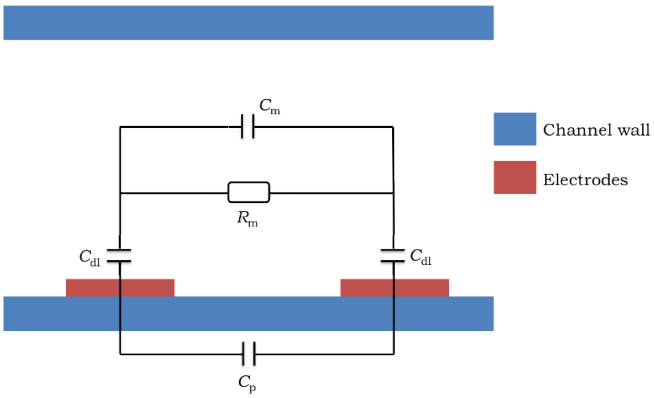

Figure 5.2: *The equivalent circuit model of the liquid filled channel without a bead. The total impedance is found from the double layer capacitance C_{dl}, that originates from the electrical double layer formed at the electrode/electrolyte interface, the medium which is modelled as a capacitor C_m and a resistor R_m in parallel and a parasitic capacitance C_p.*

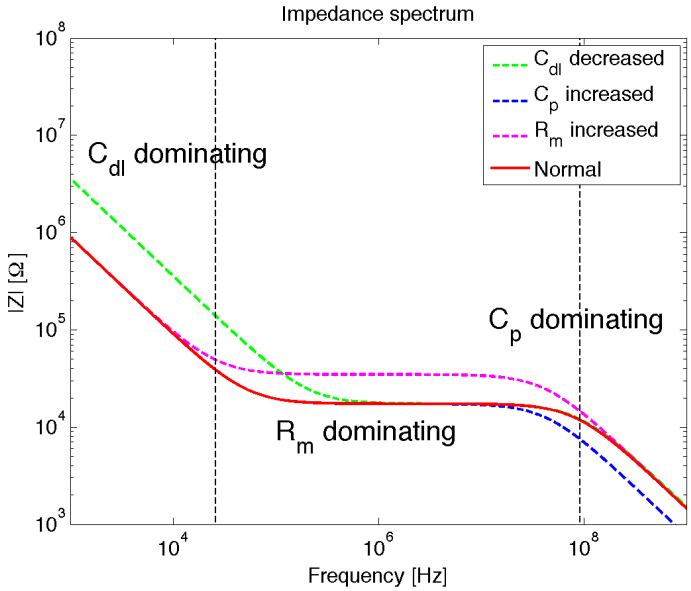

Figure 5.3: *Simulation of impedance spectrum showing the magnitude of the impedance $|Z_1|$ as function of the frequency on a double logarithmic plot. The solid red line shows the response for $w = 30\mu m$, $h = 30\mu m$, $L = 25\mu m$, $A = 300\mu m^2$, $C_{dl} = 354pF$, $R_m = 20.8k\Omega$, $C_m = 7.08fF$ and $C_p = 1pF$ The other curves shows how changing specific parameters will influence impedance at certain frequencies.*

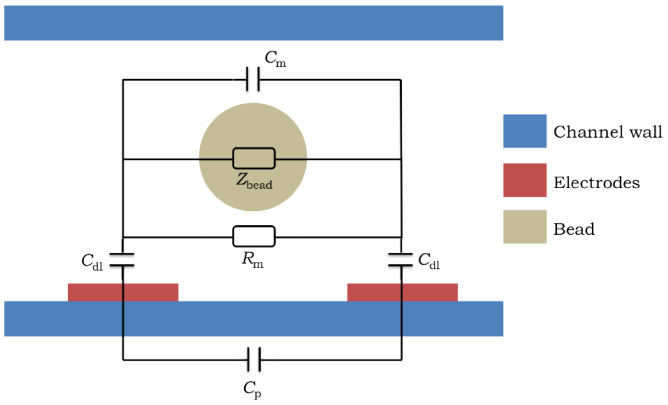

Figure 5.4: *The equivalent circuit model of the liquid filled channel with a bead. The total through the electrolyte is modeled as R_m, C_m and Z_{bead} in parallel.*

5.1.2 System Model with Bead

By introducing a bead in between the two electrodes it is necessary to include the beads contribution to the total impedance between the electrodes. The impedance of the bead is denoted Z_{bead} . The new equivalent circuit is illustrated in figure 5.4. Z_{bead} is in parallel with R_m and C_m. This means that the expression for the total impedance Z_2 can be written as:

$$Z_2 = \left(\left((\frac{1}{R_m} + j\omega C_m + \frac{1}{Z_{bead}})^{-1} + \frac{2}{j\omega C_{dl}} \right)^{-1} + j\omega C_p \right)^{-1} \tag{5.5}$$

5.1.3 Setup and Signal

The chip design used in work utilizes a set of three co-planar electrodes. This creates a non-uniform electrical field across the microfluidic channel, see figure 5.5 (A). The electrical field lines are depicted between the exciting electrode (black) and the two measuring electrodes (grey). The voltage drop between the electrodes are denoted V_1 and V_2. A bead that moves through the channel from left to right will perturb the field lines and give rise to a change in the total impedance. The system measures a voltage differential $V_d = V_1 - V_2$. The transition of the bead is illustrated at different positions labeled from $a - e$. In figure 5.5 (B) an equivalent output is sketched. At position a the bead has not yet perturbed the field lines and hence no change in V_1 i observed. At position b the bead is located between the measuring electrode and exciting electrode giving rise to the maximum change of V_1. This gives a high positive voltage differential. As the bead moves over the exciting electrode (c) it perturbs an equal amount of field lines to each measuring electrode thereby making $V_1 = V_2$ resulting in no differential voltage. The situation at d is equal to b but with an opposite sign giving a high negative voltage differential. At e the bead has move over the second measuring electrode thereby not ginving rise to any potential change.
The vertical position of the bead in the microfluidic channel influences the signal amplitude. The system response to a bead passing through the channel close to the electrodes will be larger in magnitude and thereby easier to detect and distinguish from noise, than a bead in the uppermost part of the channel.

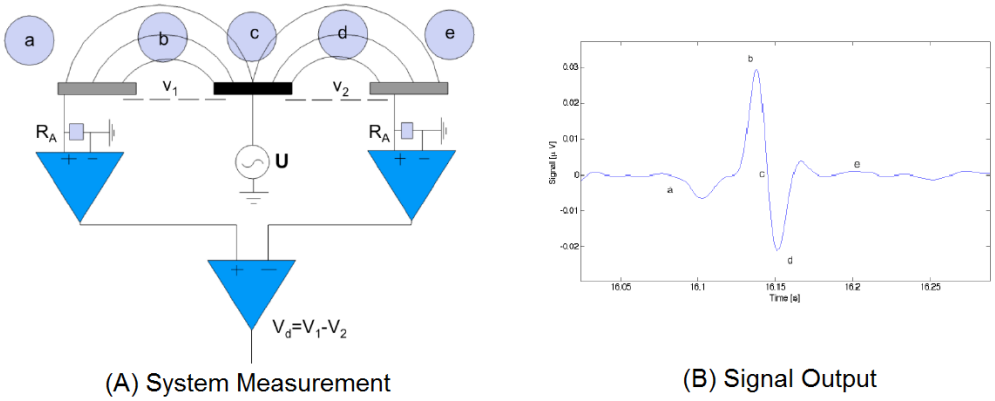

Figure 5.5: *The bead pertubs the electrical field lines and creates changes in the output signal. (A) System with three electrodes, one exciting (black), two measuring electrodes (grey) and the field lines in-between these. The voltage drops between the exciting and the measuring electrodes are denoted V_1 and V_2, and change depending on the bead position (a, b, c, d and e). The differential voltage drop is Vd. (B) The signal output V_d with the corresponding bead positions.*

5.1.4 Design and Fabrication

The chip system consists of a two mask design; a mask for the microfluidic channel and a mask for the electrodes. The design is made with three different channel widths and electrode widths to further optimize the design. The masks are designed to fit on a 4" wafer.

The channel design consists of two small chamber, with a diameter of 100 μm, used for inlet and outlet connections. These are connected by a 80 μm straight channel with a constriction of either 20 μm, 25 μm or 30 μm (the size of the constriction is denoted on the chip).

The electrodes is designed to have 8 interdigitated electrode crossing the channel at the constriction. In this work it is only intended to use 3 electrode, the extra electrodes however are practical in case of fabrication errors results in one or two electrodes not working. The extra electrodes could also be used to ground the system further if found necessary. The electrodes are designed with different widths of 5 μm, 10 μm and 15 μm all with an inter-electrode distance of 10 μm.

The chip consists of two parts which are later bonded together. The first part contains the microfluidic channel and the other part contains the electrode layout. The part containing the microfluidic channel is fabricated by hot embossing a polymer foil using a silicon master. The part containing the electrodes are made with standard photolithography.

The two parts are fabricated on Topas® (grade 5013, Topas Advanced Polymers) substrates of thicknesses of 0.3 mm and 2 mm. The silicon master is fabricated using standard photolithography and deep reactive ion etching (DRIE). The silicon master was used for hot embossing in the 2 mm thick Topas® at a temperature of 155° C and a force of 10 kN

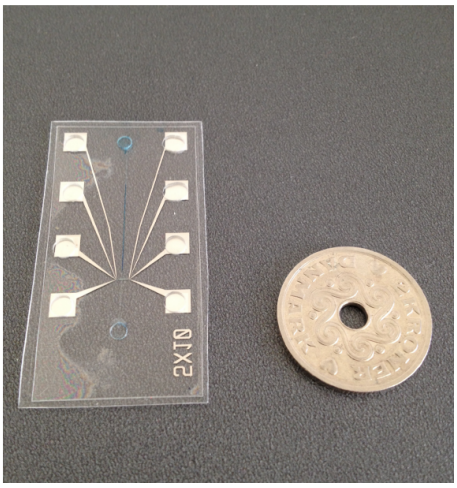

Figure 5.6: *Image of a final chip with platinum electrodes*

for a duration of 10 min.
The electrodes were fabricated on the thin 0.3 mm Topas® foil using photolithography and lift-off technique to add a 90 nm platinum layer with a 10 nm titanium layer for better adhesion. The rigid nature of the metals makes it important to avoid flexing the Topas® foil before bonding it to the thicker and more rigid 2 mm Topas® as this will make the electrodes delaminate.
The two parts were cleaned thoroughly in first ethanol and deionized (DI) water and then flooded with UV-light for 60 s. The bonding was made with a temperature of 125° C with a pressure of 5 kN for 10 min. A finished chip is depicted in figure 5.7. Further details on the fabrication can be found in appendix A.

5.1.5 Experimental Setup

To obtain a steady microfluidic flow the chip needs to be connected to a syringe pump. This is done through silicone tubing using pieces of polydimethylsiloxane (PDMS) as gaskets and clamping the whole thing between two plates of poly(methyl methacrylate)(PMMA). This setup allows for the sample to flow freely through the chip without leakage. The electrodes are connected by attaching spring connectors (P25-0822, HARWIN) to the top part of the PMMA with glue. When the the whole system is clamped the spring connectors are pressing down onto the contact areas of the platinum electrodes on the chip thereby ensuring electrical connection. Figure 5.7 (A) and (B) illustrates the chip setup without the spring connecters.

To perform the impedance measurements the following materials and equipment was used:

- The bead sample solution consist 10^6 ml^{-1} 5 μm CALIBRE® CS polystyrene beads (Microbeads A/S) diluted in 1% Tween® 20 (Sigma-Aldrich) in PBS.

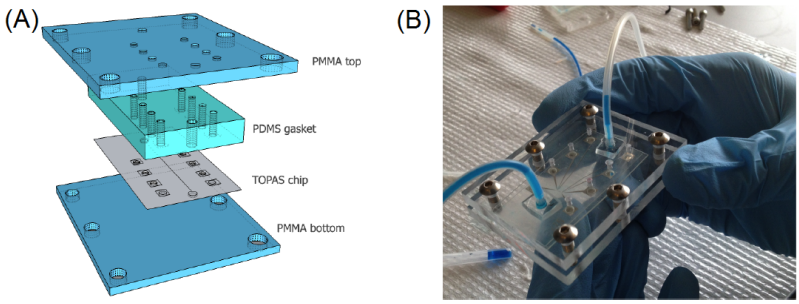

Figure 5.7: *(A) illustrates how the chip is clamped between two pieces of PMMA with a PDMS gasket. (B) shows an image of the device with a free flow of colored PBS.*

- NE1000 Single Syringe Pump.
- Syringe 1 ml (BD).
- HF2IS Impedance Spectroscope (Zürich Instruments).
- HF2CA Current Amplifier (Zürich Instruments).
- Microscope (Olympus-CKX31).
- Computer with Zürich Instruments proprietary software.

The sample was injected using the syringe pump to drive the fluidic flow. To reduce the noise from the power grid the needle on the syringe was grounded via the Impedance Spectroscope. The output AC signal from the impedance spectroscope was connected by a cable to one of the spring connectors of the chip. The signals measured by two of the chip electrodes were first pre-amplified by the current amplifier before being fed to the input terminals of the impedance spectroscope. The data acquisition was then performed by the computer and the data were available for processing in MATLAB. Experiments were performed next to a microscope which allowing optical inspection of the microfluidic channel to check for free bead passage and making sure that no clogging occurred.

5.1.6 Results

The results presented here was obtained on chips with an electrode design of a width of 5 μm and a inter-electrode distance of 10 μm. The microfluidic contraction was 30 μm wide with a channel height of 31.5 μm.

Initially the electrodes were characterized by measuring the impedance between two electrodes over a frequency sweep from 10 kHz to 30 MHz. In section 5.1.1 it was shown the the frequency should go as high as 90 MHz. The upper frequency was however limited by the equipment. The preamplifier used in this setup distorts the signal at higher frequencies. The frequency sweeps were done with PBS in the microfluidic channel (no beads or tween) and no flow. The amplitude spectrum is shown in a double logarithmic plot, figure

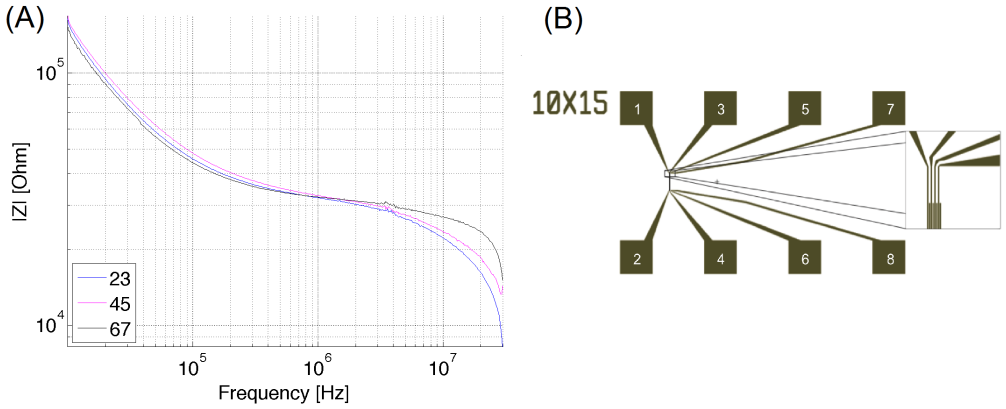

Figure 5.8: *(A) The amplitude spectra on a double logarithmic plot measured between consecutive electrode pairs. The profiles represents measurements between electrodes 2 and 3, 4 and 5, 6 and 7. (B) Shows the electrode numbering.*

5.8. Comparing this amplitude spectra to the simulated in section 5.1.1 there is seen a distortion in the signal at higher frequencies. At frequencies below 100 kHz it is seen that C_{dl} is dominating showing a high frequency dependence. The spectra is seen to flatten out with a more constant impedance between 100 kHz and 10 MHz. This fits with the expected range and is the frequency range of interest for detecting beads.

The bead sample measured by flowing the beads through the microfluidic channel at a flowrate of $\approx$1 μm/min. The resulting measurements were filtered with a 500 point moving average (MA) filter to remove a baseline drift in the system an a low pass filter with a cutoff frequency of 80 Hz. The result is seen for 1 MHz in figure 5.9 (A). There is observed a lot of peaks with both positive and negative amplitude. Each bead transition refers to a set of a positive and negative peak. This indicates that it is possible to count the number of beads flowing through the channel.

The number of beads were counted using a MATLAB script. The script detects local maximums and minimums above a certain threshold limit. If the threshold is set too high it will result in loosing sensitivity whereas a too low threshold could result in false positives. To remove outlying single peaks there was also set a threshold for the inter-peak time for giving a peak-set. This is illustrated in figure 5.10.

The systems ability to detect the right concentrations of beads in the liquid was investigated. The concentration of the bead solution was verified by using a Cell Counting chamber. In this experiment there was a concentration (C_0) of 2.83 beads ml^{-1}. Due to a large dead volume at the fluidic connections it was not possible to collect the fluid to find the equivalent volume of sample corresponding to the passing beads. Instead the volume was calculated from the mean transition time of the beads. By measuring the time

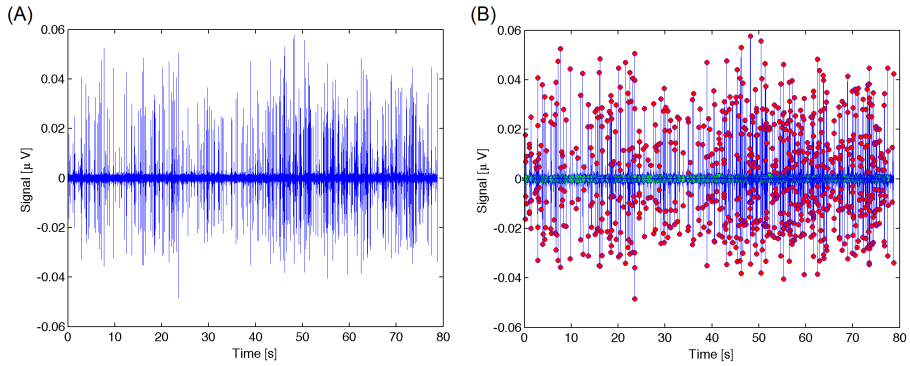

Figure 5.9: *(A) Filtered signal using a 500 point MA filter and an LP filter with cutoff frequency at 80 Hz. (B) The bead detected signal with red markings for each positive an negative peak and green markings that outline the transition of each of them.*

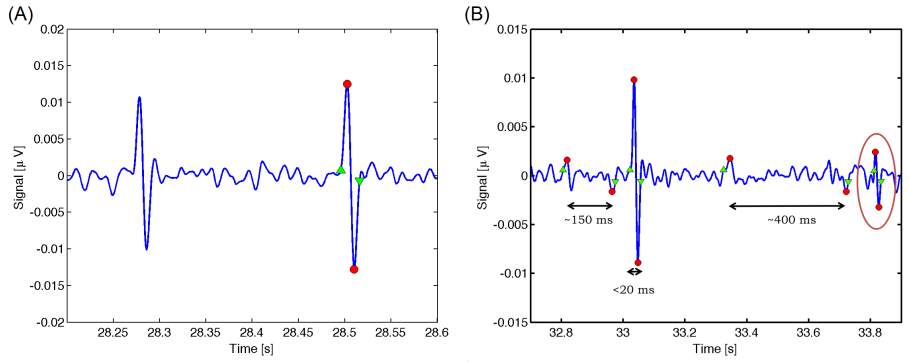

Figure 5.10: *(A) Signal where threshold-value is underestimated, resulting in undetected beads. This will eventually lead to a wrong concentration estimation. (B) Signal with overestimated threshold.*

between a beads passage of the first and second measuring electrode it is possible to find the mean velocity of the beads. For a particle less than 10 mm in diameter moving under the influence of a force F can be considered to always move at the terminal velocity of the fluid.[115] From this and the parameters of the microfluidic channel is is possible to calculate the flowrate of the fluid and concentration of beads (C_N). Measuring a concentration (C_N) of $2.74{\cdot}10^6$ beads ml^{-1} gave a concentration accuracy of 97.2% compared to original concentration C_0.

5.2 Sorting Channel

The sorting channel tested in these experiments is 100 μm wide with a height of 20 μm fabricated by micromilling. In these experiments the injected beads is allowed to sediment and bind to the channel surface. This means that the channel parameters are not of importance to the sorting. In future work the sorting is supposed be continuous. here the channel design comes into place. In a laminar flow the beads in the middle of the flow will not "see" the surface and the coated antibodies and hence not effected by the sorting channel. To make sure for all the beads to come into contact with coated antibodies it is necessary to introduce a mixing of the flow. This could be done by fabricating a herringbone mixer in the channel. The mixing effects of a herringbone mixer has previously been documented.[116,117]

5.2.1 Bio Functionalization

The prerequisites for making this sandwich assay is there is found a way to functionalize the channel and the beads with the respective antibodies. The anti bodies used in this work is 4G8 and 6E10 (Covance). The 4G8 was a pure antibody whereas the 6E10 was acquired as two types one with an Alexa Fluor® 488 label for visualization and one with a Biotin label for functionalization purposes.

To test if the sorting functions as expected it would be of great interest to have beads functionalized with antibody labeled with one fluorescence and beads with no antibody coated with another. This would allow for quantifying the number of beads being bound in the channel due to the double assay. The beads are functionalized using a streptavidin-biotin interaction. Streptavidin-coupled beads are widely used in connection with isolation of biomolecules.[118] The protein streptavidin usually exists in a tetrameric structure with four binding sites for biotin. The non-covalent interaction is very strong, approaching the strength of covalent bonds,.[118] Because of this, a biotinylated ligand will easily be bound to the streptavidin-coupled beads. The optimal combination would therefor be to purchase beads with both streptavidin and a fluorescent label or antibodies with both a biotin and fluorescent label. However, these were not available in this project, which led to the decision to simultaneously bind a fluorescent labeled biotin and the biotinylated antibody to the beads. Biotin is a relatively small molecule with a molecular weight of $\approx$244 Da whereas the antibodies are much larger with a size of $\approx$150 kDa. This means the diffusion rate of biotin is much higher than that of the antibodies. Thus is mixed with the streptavidin coated beads 1:1 the biotin would quickly uptake all the free binding sites. The experiments carried out here showed that mixing a low concentration of biotin, matching $\approx$ 25% of the available binding sites, labeled the beads while leaving free sites for the antibodies.

The binding of antibodies to the channel (Topas®) surface could not be done using the biotin-streptavidin interaction. It was considered to use simple adsorption of antibodies to the surface. Antibodies have shown to adsorb easily to polymer surfaces.[119] The intended

Solution	pre-wash	post-wash	Intensity change
6E10+Bz	46.4 (a.u.)	47.8 (a.u.)	-3%
Bz	26.9	26.7	0%
6E10	112	82.9	26%

flow in the channels would however increase the risk of removing the adsorbed antibodies again. Especially once they bind to the beads, through the A$\beta$and other antibody, due to the increased drag force. The persistence of covalent bonds is much higher than the van der Waals and hydrogen-bonds made during adsorption. To attain covalent bonds between antibodies and TOPAS, photo immobilization is used. Here, benzophenone (Bz) is used as an intermediary reactant since Bz activates the creation of covalent bonds when exposed to UV illumination.[119] The binding was tested by placing a range of Topas®pieces inside individual well in a microwell plate. The pieces are then covered with 1 ml of the following solutions:

- 0.02 mg/ml 6E10 Alexa Fluor® 488 label and 0.1 mg/ml Bz in PBS
- 0.1 mg/ml Bz in PBS
- 0.02 mg/ml 6E10 Alexa Fluor® 488 label in PBS

The covered pieces are then UV-exposed for 30 min to perform the photo immobilization. Then the intensity of the of the Alexa Fluor® is measured using a platereader. The Topas®pieces are then washed with Triton-X 100 and PBS to remove unbound antibody and re-measured in the platereader. The measured intensities can be seen in The experiment shows that when photo linking the antibody through Bz there is no significant change to the intensity. This means that there is the same amount of antibody present on the surface both before and after the wash. The negative controls shows that the purely adsorbed antibody can be washed of as the intensity is reduced 26%. This indicates that the Bz helps covalently bind the antibodies to the Topas®surface.

5.2.2 Bead Sorting

Due to the time constrains involved with this project experimental sorting of beads were held to very few tries. This section shows a positive experiment indicating that the sorting could work.
A microfluidic channel with a width of 100 μm and a height of 30 μm was fabricated in a piece of Topas®using micro milling. The channel was then closed by bonding another piece of Topas®on top using thermal bonding. The channel was connected to a syringe pump in the same way as described in sec. 5.1.5 to drive a fluidic flow.
The next step is to send beads with and without an Aβ40-coating into a 4G8 antibody-coated channel and observe possible differences - i.e. mix antibody 6E10- and Biotin 565-coated beads with antibody 6E10-, Aβ40 and Biotin 488-coated beads. The Aβ40-coated beads are expected to stay attached to the surface for significantly higher flow rates as opposed to the beads without Aβ_{40}.

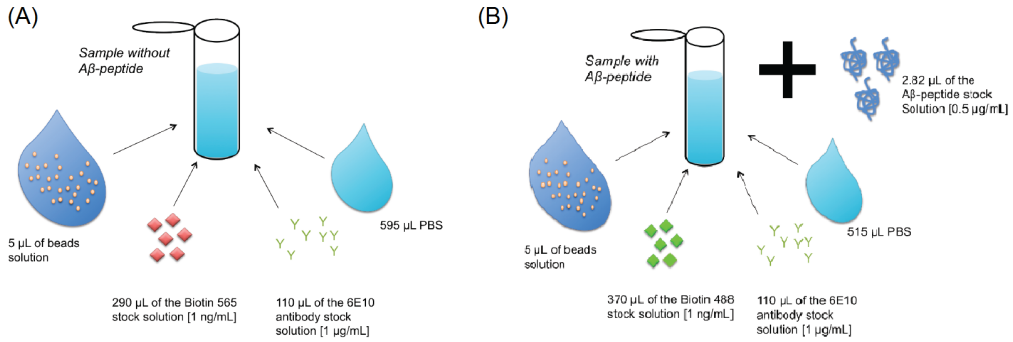

Figure 5.11: *The method of coating the beads is illustrated and the used concentrations are shown. In (A) the beads are incubated with only Biotin 565 and antibody 6E10. In (B) the beads are incubated with initially Biotin 488 and antibody 6E10, and then with the target peptide, $A\beta_{40}$.*

Two bead samples are prepared: One with Biotin 565, and one with Biotin 488 and $A\beta_{40}$. 5 μL of bead solution is added in both mixtures of 1 mL. Figure 5.11 shows the content of the two samples. In the The solution loaded into the channel consists of both $A\beta_{40}$-coated beads, beads without $A\beta_{40}$ and of PBS. The three substances are mixed in either the relation 1:1:1 or 1:1:2 in the mentioned order. This gives a total bead concentration of $1.2{\cdot}10^6$ beads/ml or $0.8{\cdot}10^6$ beads/mL respectively. The flow rate is initially set to 1-2 μL/min, but as soon as the solution of beads reaches the entrance of the channel, it is turned further down to 0.1-0.3 μl/min. The procedure of filling the tube and system with bead solution is done carefully without adding unnecessary pressure to the system. The volume of the solution added to the system is varied and generally reduced from trial to trial. Once the beads have been observed inside the channel, the system is set to rest for 45-60 minutes to let the beads sediment. The number of the respective beads are evaluated before and after the flushing process. The channel is flushed through with an increasing flow rate while observations are made of specific areas with both $A\beta_{40}$-coated beads (green fluorescent) and beads without $A\beta_{40}$ (red fluorescent).
Initially a segment of the channel was observed after sedimentation. Here there was observed 12 beads without $A\beta_{40}$ and 36 with $A\beta_{40}$. After flushing the channel there was observed 4 beads without $A\beta_{40}$ and 32 with $A\beta_{40}$. The fact that almost 90% of the beads with the target molecule $A\beta_{40}$ was left after flushing indicates that the sandwich assay immobilizes the beads.

5.3 Conclusion and Outlook

The goal of this work has been to design and test a prototype for a lab-on-a-chip system that can measure the concentration of Aβpeptide in CSF. This should be achieved through a sandwich assay sorting channel catching and immobilizing beads with the target

molecule. By counting the beads before and after the sorting channel it is possible to find the concentration of the target molecule, Aβ.
A three electrode chip system was designed to fabricate a prototype Lab-on-a-chip system for counting beads. It was shown that each individual bead correspond to a double peak of the impedance system. It was also shown was the coulter counter could measure the concentration of a bead solution with up to 97.2% accuracy.

A prototype for the sorting channel were also designed and fabricated during this project. It was successfully tried to biofunctionalize the Topas®surface and polystyrene beads with two different antibodies. An initial experiment with sorting between beads coated with antibodies and Aβ_{40} and beads without was promising. It is however clear that a lot more experiments would be needed for more conclusive evidence.

Chapter 6

PEDOT Nanowire Review

Since the original article on silicon nanowire demonstrating the potential of these new types of biosensors was published more than a decade ago[120] the field of silicon nanowires has received a lot of attention and many articles exploring this specific field have been published.[121–124] Nanowires offers very versatile and good assets for chemical and biological sensing. The main reson for this stems from the high surface to volume ratio.[125,126] Using silicon nanowires as biological field effect transistors (BIO-FET) has proven to be very sensitive towards a large range of biological targets e.g. proteins,[17,120,127] lipoproteins,[128] DNA[129] or virus.[125] The fabrication costs of the silicon nanowire devices remains the main challenge of fully exploring the nanowire devices as possible biosensors.[130] Recently conductive polymers have received a lot of attention across scientific and engineering disciplines due to their remarkable properties such as; light weight, low cost, ease of processing, transparency and scalable production. As a result conductive polymer nanowires have become prime candidates for replacing the conventional bulk semi-conducting materials for fabrication of nanowires.[131] Among the most common materials used for fabricating conducting polymer nanowires are Polyalinine, Polypyrole and PEDOT. As this work solely focusses on PEDOT we will take a closer look on the fabrication methods and utilities of PEDOT nanowires.
This chapter reviews the recently published advances in fabrication, characterization and possible applications of PEDOT nanowires.

6.1 Fabrication Methods

6.1.1 Maskless Electro Polymerization

Maskless electro polymerization has been showed to be a plausible path for making PEDOT nanowires.[132,133] Kannan and his colleagues[133,134] has recently had success using PEDOT nanowires as biosensors for detecting DNA. These nanowires were fabricated using maskless electro polymerization. By fabricating a set of triangular gold electrodes with sharp ends separated by 10 μm the electrical field between the anode and cathode is highly focussed in a small area. The PEDOT solution (10 mM 3,4,-ethlendioxythiophene (EDOT) $2{\cdot}10^{-4}$ 3,4-ethlendioxythiophene-yl-methoxy acetic acid

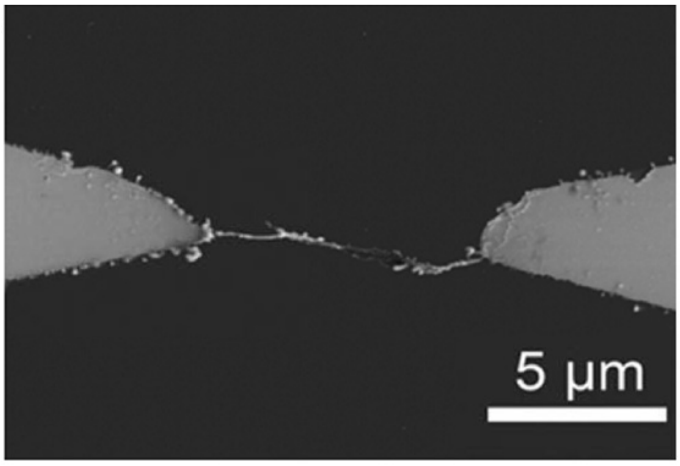

Figure 6.1: *ESEM image of a single CONW grown between the tips of wedge shaped gold electrodes on a glass substrate. Figure is modified from Kannan et al. 2012*[133]

(C2-EDOT-COOH), 1μM Poly(styrene sulfonic acid) (PSSA) and 0.1 mM $LiClO_4$ in acetonitrile (ACN)) was placed between the electrodes. By applying an AC electrical field with a peak to peak current of $\pm$7 V with a frequency of 35 kHz the polymerization was initiated along the electrical field lines. The potential was then slowly increased until the first signs of convection showed. The amplitude was then increased slowly a little further (0.2-0.5 V) until a black dot was observable. After a short pause of $\approx$ 2 s the amplitude was reduced to 0 V. A PEDOT nanowire is shown on figure 6.1.

6.1.2 Masked Electro Polymerization

Electro polymerization gives great possibilities for fabricating PEDOT nanowires. By using a mask or a template for fabricating the PEDOT nanowires it is possible to fabricate a large amount of uniform nanowires at low cost.[128,135–141] There has been two governing methods for masked electro polymerization; nanopore assisted polymerization and Lithographically patterned nanowire electroposition (LPNE). Suitable nano porous templates can be made or obtained by a variety of methods. Long and Duvail et al. has recently published a range of articles where they use track-etched polycarbonate membranes as templates[141135142143144] this approach has also been used by Carstens et al.[136] another template was suggested by Hangarter and his colleagues who has used a nanoporous alumina host[137138].[145] The fabrication method within these is very similar. Both approaches sputter a thin gold layer on one side of the template to function as a seed layer and working electrode, a platinum plate or electrode is in both cases used as counter electrode with saturated calomel electrode (SCE) as reference. By submerging the template into an EDOT solution and applying a fixed potential the nanopores are filled with polymerized PEDOT. The template is then etched away to obtain the wires. The fabrication process

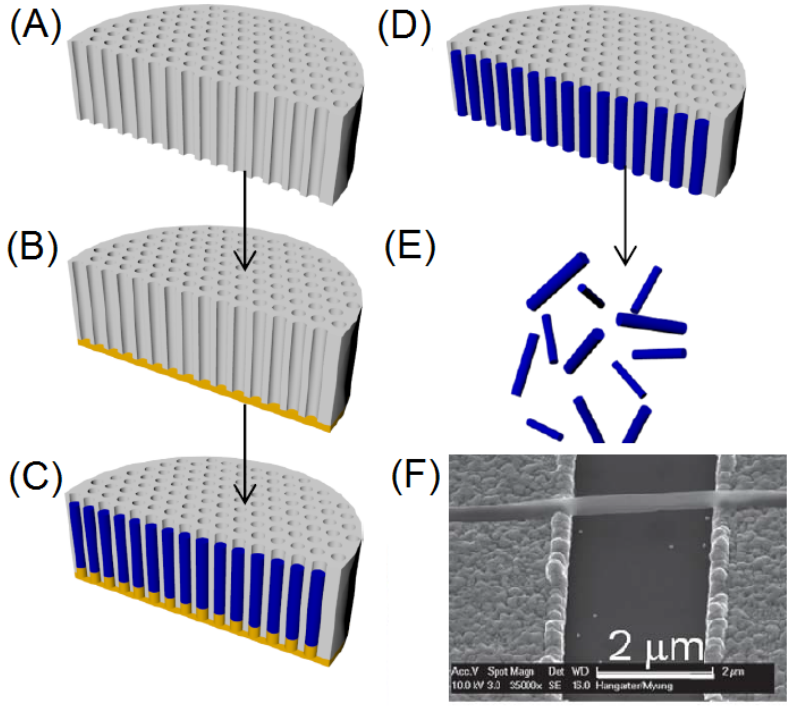

Figure 6.2: *Illustration of the fabrication process modified from Hangarter et al. 2011.*[138] *(A) Shows the nanoporous aluminium templater. (B) The gold seed layer is sputted onto the backside of the template, (C) followed by the electropolymerization of PEDOT. (D) The gold seed layer is removed by polishing and (E) the nanowires are released by etching of the template. (F) Shows a nanowire deposited between two gold electrodes.*

using aluminum template is illustrated in figure 6.2.

The masked electro polymerization provides an easy and reproducible fabrication of the wires themselves as the template defines the size. However, since the template is etched away after every fabrication the process is not low cost. Another issue is that the loose nanowires needs to be connected to macro scale electrodes. Hangarter et al. and Long and Duvail et al. are taking two different approaches to connecting the nanowires. Hangarter et al.[138] collect the nanowires and resuspend them in distilled water, washing them by centrifugation. The resuspended nanowire solution is placed on top of a set of opposing gold contact electrodes, fabricated by standard photolithography and lift-off techniques, using dielectrophoresis to align the nanowires between the electrode, see figure 6.2 (F). Long and Duvail et al.[135,141–143] takes a different approach. After etching the template away the nanowires are dispersed onto a SiO_2/Si wafer. Then platinum leads are attached to single PEDOT nanowires. A SEM is used to locate appropriate nanowires. then, the platinum leads are made using focussed ion beam deposition.

Taggart et al.[140] and Arter et al.[128139] have recently fabricated PEDOT nanowires using

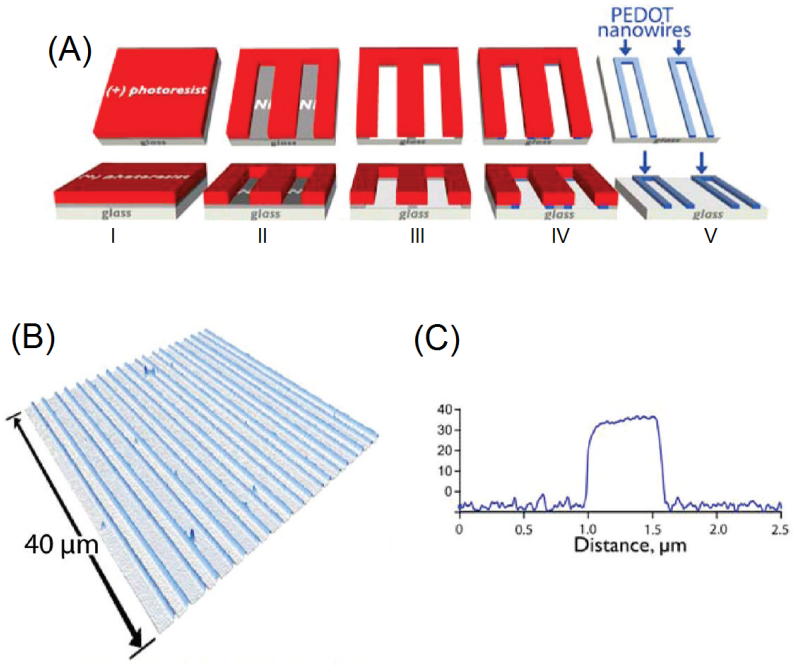

Figure 6.3: *Illustration of PEDOT nanowires made from LPNE. (A) shows the frabrication process. I) shows the nickel film covered with photoresist.(II) The photoresist is patterned by photolithography. (III) The exposed nickel is etched isotropic. (IV) the PEDOT is electro polymerized using the remaining nickel as working electrode. (VI) The remaining photoresist and nickel is stripped. (B) shows an AFM image of an array of 40 x 200 nm PEDOT nanowires on glass. (C) shows a high magnification AFM image of a single PEDOT nanowire. The figure is modified from Taggart et al. 2011* [140]

LPNE. The LPNE process involves a vapor deposition of a thin nickel film on a glass substrate. The thin film is then coated with a photoresist which is patterned into an array of straight lines using photolithography. The photoresist is used as an etch mask where the uncovered nickel is removed using oxidative degradation. The isotropic nature of the oxidation creates and under etch at the etches of the photoresist. This creates nano sized trenches. The nickel in the trench can be used a working electrode for electro polymerization in a three electrode cell with an aqueous solution of EDOT and $LiClO_4$. The resulting nanowires have cross-sectional dimensions determined by the time of the electro polymerization (width) and the height of the nickel layer (height) and lengths defined by the photolithographic process. The process is illustrated in figure 6.3.

6.1.3 Molecular Combing

Molecular combing was first developed by Bensimon et al. 1994.[146] The process was originally developed to stretch out DNA strands on a glass surface. Molecular combing is carried out by having DNA molecules attached at one end to a solid surface and then stretch them through a receding air-water interface leaving them to dry on the surface. In the original paper[146] a drop of the DNA solution is added onto a silanated cover slide (the silane anchors the DNA to the cover slide at the DNA's extremities) and covered with an untreated cover slide. When the solution between the two starts to evaporate the surface tension of the receding air-water interface drags stretches the DNA out. Since evaporation is not necessarily directional controlled another method using the same principles has been shown. By slowly retreating a silanated coverslide out of a solution containing DNA the same effect occurs.[147] Samitsu et al.[148] has used the method of molecular combing to fabricate PEDOT:PSS nanowire aligned across two platinum electrodes. The process is started by adding a small droplet of diluted PEDOT:PSS covering the gap between to parallel platinum electrodes. The droplet is subsequently sucked away, with a syringe al a very low speed, in the direction of one of the electrode. This effectively creates a moving air-solution interface which aligns the PEDOT:PSS nanowires.

6.1.4 DNA polymerization

In the past decade there has been huge advances in using DNA as motifs and templates for nanotechnology. There has recently been a development within the field of water-soluble cationic conductive polymer biosensors, where the polymer has been assembled onto oppositely charged biomolecules. Hamedi et al.[149] has utilized DNA as templates for fabricating PEDOT-S nanowires. PEDOT-S is a short water soluble polymer that is self-doped with $\approx 1/3$ of the sulfonate side groups acting as self-doping sites. The remaining sulfonate groups adds up to a net anionic charge with a bulk of the polymer having an intrinsic conductivity of 30 S/cm.[150] The group of Inganäs has previously proved that PEDOT-S can bind to oppositely charged amyloidprotein structures,[151] see figure 6.4 (A). The synthesis of PEDOT-S nanowires were done by diluting λDNA in milliQ-water and mixing it at a molar ratio of 1/2 with PEDOT:S in solution. The final solution was then incubated for two hours.[149] The nanowires were aligned over a set of electrodes using molecular combing leaving stretched out nanowires, see figure 6.4 (B).

6.1.5 Dip-Pen Nanolithography

Dip-Pen Nanolithography (DPN) is a direct writing alternative to the electro polymerization approaches, which often require lengthy steps before the polymerization can be condoned. The principle of DPN is using an AFM tip as a pen. The major advantage of DPN is that the dimensions of the resulting nanowires can easily be controlled by the size of the AFM tip, the dwell time and environmental parameters such as temperature and relative humidity. DPN offers a high flexibility of processes and fabrication procedures while eliminating the need for photolithography.[152] Lu et al. has recently fabricated PEDOT nanowires using DPN. PEDOT:PSS was used as an ink. A soft (0.016 Nm^{-1}) cantilever

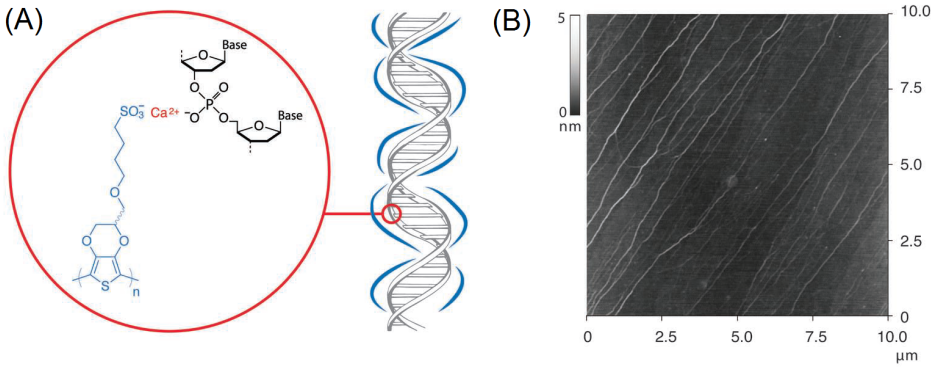

Figure 6.4: *(A) Schematic illustration of the PEDOT-S/DNA molecular self-assembly. (B) AFM topography image of the stretched out PEDOT-S/DNA nanowires. The figure has been modified from Hamedi et al. 2013.*[149]

was used for the AFM and the tip was dipped into the concentrated PEDOT:PSS solution for 30 to 40 s and dried gently using a nitrogen gas. By scanning the tip across the substrate surface a set of PEDOT:PSS nanowires can be directly written. In the case of Lu et al. an array of 64 PEDOT:PSS were written between two gold microelectrodes, which had been previously prepared by standard photolithography process.

6.2 Electrical Characterization

The current-voltage response (I-V) is the simplest technique to gauge the electrical properties of the PEDOT nanowires. A linear response indicate an ohmic resistance whereas a non-linear response indicate a semi-conductor Schotktky like behavior. Many of the groups who has presented the above fabrication techniques has also characterized the I-V response. Due to the different nanowire sizes, fabrication methods and doping agents it is difficult to compare the responses. This section will however try to give an overview of the electrical properties of the PEDOT nanowires.
The most widely used PEDOT in the literature is PEDOT:PSS. Kannan et al.[133] and Das et al.[132] fabricated very thin PEDOT:PSS nanowires using maskless electro polymerization, Samitsu et al.[148] mae similar sized nanowires using molecular combing, Hangarter et al.[137,138] and Long et. al[141,143] fabricated slightly larger nanowires using masked electro polymerization. They all characterized the PEDOT:PSS nanowires' I-V response. It was generally agreed that the nanowires at room temperature showed a linear ohmic response with a potential amplitude of ±200-600 mV, see an example in figure 6.5 (A). Lu et al.[153] and Das et al.[132] reports that at higher potentials the response shows a non-linear tendency. Das et al. 2006[132] describes that as the voltage increases the additional space charge is also injected and therefore, a transition from Ohmic to space charge limit behavior is observed.

PEDOT nanowires I-V characteristics has been reported to show a strong temperature

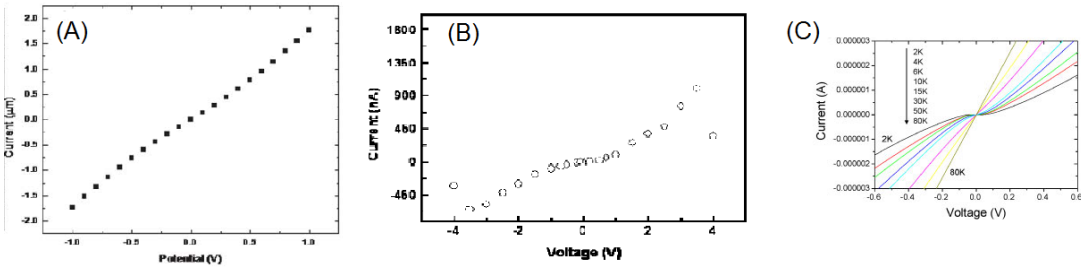

Figure 6.5: *(A)I-V response with a potential of ± 1 V. Modified from Hangarter et al. 2011.*[138] *(B) I-V response with a potential of ± 4 V. Modified from Das et al. 2006,*[132] *(C) I-V characteristics of PEDOT nanowires fabricated from masked electropolymerization. Modified from Long et al. 2008*[141]

dependence.[84,141,148,153] There is a clear tendency for all the different nanowires to have a linear ohmic response for applied voltages below 200 mV. Samitsu et al. 2005[148] reports that the conductivity of the PEDOT nanowire is reduced with reduced temperature. Both Samitsu et al. and Long et al. 2008[141] shows that the PEDOT nanowires exhibits a linear ohmic response around room temperature and becomes more non-linear as the temperature is decreased further. Figure 6.5 (C) shows the shift from linear I-V response to a non-linear I-V response from 80K down to 2K.

6.3 Applications of PEDOT nanowires

6.3.1 Label-free Gene Sensor

Kannan et al. 2012[133] has presented a maskless electro polymerized PEDOT nanowire as a highly sensitive, label-free gene sensor. single PEDOT nanowires were fabricated between gold electrodes followed by covalent attachment of amino-modified probe oligonucleotide (ODN). The nanowire was measured both in situ and ex situ. In the ex situ measurement the nanowire were performed by using two terminal device setup and the changes in the interface of the nanowire associated with the association or dissociation of ODNs were measured as change in resistance. The presence of the charged complementary ODN on the nanowire surface modulates the electrical properties of the nanowires specifically resistance. The results can be seen in figure 6.6. The results indicate that the ex situ measured resistance is directly related to the solution ODN concentration.

Kannan and his colleagues also measured in situ. These measurement were constructed using Scanning Ion Conductance Microscopy (SICM). A double barrel pipette (≈10 μm diameter) filled with PBS solution holds an Ag wire as a quasi-reference electrode and an Ag/AgCl wire as a counter electrode. This is placed right on top of the nanowire. The setup is illustrated in figure 6.7 (A). The resistance in the nanowire changes upon hybridization of the ODN can be seen in figure 6.6 (B). These results demonstrates the ability of PEDOT based nanowire devices can function as a highly sensitive sensor.

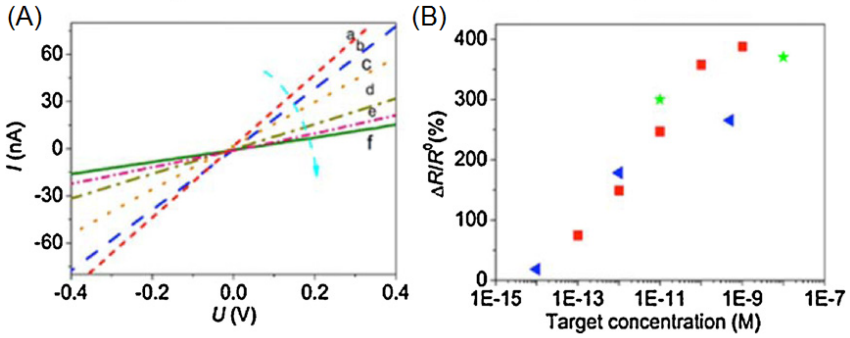

Figure 6.6: *(A) Overlay of I-V curves of probe-oligonucleotide modified nanowire after hybridization with increasing concentrations of the target sequence (a) 0 pM, (b) 0.1 pM, (c) 1 pM, (d) 10 pM, (e) 100 pM and (f) 1000 pM. The target hybridised probe modified copolymer nanowires were measured in the dry state after removal from the solution. (B) Normalised percentage change in the resistance as a function of target oligonucleotide concentration. The different colored and shaped data points correspond to different sets of sensor results obtained from different single nanowires. The figure is modified from Kannan et al. 2012*[133]

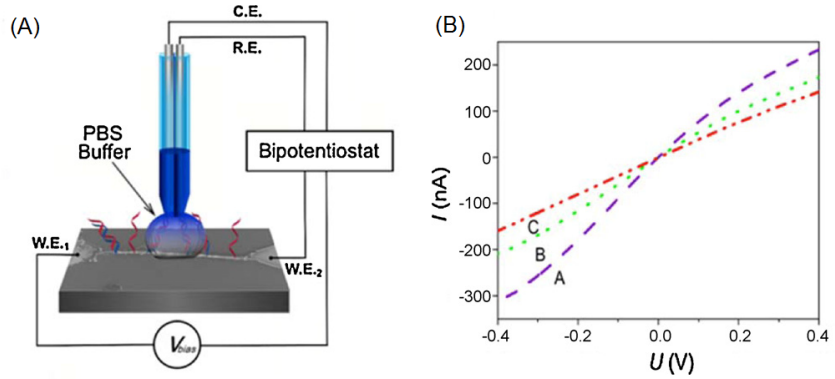

Figure 6.7: *(A) Experimental setup of SICM based Bio-FET. (B) Overlay of I-CV curves of ODN modified nanowire after hybridization with different (increasing) concentration of the complementary target ODN:* ***A*** *0.023 pM* ***B*** *0.5 pM and* ***C*** *33.3 pM. The length of CONWs used was ≈15 µm. The figure is modified from Kannan et al. 2012*[133]

6.3.2 Gas Sensor

PEDOT nanowires has been presented to be potentially very sensitive gas sensor.[131,138,153] Lu et al. 2009 demonstrates that PEDOT nanowire sensors has the potential to sense nitric oxide (NO) concentrations at a limit ≈10 ppm which would be above the current limit for practical environmental applications.[153] Figure 6.8 shows the measured I-V curves for 0 ppm, 50 ppm and 100 ppm NO gas over an bias voltage of 0 to -6 V. The current is increasing with an increased concentration of the NO. Lu et al. explains the

changes in the sensing mechanism by changes in the electron density upon the physical adsorption/desorption of gas molecules by the PEDOT.
Hangarter et al. investigated the sensing performance of PEDOT nanowires by analyzing changes in resistance upoon exposure to humidity and various volatile organic compound vapors (VOC); water, acetone, methanol, ethanol and methyl ethyl ketone (MEK). The analyte concentrations were reported at percentages of their respective saturation vapor pressures. exposure profiles for acetone, water, methanol and ethanol can be seen in figure 6.9.

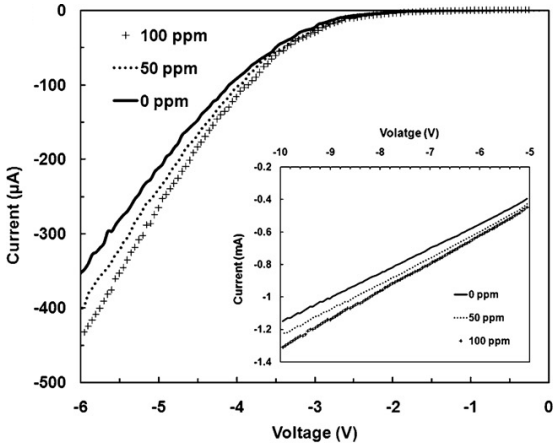

Figure 6.8: *Measured I-V curves for different concentrations of NO at 353 K with applied biases of 0 V to -6V with a gas flowrate of 250 mL/min. The insert extends the curve from -5 V to -10 V. The figure is modified from Lu et al. 2009*[153]

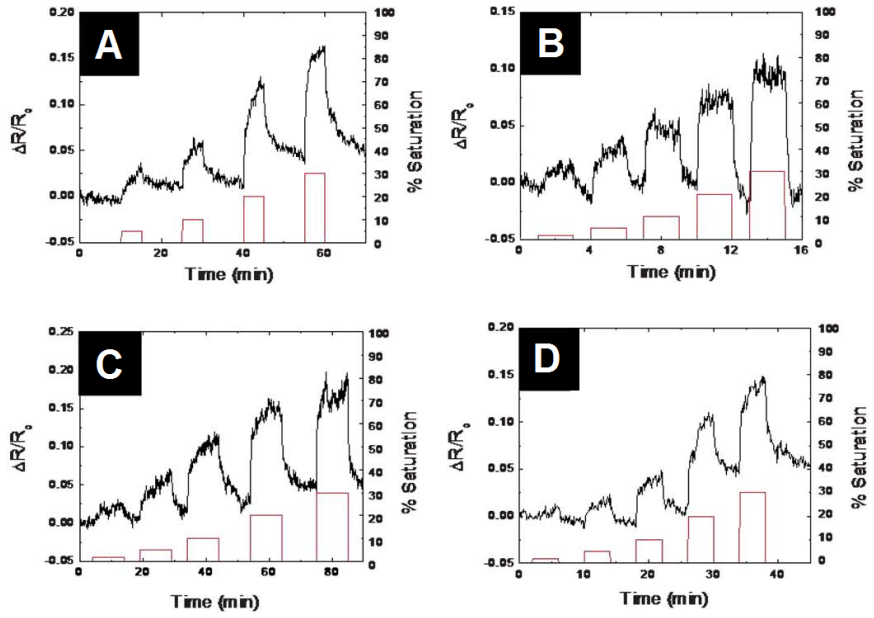

Figure 6.9: *Transient sensing profiles for PEDOT:PSS nanowires in response to* ***A*** *Acetone,* ***B*** *water,* ***C*** *Methanol and* ***D*** *Ethanol. The device resistance is normalized to* $\Delta R/R_0$ *(the black lines). The analyte concentration (red lines) is increased with each exposure and are reported in percent of their partial pressures. The figure is modified from Hangarter et al. 2011* [138]

6.3.3 Antigen Detection

Arter et al. have solved the biological molecular recognition challenge by incorporating a virus M13 into the PEDOT.[128] M13 is a bacteria-infecting virus that can recognize essentially any analyte by binding to engineered polypeptides on its surface.[128] The combination of virus and PEDOT offers chemical and biological selectivity to the nanowire, without requiring postsynthesis functionalization. This results in a label-free biosensing platform. The initial paper Arter et al. 2010 investigated the selectivity and sensitivity of the PEDOT/virus nanowires using positive and negative antibodies. This study observed a detection limit down to 20 nM of the positive antibody and no significant change to the negative antibodies. Recently a new work has been published demonstrating the detection of prostatespecific membrane antigen (PSMA).[139] The electrical resistance of an array of these nanowires increases linearly with the PSMA concentration from 20 to 120 nM in high ionic strength phosphate-buffered fluoride (PBF) buffer, yielding a limit of detection (LOD) for PSMA of 56 nM. Real time biosensing of the binding of PSMA to the nanowire can be seen in figure 6.10 (A). 6.10 (B) demonstrates a linear correlation between the normalized change in resistance ($\Delta R/R_0$) and the concentration of the added PSMA. PEDOT:virus nanowires bearing the PSMA-binding recognition motif showed specific binding to PSMA in synthetic urine, with sensitivity measurable for PSMA concentrations above 66 nM.

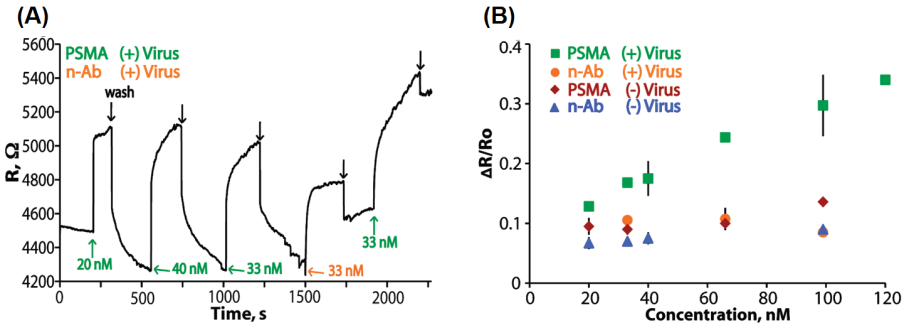

Figure 6.10: *Real-time biosensing with PSMA-binding PEDOT nanowires. (A) A real-time trace of biosensing data, with the indicated injections of negative antibody (n-Ab), PSMA, or washes with PBF buffer (black arrows). (B) A compilation of all real-time biosensing data, depicted as a calibration curve with error bars indicating standard deviation (n = 3). The change in resistance upon injection is plotted versus analyte concentration. The figure is added from Arter et al. 2012*[139]

Chapter 7

Fabrication of PEDOT Thin Films and PEDOT wires

PEDOT nanowires potential as biosensors were described in chapter 6. This chapter and chapter 8 investigates a possibility for a low cost and fast fabrication method for producing PEDOT nanowires.

As stated previously one of the main criteria for Lab-on-a-chip devices is cost effectiveness. This is one of the main agitators for using conductive polymer instead of more costly materials as metals and silicon. To keep costs low it's not only interesting to investigate low cost materials but also cost efficient methods for handling them. There has been suggested a range of different fabrication methods for producing PEDOT nanowires. We have chosen a simpler method for polymerization through chemical oxidation in liquid. This allows us to spin a polymer thin film on a desired substrate very easily.
After spinning on the PEDOT it is also necessary to pattern it. The traditional way of patterning the PEDOT is using reactive ion etching (RIE), which is very well characterized and gives a very precise transfer of the pattern to the PEDOT. In this chapter a cheaper and simpler method of patterning PEDOT thin films is tested. The patterning is a chemical wet etch controlled by containing the chemical inside an agarose stamp, which is placed on top of the PEDOT thin film.
The investigations into spinning of PEDOT thin film and patterning using agarose stamping are of generic interest to our group as we are working with a range of different PEDOT based transducers. However, the main focus of these experiments has been to investigate if it is possible to use this fabrication method for making PEDOT nano wires or Nano ribbons.

7.1 Materials and Methods

7.1.1 Spin Coating of PEDOT Thin Films

As written in section 2.3 PEDOT can be synthesized by either oxidative polymerization or electrochemical polymerization. To favor batch processes and keep costs low the former is used in this work.
The Polymer solution used to make the thin films was made by mixing 13ml Baytron C(40%Fe(III)tosylate) with 4ml butanol and 300μl pyridine. The solution was mixed thoroughly and kept at room temperature for 30min. The initial solution was then mixed thoroughly with 440 μl EDOT monomer (Baytron M). The final solution was then spin-coated onto the desired substrate. The parameters of the spin-coating can be varied for different thicknesses. However, in this chapter all films were made with an acceleration of 500rpm/s and a final duration of 30s with only a maximum speed. The final thickness is of the film depends on the centrifugal force of the spinning and the viscous resisting forces of the polymer solution.[154]
After spin-coating the substrate was placed on a hotplate at 70°C 15min thereby evaporating the pyridine and initializing the polymerization. After the heat treatment the substrates are gently flushed with Milli-Q water and dried using a nitrogen flow.

7.1.2 Patterning on PEDOT Thin Films

The silicon mold for stamp fabrication was manufactured using standard cleanroom silicon processing techniques and will not be explained in depth here. The stamp was fabricated from a 10 wt% agarose solution in Milli-Q water. The agarose was stirred into a liquid and heated to the boiling temperature using a microwave oven The procedure was repeated several times until the solution was transparent and free of bubbles. The liquid agarose were poured onto the silicon mold and heated to 70-80°C on a hotplate for 10min. A plastic cover was applied on top to minimize evaporation. The cast agarose solidified by placing it inside a fridge (5°C) for 15min.
The cast stamp was soaked for 5min. in 1 wt% NaOCl prepared by mixing 1.5 ml 10-15% NaOCl with 13.45 ml Milli-Q water and 150 μl 10% Triton X in Milli-Q water. The surface of the saturated stamp was dried off using a nitrogen flow. The PEDOT thin film was etch by placing the agarose stamp on top. To assure contact a light pressure is applied. After etching the over oxidized PEDOT is washed away using Milli-Q water. In certain cases The resulting PEDOT pattern was cleaned with 2% Tritton X in Milli-Q water, then rinsed with ethanol and Milli-Q water before being immersed in Dimethyl sulfoxide (DMSO) for 1 min followed by additional washing step of ethanol and Milli-Q water. If the extra washing step was used it will be mentioned explicitly. The patterning method is illustrated in figure 7.1.

7.1.3 Surface Probe Measurements

The sheet resistance of the PEDOT:TsO thin films were measured using 4-point probe measurements. A Keithley 2400 Sourcemeter with custom software was used with a 4-

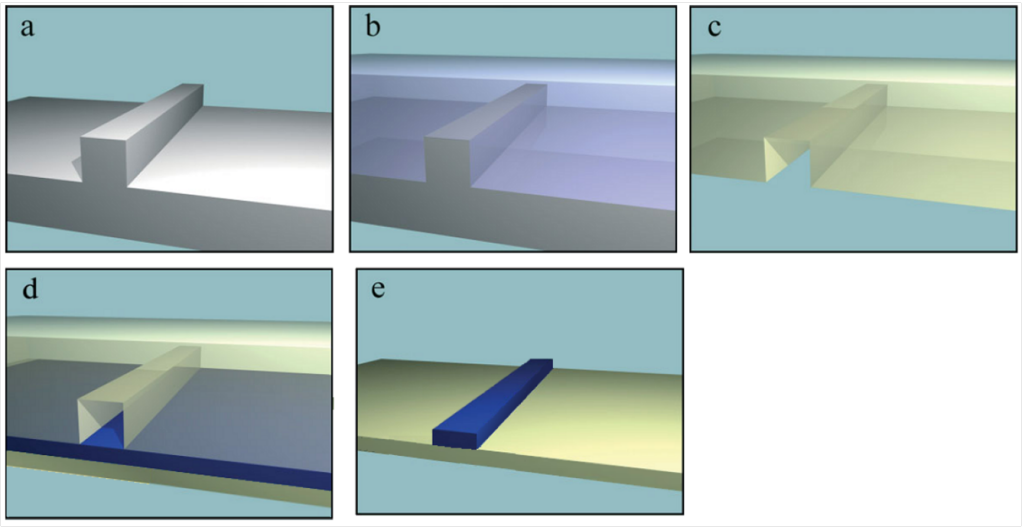

Figure 7.1: *Fabrication of an agarose stamp and patterning of PEDOT thin film. a) A structured silicon surface which can function as the agarose master. b) Melted agarose is added on top of the silicon master. The cast agarose is gently removed from the mold and immersed into NaOCl. d) The stamp is applied ontop of a PEDOT thin film, etching the PEDOT where it is in contact with the stamp. e) The stamp is removed and the substrate is washed with water leaving the patterned PEDOT. This figure is modified from Hansen et al. 2007*[155]

point probe with a spacing of 1 mm.
The thickness of the thin films were measured by either a profilomer (Dektak 8) or for more precise measurement Atomic Force Microscop (AFM) in tapping mode. The AFM used in this work was a XE-150 PSIA Advanced Scanning Probe Microscope. For Conductive AFM (C-AFM) a conductive Cr/Pt coated cantilever was inserted into the AFM, which was operated in contact mode. The PEDOT:TsO was connected in a closed circuit by contacting through a the AFM tip and an electrical wire connected to the substrate with conductive tape. A bias potential was applied over the sample and tip drawing an electrical current between the tip and sample.

7.2 Results and Discussion

7.2.1 Film Thickness

To minimize the volume and cross sectional area of the PEDOT nanowires it is necessary to control the height of the PEDOT thin films. In this work we have investigated the correlation of the height of the PEDOT with the spin rate when spin coating a substrate. We have done this for two different substrates; Silicon dioxide (SiO_2)and Topas®. The film thickness on Topas®was found using a Dektak 8 profilometer, while the film thickness on SiO_2 was measured using AFM (XE150, Park Systems, South Korea). It was found

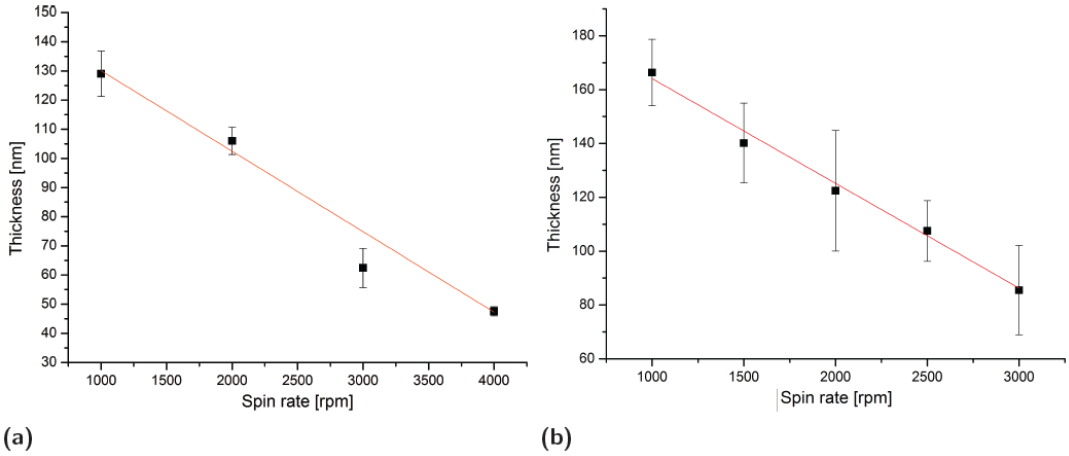

Figure 7.2: *The PEDOT:TsO thin film thickness is plotted against the spin rate on SiO_2 (a) and Topas® (b). It is observed that the film thickness is generally higher on Topas®*

that the thickness of the PEDOT film has a linear dependence to the spin rate for the range of 1000rpm-4000rpm, see figure 7.2. It is seen that the results between the two surfaces clearly differers. This is due to the different surface energy between SiO_2 and Topas®. The results are shown in figure 7.2. It is observed that the obtained film on SiO_2 in general were thinner than the on Topas®. This can be explained by the more hydrophilic properties of SiO_2 compared to Topas®causing a lower contact angle of the relatively polar reactive polymer. On figure 7.2 it is also observed that the standard deviations of thickness on SiO_2 are significantly lower than on Topas®. However, this can be attributed to both different instrumentation as well as the smoother surface of SiO_2 compared to the injection molded Topas®substrate.

7.2.2 Film Conductivity

The sheet resistance of the thin film were measured using four point probe measurements. The data recorded with the four point probe measurements had some large outliers and low currents. This stems from the contact resistance. To avoid this influence in the further data interpretation it was decided to use the median for all further use. The sheet resistance $\rho_\square$ is related to the film thickness d and the resistivity ρ.

$$\rho = \rho_\square \cdot d \tag{7.1}$$

The calculated resistivity can be seen in table 7.1. The difference between the two substrates can be explained by a slight difference in the preparation of the films. The PEDOT:TsO deposited on SiO_2 was filtered using a 0.2 μm syringe filter, whereas the PEDOT:TsO applied to the Topas®was unfiltered. This could mean that small impurities were incorporated into the films. This could create grains of nonconductive material in the film lowering the conductance. To test this statement it would be easy to fabricate a range

Table 7.1: Characterization of PEDOT:TsO film conductivity and thickness related to spin rate

Spin rate (rpm)	Thickness (nm)	SD (nm)	Resistivity (Ωm)	SD (Ωm)	Substrate
4000	48	2	$2.2{\cdot}10^{-5}$	$5{\cdot}10^{-6}$	SiO_2
3000	62	7	$2.5{\cdot}10^{-5}$	$4{\cdot}10^{-6}$	SiO_2
2000	106	5	$3.1{\cdot}10^{-5}$	$8{\cdot}10^{-6}$	SiO_2
1000	129	8	$1.8{\cdot}10^{-5}$	$1{\cdot}10^{-5}$	SiO_2
3000	86	17	$4.3{\cdot}10^{-5}$	$5{\cdot}10^{-6}$	Topas®
2500	108	11	$4.4{\cdot}10^{-5}$	$4{\cdot}10^{-6}$	Topas®
2000	122	22	$4.3{\cdot}10^{-5}$	$3{\cdot}10^{-6}$	Topas®
1500	140	15	$3.0{\cdot}10^{-5}$	$2{\cdot}10^{-6}$	Topas®
1000	166	12	$2.5{\cdot}10^{-5}$	$5{\cdot}10^{-6}$	Topas®

of filtered and unfiltered PEDOT:TsO thin films on the same substrate. However, due to the time constrains in this work this was not carried out. Calculating the conductance σ based on the sheet resistance measurements showed the conductance of PEDOT:TsO $\sigma = 424 \pm 57.2$S/cm. This value is within the expected range based on previously published results.[51,155]

The statement that impurities in the polymer can influence the overall conductivity of the film was investigated using conductive AFM. Comparing the topography mapping and conductance mapping on figure 7.3 it is observed the elevations in the topography gives rise to a correlating loss of conductance. To enhance the visualization of the correlation we applied a mean filtering of the pixels. The filter averages the pixels out from n number of the nearest neighboring pixels.

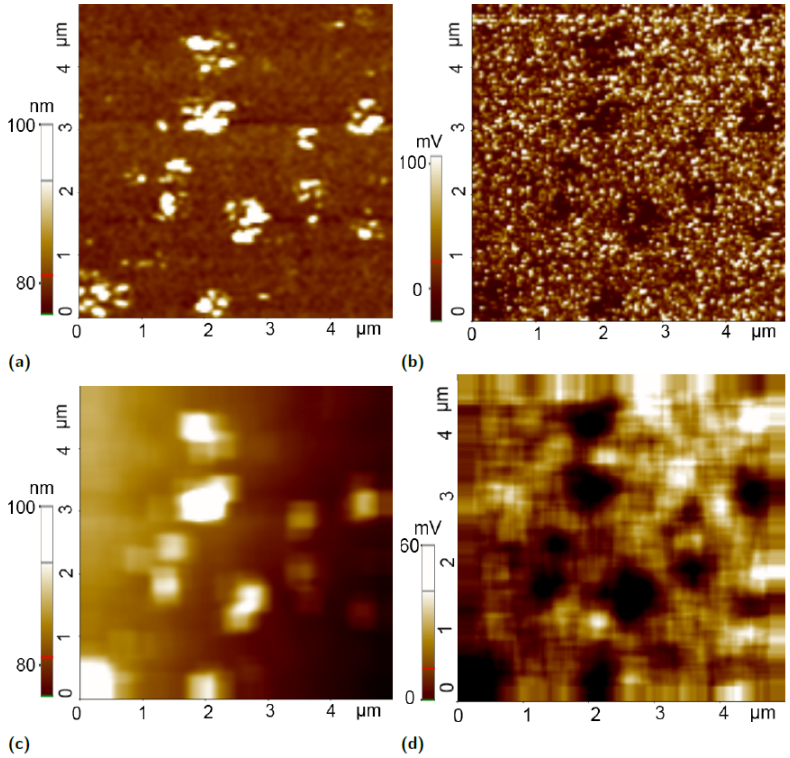

Figure 7.3: *C-AFM imaging of a PEDOT:TsO thin film. (a) 5 µm x 5 µm topographical image of a PEDOT:TsO thin film surface. The topography is obtained in contact mode. (b) Conductivity mapping of the measured area. The dark spots indicates little or no conductivity. It is observed that these correlate to the elevated areas in the topography image. (c) The topography image with a mean pixel filtering of n=11. (d) The conductivity image with a mean pixel filtering of n=11*

7.2.3 PEDOT Wire Fabrication

The aim of this series of experiments was to investigate the influence of agarose stamping time with the conductivity and geometrical output when trying to fabricate PEDOT:TsO wires. To find out if agarose stamping is a viable option for fabricating PEDOT micro or nano wires it is important to know how small wires it is possible to stamp and how size affects the conductivity. Another feature to investigate is reproducibility. The experiments were carried out by designing a stamp with a simple structure comprised of different sized microwires, ranging from 2 μm-20 μm, connected to single contact electrodes, the design can be seen on figure 7.4. The lower limit of 2 μm was determined by the the limits of photolithography in our cleanroom facility. The stamp was prepared as described in section 7.1.2. However, the fabrication of the 2 μm wire didn't succeed so only measurements of the 4 remaining wires are presented here.
A series of patterns were stamped on PEDOT:TsO thin films with 1% NaOCl and vary-

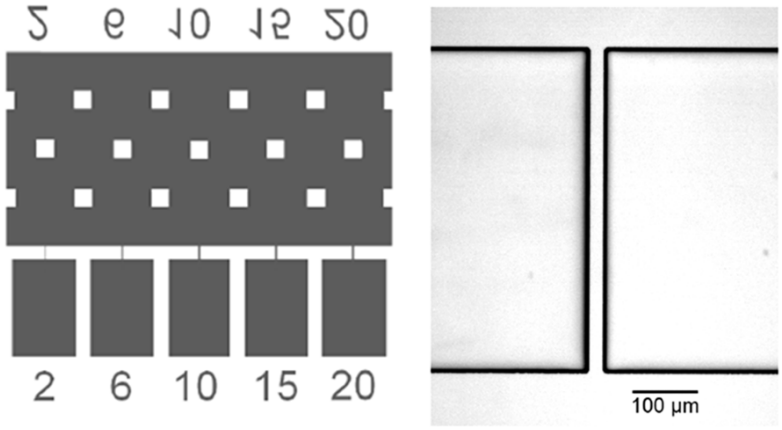

Figure 7.4: *(a)Image of the mask used for making silicon structures. (b) Microscope image of 400 µm long and 20 µm wide silicon wire on the template.*

ing stamping time between 30s-120s. The resulting width was measured using optical microscopy. The uncertainty of the measurements were estimated to be within 50 pixels corresponding to 1μ. The resistance of the wires were measured with an uncertainty of 0.01%. The resistance of the etched wires are plotted against the measured wire width in figure 7.5. It is observed that the resistance increase several orders of magnitude at etching times above 60s. Considering the ideal wire the resistance R is related to the material resistivity ρ, the length of the wire l and the cross-sectional area, by assuming the PEDOT:TsO wires to be rectangular the cross-sectional area is given as the wire width d and times the height h.

$$R = \frac{\rho l}{d \cdot h} \tag{7.2}$$

The length of the nanowire ($l = 400$ μm) is fixed from the mask design. This means that the oresistance should be inversely proportional to the width d of the nanowire. This does not fit with the results shown in figure 7.5. A powerfit with the function $y = ax^b$ was fitted to the plot. If the resistance is infact inversely proportional the coefficient b should be $b = -1$. However, it was seen that the coefficient was changing with etching times up to $b = -3.5$ for the 120s measurements. This shows that the cross-sectional area does not correspond linearly to $d \cdot h$.

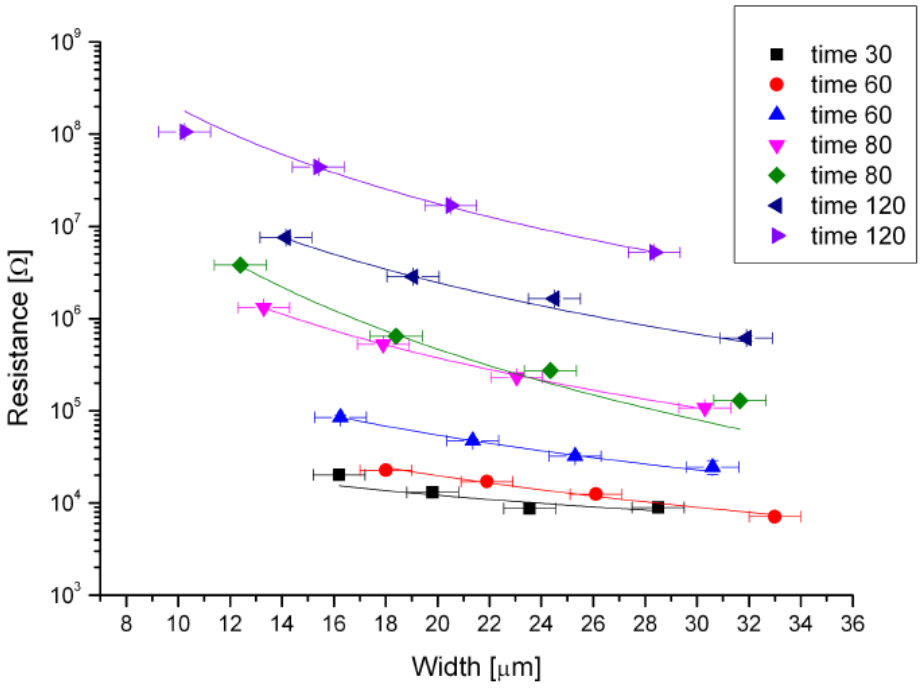

Figure 7.5: *Wire resistances, of pattern stamped with durations of: 30 s, 60 s, 80 s and 120 s. Where the resistance is plotted as a function of wire width.*

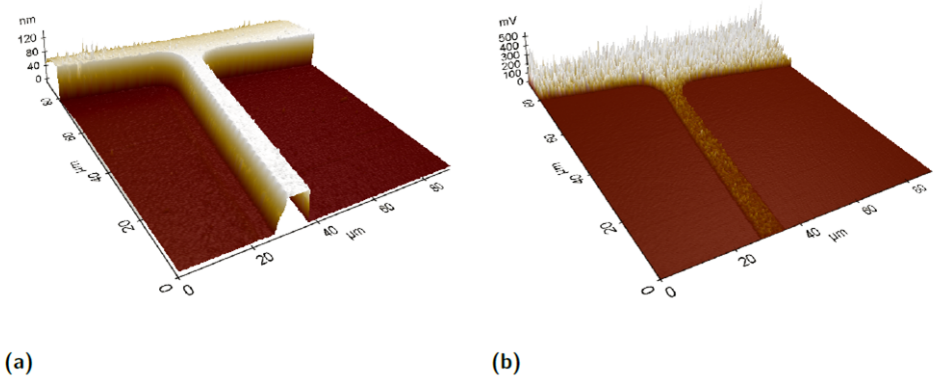

Figure 7.6: *C-AFM measurement PEDOT pattern on SiO2. (a) Topography of 6 µm wire connected to the contact electrode. (b) Conductance mapping of the measured 6 µm wire.*

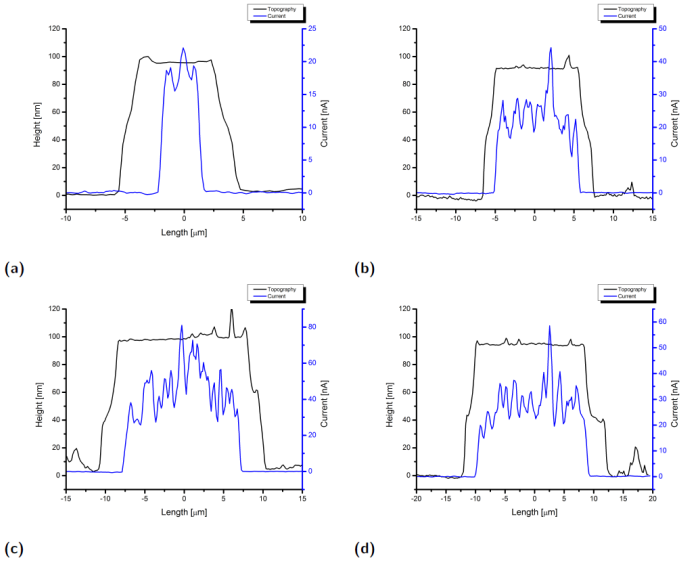

Figure 7.7: *Two-Dimensional line profiles of the topography (black) and conductivity (blue) of the PEDOT:TsO wires; (a) = 6 µm, (b) = 10 µm, (c) = 15 µm, (d) = 20 µm*

This irregularity was investigated futher by the use of C-AFM. a PEDOT:TsO thin film of 105 nm were prepared and etched for 60s. By comparing the topography and conductivity mapping of a PEDOT:TsO wire it is observed that the conductivity of the wire is much lower than that of the contact electrode, even though the height is the same, see figure 7.6. Figure 7.7 shows the two-dimensional line profiles of the topography and conductivity measurements. It is seen that the wire is wider at the bottom than at the top. This could be due to the tip effect of the AFM measurement. However, it could also be a diffusion based effect. There is observed a clear difference in the width of the conducting area and the width of the PEDOT:TsO wire. This shows that, in average, 5.5 $\pm$ 1.6 μm of the wires are now non-conductive. This indicates that the the over oxidation that etches the PEDOT:TsO thin film is not completely anisotropic. NaOCl, or gaseous chlorine, is properly diffusing into the remaining PEDOT:TsO wire during etching thereby over oxidizing the surface of the wire. This effect has previously been reported,[155] and is illustrated in figure 7.8. This diffusion could explain the results presented in figure 7.5 where it was found that the resistance increased several orders of magnitude at longer etching times. On this background it was decided to fabricate all future electrodes using etching times of 60s as this completely removes the desired PEDOT:TsO, while only showing minor indications of over oxidized surface area on the wires.

When stamping a range of wires repeatedly on a batch of Topas®discs using the same stamp it was found that the resulting wire width were increasing, this is also evident from the results presented in figure 7.5. To investigate this further a time series experiment were set up. The same stamp was used repeatedly with 5 min. intervals and a etching time of 60s. The width of the stamp was measured using optical microscopy between every stamping. To minimize the source of error a new bottle of NaOCl was used and the NaOCl

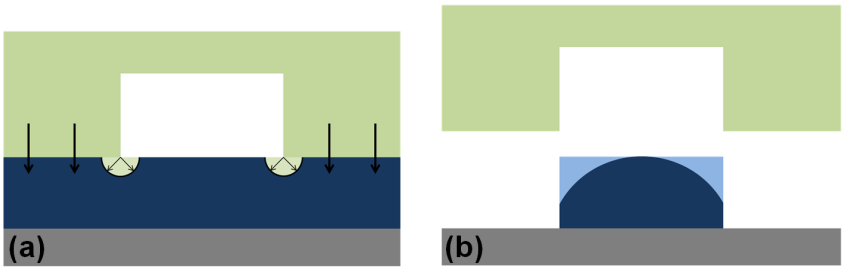

Figure 7.8: *Illustration of how the stamp NaOCl could diffuse into the stamp, resulting in edge effects on the PEDOT pattern. Long exposure times will enhance the effects.*

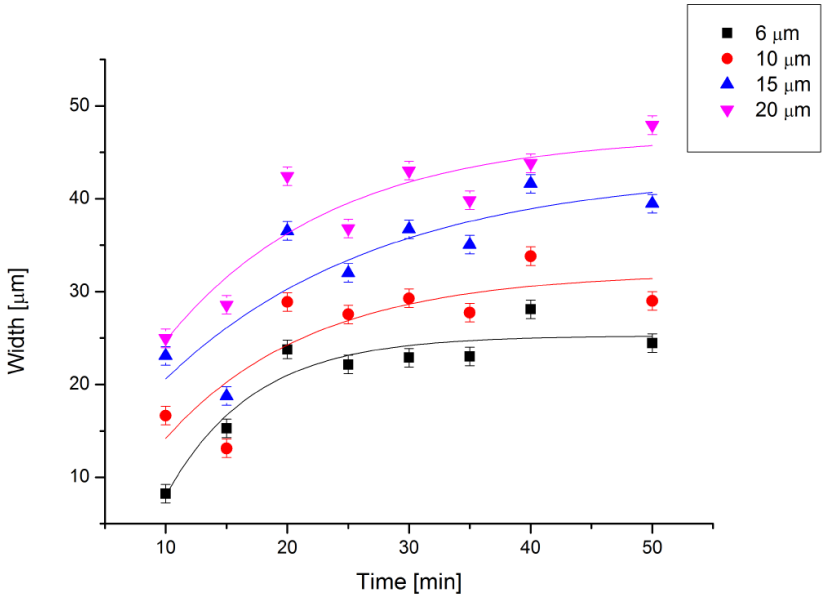

Figure 7.9: *PEDOT wire widths plotted as a function of time, after the immersion of agarose stamp in NaOCl. The width is plotted in individual series, labeled for with the corresponding template wire width.*

solution used to soak the stamp in was exchanged every 10 min to avoid concentration change due to evaporation. In total 18 PEDOT:TsO wires were stamped with the same parameters. After stamping the width of all the etched wires were measured and plotted against to total usage time of the stamp. It was observed that the PEDOT:TsO wires width increases with time, see figure 7.9. They seem to reach a plateau after 40-50min. The change in size seems to stem from a contraction of the agarose stamp. This can be seen in figure 7.10

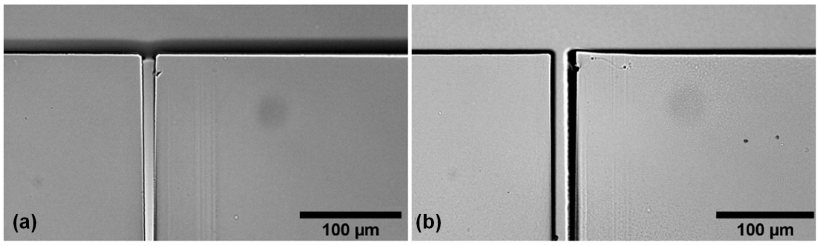

Figure 7.10: *The agarose stamp before use (a) and after use (b)*

7.2.4 Electrical Characterization

From the C-AFM mapping it is seen that the PEDOT:TsO wire is conductive. however, to investigate the system as a whole it is necessary to measure the conductivity through the wire from the contact electrodes. Initially the electrodes were imbedded into a microfluidic channel isolating the wires from the contact electrodes. A potential varying from -100mV to 10mV was applied across the wire while measuring the current output. The potential sweep gave a linear response indicating an ohmic resistance, see figure 7.11. For a second experiment the microfluidic channel was filled with Milli-Q water still showing an ohmic resistance. The conductance, however, seemed to increase $\approx$ 40%. Similar increase in PEDOT:PSS has previously been reported for different solvent treatments.[156] It is interesting that the conductivity of the PEDOT:TsO wire changes this much in Milli-Q water as it is not adding any charge carriers to the wire. The change in conductance is expected to stem from a conformation change of the polymer when it swells up due to the liquid. However, if another liquid is used for measurement e.g. a buffer like Phosphate buffered saline (PBS) it is likely that the ions in the solution will influence the conductivity even further.

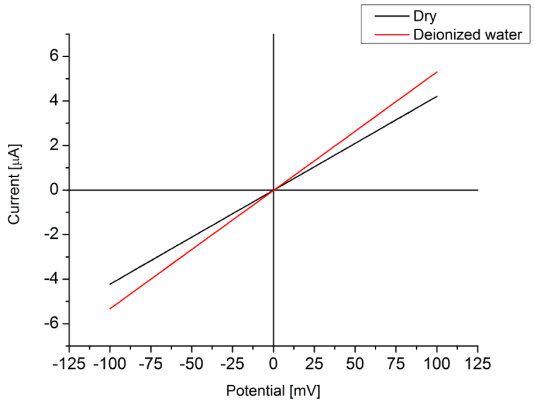

Figure 7.11: *Current response of a potential sweep from -100mV to 100mV with a step size i 1mV. The two lines shows the response of the wire in dry ambient surroundings and Milli-Q water respectively. The linear behavior shows and ohmic conductance of the wire. It is seen that the conductance increases when the wire is covered in Milli-Q water.*

7.3 Discussion and Conclusion

The possibility of using PEDOT:TsO to fabricate nano wires or nano ribbons depends on the ability to control the dimensions of the PEDOT:TsO. And also how the conductivity of PEDOT:TsO change with different fabrications methods.
Controlled coating of Topas®discs and silicon wafers with PEDOT:TsO thin films was studied. It was found that it is possible to control the thickness down to at least 40 nm on silicon. This means that polymerization by oxidation can be a viable and inexpensive method for fabricating nano wires or nano ribbons as we can go to nanometer scale in at least one dimension.
It was shown that the PEDOT:TsO thin films could be patterned using agarose stamping, with NaOCl as oxidizing agent, as expected. However, it was discovered that the agarose stamp showed a contraction over the first 50min of use giving rise to a change of up to 300% in wire width compared to the expected width. The relative change is lesser for the larger wires or electrodes. The contraction needs to be taken into account when designing the next pattern layout. Baring an optimization in mind these results suggests that the stamping technique might be most applicable for patterns with feature sizes above 20 μm. Using C-AFM it was shown that the NaOCl from the agarose stamp diffuse into the PEDOT:TsO pattern. This can actually be exploited to create even smaller wires. As the effective radius of the PEDOT:TsO wire is smaller than the actual size. However, for the purpose of using the nano wire as a Bio-FET this would properly not work as the non-conductive PEDOT:TsO layer at the surface would screen the target analyte.

Chapter 8

PEDOT Nanowire Produced by Self-Assembled Peptides.

8.1 Introduction

Since the original article on silicon nanowire demonstrating the potential of these new types of biosensors was published more than a decade ago[120] the field of silicon nanowires has received a lot of attention and many articles exploring this specific field have been published.[121–124] However, the fabrication costs of the nanowire devices still are a challenge hindering the full exploration of the nanowire devices as biosensors for diagnostic use.[130] One of the approaches explored to face this challenge has been the fabrication of nanowires in cheaper materials, for instance conductive polymers such as polyanaline[110,157,158] and poly(3,4-ethylenedioxythiophene) (PEDOT).[132,141,159] The benefits of the cheaper nanowire devices have been demonstrated in various applications ranging from chemical gas and liquid sensors,[138,160] over temperature sensors[135] to biosensors.[128,133,139] However, the fabrication procedure for the polymer nanowire devices still is challenging and/or time consuming due to the incompatibility of the polymers with organic solvents used in traditional nanofabrication techniques.[161] Recently, we have demonstrated the use of self-assembled diphenylalanine peptide nanotubes (PNT's) as dry etching masks for the low cost, mild and rapid clean room fabrication of silicon nanowire devices.[72,86] Diphenylalanine self-assembled peptide nanostructures are biological entities able to self-organize in a rapid way under mild conditions. Its on-chip fabrication, structural and electrical characterization, manipulation and application in the development of biosensors were recently reported.[76,79–81,85] In this work we have demonstrated the rapid fabrication of polymerized p-toluenesulfonate doped poly(3,4-ethylenedioxythiophene) (PEDOT:TsO) nanowire devices (the whole process can be conducted in approximately 5 h) based on the self-assembled PNT lithography. The benefit of this fabrication procedure is that any contact between PEDOT:TsO and organic solvents, such as acetone, can be avoided since the PNT's dissolve rapidly in Milli Q water after the dry etching pattern transfer.[71]

8.2 Materials and Methods

8.2.1 Chemicals

The lyophilized diphenylalanine dipeptide powder was purchased from Bachem (product number: G-2925). All other chemicals utilized were purchased from Sigma- Aldrich.

8.2.2 PEDOT:TsO Preparation

260 ll Baytron C (40% Fe^{III}tosylate in butanol), 80 μl butanol, 6 μl pyridine and 8.8 μl EDOT were thoroughly mixed and spun on the substrate wafer with 4000 rpm for 60 s. The coated wafers were heated to 70 °C for 10 min to evaporate the inhibitor Pyradine and start the polymerization process. The wafers were finally rinsed in de-ionized water to wash away excess reactants. This procedure ensures a PEDOT:TsO film thickness of 75 nm.

8.2.3 Preparation of Diphenylalanine Peptide Nanotubes

The PNT's were prepared from a stock solution, where the lyophilized form of the peptide monomers was dissolved at a concentration of 100 mg/ml in 1,1,1,3,3,3-hexafluoro- 2-propanol (HFP). The HFP stock solution was diluted to a final peptide concentration of 2 mg/ml in water in which process the PNT's are formed. Fresh stock solution was prepared prior to experiments to avoid pre-aggregates.

8.2.4 Spin Casting Procedure

The PNT's were positioned across the electrodes in a spin casting procedure as described in.[139] In short, the solution containing the newly formed PNT's is dropped in individual drops on the spinning substrate. This spin casting procedure ensures that the PNT's on the surface of the wafer are oriented along the axial direction. In this work a spin rate of 4000 rpm was utilized in all the experiments.

8.2.5 Reactive Ion Etching Procedure

The reactive ion etching procedure was conducted in a STS Cluster System C010 with a pressure of 300 mTorr and a power of 100 W. For the patterning of the PEDOT:TsO an oxygen based plasma was used (98 SCCM O2 and 20 SCCM N2). The wafers were subjected to the plasma for 15 s, which was enough to etch through the thin PEDOT:TsO layer.

8.2.6 Visualization

All scanning electron microscopic (SEM) images were acquired using a Zeiss SUPRA® 40 VP operated in the inlens mode with an acceleration voltage of 3 kV. The atomic force microscopy (AFM) measurements were conducted using a PSIA XE 150 in both tapping (for topography imaging) and contact (for conductive recordings with a tip bias of 0.7

V) mode. The conductive AFM images were acquired with a Cr/Pt coated cantilever (ContE-Al, Budget Sensors) with a force constant of 0.3 N/m. The current between the AFM tip and sample was measured using an inverting current amplifier and one of the analog-digital converter inputs of the AFM controller.

8.2.7 Electrical Readout

The impedance of the PEDOT:TsO nanowire device was recorded with a custom build lab view controlled experimental set-up, as described in.[122] In this set-up the current through the PEDOT:TsO nanowire is externally amplified using a low-noise current preamplifier model: SR570 from Stanford Research Systems and finally recorded using a National Instruments data acquisition card model BNC-2111.

8.2.8 Temperature Measurements

The initial temperature measurements were conducted in a water bath with a temperature controlled feedback loop. The real temperature of the water bath was measured using an external thermometer model VT5-S40 from VWR. To investigate the response time of the PEDOT:TsO nanowire to a change in temperature two water baths at different temperatures were prepared and the PEDOT:TsO nanowire devices were moved manually from one to the other while the impedance of the wire was continuously monitored.

8.2.9 Backgating Measurements

To backgate the nanowires it is necessary to ensure a good electrical contact on the backside of the chip. To do this a 100 nm aluminium layer is deposited on the backside of the silicon wafer before fabricating the nanowires. The PEDOT nanowire chips were then produced in the same way as previously described. The impedance is measured while a gating potential is applied to the backside of the chip. A schematic of the setup can be seen in figure 8.1

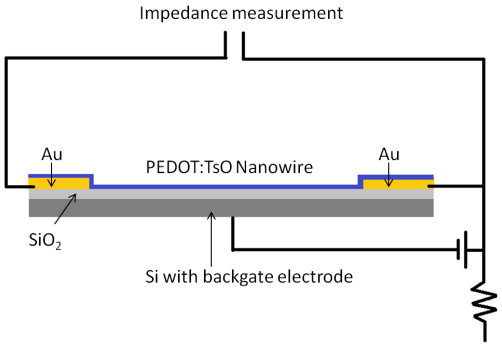

Figure 8.1: *Illustration of the experimental setup for the backgating measurements. The impedance is measured between the two gold electrodes (source and drain) while applying a backgating potential through the backside aluminium contact.*

8.3 Results and Discussion

8.3.1 Fabrication of PEDOT:TsO Nanowires

In a previous work, we have demonstrated the use of the diphenylalanine PNT's as a dry etching mask for the fabrication of poly silicon nanowires.[72,86] One of the benefits of utilizing the PNT's besides the low cost and rapid fabrication process is that they can be removed in Milli Q water after processing.[71] In this way, acetone traditionally required for the removal of photoresists, can be avoided. This enables the patterning of new types of materials normally incompatible with such organic solvents. In this work, a modified version of this fabrication procedure has been utilized for the rapid and low cost fabrication of PEDOT:TsO nanowire devices. In fact the entire fabrication procedure can be conducted in approximately 5 h yielding at the moment around 200 ready to use PEDOT:TsO nanowire devices. In figure 8.2, the fabrication steps in the process are illustrated. The first and most time consuming part of the fabrication was the deposition and patterning of the gold electrodes and contact pads allowing electrical connection to the PEDOT:TsO nanowires. In this work 90 nm of gold was deposited on 500 nm thick silicon dioxide layer grown from a bare silicon wafer utilizing a 10 nm chromium adhesion layer. The metal layers were patterned in a traditional lift off procedure. The only difference being that the wafer was dipped in a 5% buffered hydrofluoric acid solution for 20 s prior to metal deposition. This ensure a smooth corner on the edge of the gold electrodes to provide electrical connection between the electrodes and the PEDOT:TsO nanowire.

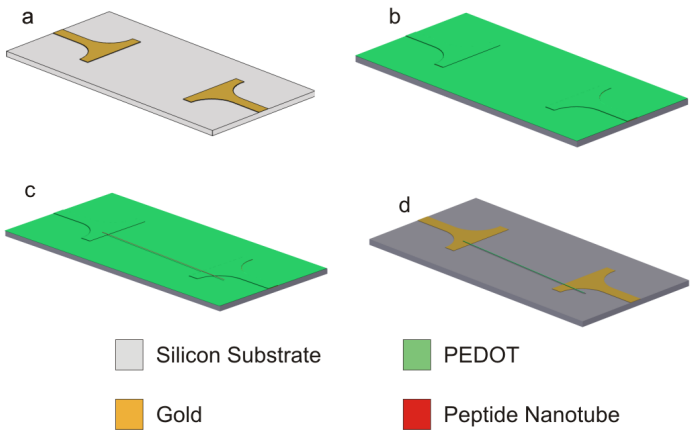

Figure 8.2: *Illustration of the fabrication procedure developed and utilized in this article. In this approach the gold electrodes were initially defined by a lift off procedure. The PEDOT:TsO was spincoated on the wafer and finally the peptide nanotubes were spin casted on the coated wafer to ensure prober alignment of the structures to the electrodes. In the last step the pattern of the nanotubes was transferred to the PEDOT:TsO layer in a reactive ion etching procedure and finally the peptide nanotubes were dissolved in Milli Q water. The process can be completed in approximately* 5 *hours.*

In the second step, the PEDOT:TsO layer was spin coated on the wafer with a spin rate of 4000 rpm followed by a post backing step as explained above. The PNT's forming the dry etching mask were positioned across the electrodes in a modified spin casting technique described in.[72] In this manipulation procedure the PNT's aligned according to the axial direction on the wafer. The gold electrodes were positioned perpendicular to this direction. In this way the aligned peptide nanotubes were able to bridge the gap at the electrode position and not at other locations in order to avoid potential short circuits as described in our previous work.[72] The final step in the fabrication process was to transfer the pattern of the self-assembled peptide nanotubes to the spin coated PEDOT:TsO layer. After pattern transfer the PNT's were removed in pure Milli Q water.

8.3.2 Characterization of PEDOT:TsO Nanowires

The fabricated PEDOT:TsO nanowire devices were characterized using both SEM and AFM. A SEM image of a PEDOT: TsO nanowire spanning the gap between two gold electrodes is shown in figure 8.3 (a). Figure8.3 (b) displays a zoom of the contact between the PEDOT:TsO nanowire and the gold electrode illustrating the smooth step coverage of the PEDOT: TsO nanowire across the step from the oxide substrate to the top of the gold electrodes. The large contact area between the gold electrodes and the PEDOT:TsO nanowire and the smooth coverage of the step from the electrode to the substrate by the PEDOT:TsO, as seen in the figure, ensured proper electrical contact in the devices. This is also evident from the small impedance and linear current voltage characteristics, even at room temperature, of these devices as described below. In figure 8.3 (c), a topography image of the surface of the PEDOT:TsO nanowire recorded with an AFM in tapping mode is shown. Based on the line profile shown in figure 8.3 (d), the height of the PEDOT:TsO nanowire can be determined to be 75 nm. In this image the surface roughness of the PEDOT:TsO nanowire is also clearly seen. The roughness of the surface introduces a larger surface to volume ratio than comparable flat nanowires and should therefore increase the sensitivity of the measurements. Using conductive AFM the complete removal of the PNT's from the PEDOT:TsO surface after etching was verified as seen in Fig. 3b. From this AFM image it is seen that the surface of the PEDOT:TsO nanowire is highly conductive and hence the isolating PNT's must have dissolved.

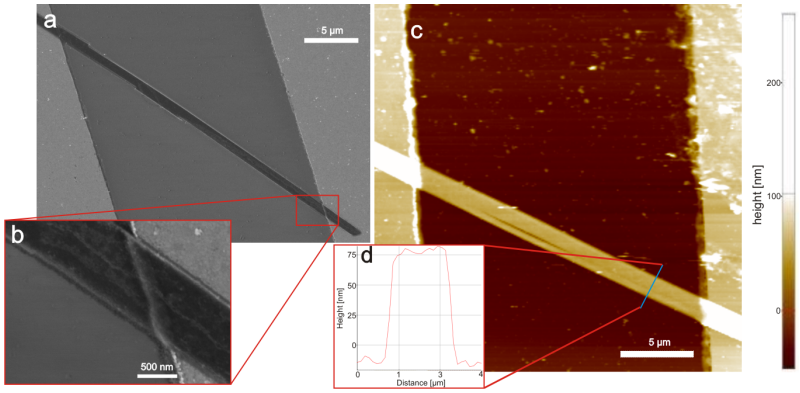

Figure 8.3: *Visualization of the fabricated PEDOT:TsO nanowire structures with the gold contact pads visible. A SEM image of the whole PEDOT:TsO nanowire spanning the gap between two of the gold electrodes is seen in a. And in b a zoom of the contact area between the PEDOT:TsO nanowire and the gold contacts is shown. In this image it is seen that the PEDOT:TsO nanowire covers the step of the gold contact very well, which is also evident in the electrical recordings presented below. In c an AFM image of the junction between the PEDOT:TsO nanowire and the gold contact pads is seen and in d a line scan covering the PEDOT:TsO wire is included to verify the height of the fabricated PEDOT:TsO nanowire. From this scan the thickness of the nanowire can be estimated to* 75 *nm.*

8.3.3 Electrical Characterization

From the SEM images in figure 8.3 (a) and (b) a continuous connection between the PEDOT:TsO nanowire and the gold surface without any fracture in the structure can be seen, indicating a good electrical connection. To verify this, the current-voltage relationship of a single PEDOT:TsO nanowire was recorded and plotted in figure 8.4 (a) for a range of different temperatures. From this plot is clear that an ohmic electrical contact between the gold contact pads and the PEDOT:TsO nanowires was established as the current voltage relation was linear. The proper electrical contact is ensured by the large contact area between the PEDOT:TsO nanowires and the gold electrodes combined with the smooth corner of the electrodes. The major difference, between this and previous fabrication approaches, is that the PEDOT:TsO in this case is first spin coated on the electrodes and patterned at the electrodes yielding the good electrical contact. In figure 8.4 (b), an image acquired with conductive AFM is included to show the complete removal of the isolating peptide nanotubes from the surface of the PEDOT:TsO.

8.3.4 Temperature Measurements

Finally, to demonstrate the potential of the PEDOT:TsO nanowires they were used as temperature sensors. The impedance of the PEDOT:TsO nanowire was monitored as the temperature was changed. In figure 8.5 (a), the impedance of the wire is plotted as a function of the temperature of the solution in which the PEDOT:TsO nanowires devices wrapped in a thin polymer foil were submerged (determined by external temperature sens-

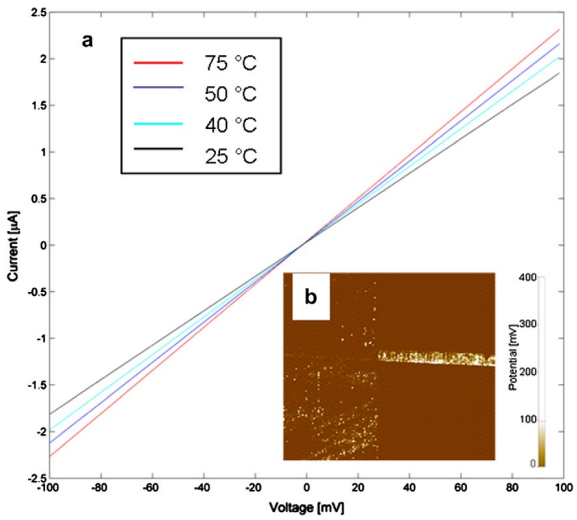

Figure 8.4: *An image acquired with conductive AFM is shown in b demonstrating the complete removal of the isolating peptide nanotubes from the surface of the PEDOT:TsO nanowire. I-V curves for the nanowire devices at different temperatures is plotted to demonstrate the completely linear ohmic behavior of the PEDOT:TsO nanowire indicating a good contact between the gold electrodes and the PEDOT:TsO nanowire in a.*

ing). In this experiment, a linear correlation between the impedance of the PEDOT:TsO nanowires and the external temperature was seen. From this plot it is also evident a low noise level in the PEDOT:TsO nanowire, corresponding to less than 0.05 °C. This is further demonstrated in figure 8.5 (b) where the impedance is monitored while the temperature is changed 0.2 °C. As a result of this change in temperature the impedance of the PEDOT:TsO nanowire increased more than 8 times the noise level. Note that in this measurement no shielding of the signal was conducted to mimic the situation in real temperature sensing environments. Performing the measurements in a faraday cage would result in an even smaller noise level and hence higher sensitivity. During the experiments it was also noted that the response time of the PEDOT:TsO nanowire temperature sensor was shorter than that of the traditional external temperature sensor. Therefore in figure 8.5 the response time of the PEDOT: TsO nanowire device is investigated by the repeated change of external temperature of the wire. From this measurement it is seen that within 10 s the PEDOT:TsO nanowire device has equilibrated to the new temperature. The fast response of the PEDOT:TsO nanowire stem from the small thermal mass of the wire. In the specific experiments, in fact, the major part of the thermal mass and hence the major contribution to the response time stems from thermal mass of the substrate wafer on which the PEDOT:TsO nanowire is fabricated. The PEDOT:TsO nanowire itself has a thickness of 50 nm, a length of 10 μm and a width in the order of 500 nm and hence the volume of the wire is only 0.25 μm^3 compared to the $\approx 10^{17}$ μm^3 of the substrate. In comparison with other temperature sensors such as strings and bimetallic geometries relying on optical readout,[72,162–164] the PEDOT:TsO nanowire only requires a 2 point electrical readout

that, due to the small impedance, in principle can be read using a multimeter depending on the desired precision. Temperature measurement with nanowire structures is not a new principle and has previously been demonstrated with both PEDOT nanowires[135] and nanowires of other materials.[165–167] The PEDOT:TsO nanowire fabricated in this work has a much lower resistivity than the previously demonstrated nanowire devices. Therefore the readout procedure for the nanowire devices fabricated in this work is easier and as mentioned above can be conducted with a standard 2 point electrical read out procedure. The main benefit is however the easy fabrication scheme demonstrated in our work allowing the fabrication of nanowire devices in less than half a day. The very low contact resistance between the gold electrode and the PEDOT:TsO nanowire ensure very sensitive measurements since the dominant change to the impedance of the device is the impedance of the PEDOT:TsO nanowire. Hence, any smaller change in the impedance in the gold contact pads and electrodes due to the temperature change can be disregarded. In order to utilize the PEDOT:TsO nanowires as biosensors in liquid conditions one will have to pattern a passivation layer covering the gold electrodes to ensure no parasitic current through the medium in which the sensors are operated.

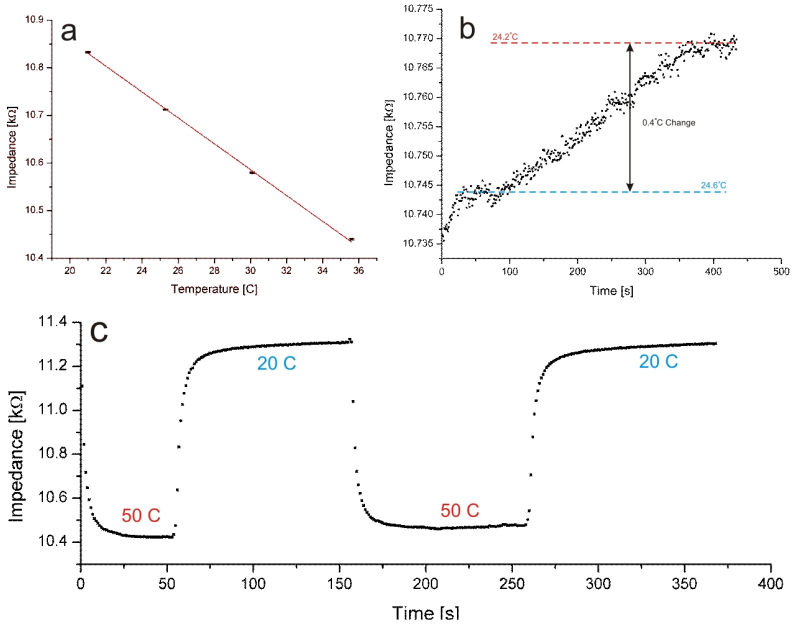

Figure 8.5: *To demonstrate the potential of these PEDOT:TsO nanowire devices they have been utilized as temperature sensors. In a the relationship between temperature and impedance is plotted and from this plot it is seen that the temperature-impedance relation seems very linear. And in b the sensitivity of the PEDOT:TsO nanowire device to temperature changes is illustrated. To determine the response time of the PEDOT:TsO nanowire devices to change in external temperatures the impedance of the nanowire was continuously monitored as the device was transferred between two water baths with different temperatures as seen in c.*

8.3.5 Backgating Experiment

The traditional silicon nanowire devices functions as a FET. The current is running between the source and drain electrode when applying a gate potential the conductance will either increase or decrease. The conductance dependency on the gate voltage has led to the idea of using FETs for electrical sensing. Imagining a number of charged target molecules attaching to the nanowire, this is analogous to applying a potential using a gate electrode.[125] To demonstrate an initial requirements for using the PEDOT:TsO nanowire as an alternative to the traditional silicon nanowire we were backgating the PEDOT:TsO nanowires. As previously described a backside contact in Al was added to the device. By connecting an external power supply to the backside of the device and to ground the backgating potential could be applied. The potential was applied in steps of 10V from 0V to 60V in time intervals of 1 min. The potential was turned off between each step to ensure the PEDOT:TsO was not simply being reduced. Figure 8.6 show the increase in impedance when applying a gating potential. It is seen that a change in backgate potential of 50 V shows a corresponding increase in impedance oh 5-10 $k\Omega$

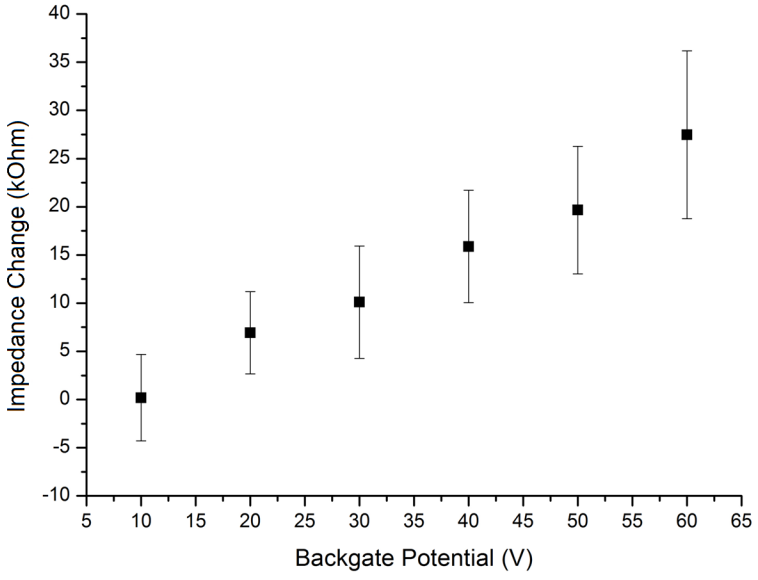

Figure 8.6: *The measured impedance is plotted against the applied backgating potential. There is seen a linear increase in impedance when increasing the potential.*

8.4 Conclusion

In this work, we have combined the benefits of bottom up fabrication using self-assembled peptide structures for the patterning of PEDOT:TsO nanowires with the benefits of top down fabrication of macroscopic gold electrode patterns to provide contact pads for reliable electrical contact. In this way we have demonstrated a rapid and low cost fabrication method for the preparation of PEDOT:TsO nanowire devices (the entire fabrication process can be conducted in approximately 5 h). The fabrication procedure of the PEDOT:TsO layer avoided the use of organic solvents due to the easy removal of the peptide nanotubes in water.
The fabricated PEDOT:TsO nanowires were used as sensitive sensors to measure temperature changes (down to 0.05 °C changes can be detected with the current setup) with a fast response time (in this setup approximately 10 s).
We have also demonstrated the potential for backgating the PEDOT:TsO nanowires. The impedance change due to a change in charge indicates that the PEDOT:TsO nanowires can be a viable system for a FET-like system e.g. as a BIO-FET used for sensing.

Chapter 9

Cellular Studies

We have previously presented work on a cell based based on EIS. This type of sensor combines the transducer signal with a cell response to the target analyte. This work was done as a side project investigating the PEDOT:TsO nanowires promise for single cell studies.

Cell based biosensors are a sophisticated bred of biosensors basically using two actuators in combination; a sensing element e.g. an impedance electrode, and immobilized living cells. Cells are by nature very sensitive to changes in their respective environment. This allows studies of physiological relevant studies of cellular responds to different target analytes. The cell based biosensors are very versatile and have a wide range of applications. A recently highlighted application is for screening of known and unknown drug candidates. The development and testing of new pharmaceutical is very expensive. This creates an insensitive to create new technologies for accelerate the process. As the biosensor creates the opportunity to monitor the cells direct responds to the drug candidate it provides a cost efficient platform for fast and accurate screening of known and unknown drug candidates.

In this work we have chosen to combine the cell with electrochemical impedance spectroscopy (EIS). It has been shown that immobilized cells on top of a electrode array provides a platform for label free detection of the cellular response to different drugs or pathogens.[168,169] The interaction between a cell monolayer and the electrode surface can be monitored in real time by applying a small alternating electrical field over the electrodes. The cell membrane can be portrait as a capacitor meaning at low frequencies it is non conducting. This means that the cell offers a significant barrier to the current. This means that the amplitude of the electrical field is an indication of the size of the cell.[170] Impedance measurements on cells cultured on electrodes is very sensitive to small changes in the cell membrane. These changes alters the capacitance and resistance of the membrane. This can be related to the well being of the cells at given morphologies. Real time impedance on cells is an efficient and rapid technique for non invasive monitoring of the response of human cells in culture to the challenge of e.g. a viral infection.[171,172] In our group we have recently shown that we can detect H1N1 virus with a response time of

less than 15 min. using EIS.[173]

9.0.1 Single Cell Studies

Sensing at a single cell level is an emerging field that gives rise to a new opportunities in medical diagnostics and has been recognized as a key technology for elucidation of cellular functions, which are not accessible from the standard cell studies as these are carried out in a bulk population level. The possibility to track and record the heterogeneity of single cells can be used to address fundamental questions on their biochemistry and functionality. Most traditional cellular assays are based on averaging over larger population on cells and hence not obtaining the single cell dynamics. This could lead to misleading conclusions on single cell level. To improve this single cell measurements are slowly becoming a requirement in modern medicine. The current techniques for single cell studies include capillary electrophoresis and flow cytometry. Both methods include labeling the cells with fluorescent conjugates. The binding of these could prove to be invasive and alter the original cellular functions.[174] Our chip allows for a non invasive label free studies of single cells within a population of cells to preserve their natural cellular environment.

9.1 Experimental Setup

The PEDOT:TsO nanowires was fabricated as described in chapter 8. However to insulate the cells from the gold electrodes a thin layer of SU-8 spun on top of the chip and patterned into a micro fluidic reservoir leaving the nanowire free but covering the gold patches, the chip is illustrated in figure 9.1. The cell's initial attachment and spreading on top of the PEDOT:TsO nanowire was measured using impedance spectroscopy (EIS). control experiments were conducted in cell medium.
Healthy fibroblast cells were seeded in the chip and the EIS measurements (no redox couple added) was carried out in a tightly controlled environment at 37 °C and 5% CO_2. The EIS were carried out with a frequency range of 1 Hz to 10 kHz over 33 s with an amplitude of 20 mV. The optimal time dependent analysis was found to be 1 Hz. This was determined by the highest response to changes on the cells.

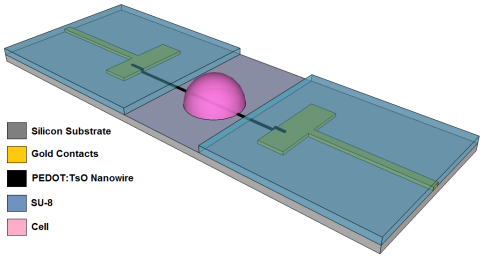

Figure 9.1: *Illustrates the PEDOT:TsO nanowire chip. The PEDOT:TsO is contacted through the gold contacts. The cells is grown on the nanowire while the SU-8 is insulating the gold contacts*

9.2 Results and Discussion

The single cell adhesion on the PEDOT:TsO nanowire was in real time. Figure 9.2 shows two typical measurements. In (a) it is seen that the initial attachment and spreading out of the cell is related to an increase in impedance until a plateau is reached after approximately 2.5 hours. Previous work in our group has shown that the adhesion of a cell population follow a similar trend.[175] In (b) the impedance change occurred at a faster pace peaking within the first two hours and the showing a drop off before eventually stabilizing. The difference between the two measurements could result from a lot of factors such as the cell's position on the nanowire, the covering percentage of the nanowire, the nanowire's dimensions, cell morphology or cell motility. An actual PEDOT:TsO nanowire is seen spanning the gold contacts in figure 9.3 (a). Using AFM (b-d) it is observed that a cell is immobilized on the nanowire.

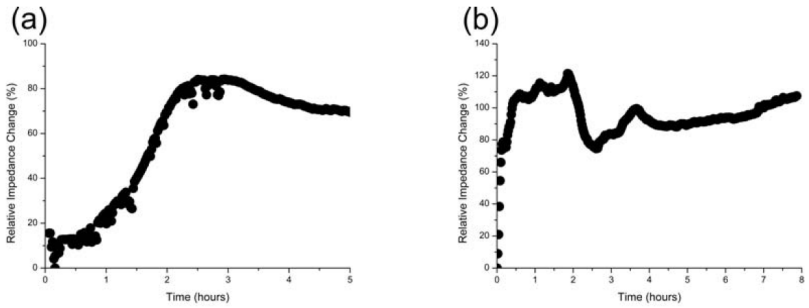

Figure 9.2: *EIS measurement of a single cell adhesion on conductive polymer (PEDOT:TsO) nanowire. (a) and (b) are two independent samples displaying the relative impedance change at a frequency of 1 Hz.*

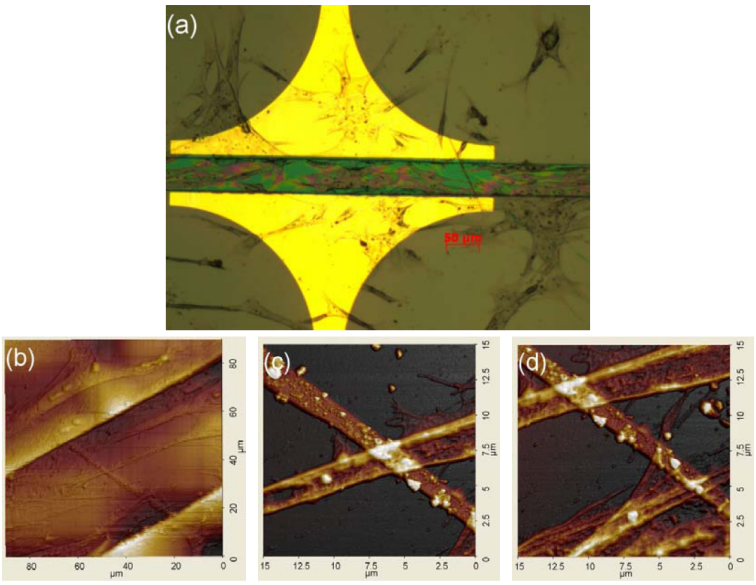

Figure 9.3: *Shows a cell adhered on a PEDOT:TsO nanowire. (a) Microscope image showing a nanowire spanning the two gold contacts. (b) AFM topography image of a cell on a nanowire. (c) and (d) shows AFM topography images of a cell on a nanowire at high magnification.*

9.3 Conclusion

It was shown that the PEDOT:TsO nanowires has a potential for being used for single cell studies. The adhesion of a cell on the nanowire gives a clear change in impedance. There is however a optimizations necessary before this setup can produce more precise and consistent measurements. The current fabrication procedure does not allow any control of the size and and location of the nanowires. Since the location and covering percentage of the cell on the nanowire is an important parameter it would be preferable to do video time laps microscopy while conducting the EIS measurements. This could be solved by fabricating the nanowire system on a transparent substrate e.g. glass or Topas®.
The microscopy and AFM verified that the cells can adhere on the surface. The images also showed, as expected, a large difference between the alignment of the cells on the nanowire between experiments. Again showing that the possibility of time laps video would be a welcome addition to the measurements to ensure propper data treatment.

Adding the possibility of video time laps would subsequently lead to studies on the early effects of virus or drug induced cell death of a single cell. The cellular response to toxins or chemicals are usually measured as an average over a population of cells.[175] With this setup it could be possible to measure the immediate response to a drug or a virus at a single cell level in real time.

Chapter 10

General Conclusion and Outlook

The aim of this thesis was to investigate a range of possible methods for detecting Aβ_{42} concentrations in CSF. The kinetics of Aβ_{42} fibrillation was also studied with the purpose of investigating if an accelerated fibrillation could be used for pre-concentrating the Aβ_{42} samples and possibly increase a given transducer output.

The studies performed on Aβ_{42} found a method for obtaining a pure monomer population through FPLC purification. It was observed that very careful handling (low temperature and concentrations) are necessary to avoid unwanted formation of protofibrils. The study also verified that it was possible to artificially fibrillate Aβ_{42} by incubation and monitor this fibrillation using ThT fluorescence. It was tried to accelerating the process by adding a fibril seeds to the solution. Initial experiments showed a slight tendency to initiate a higher fibrillation, but no significant decrease in fibrillation time. It was therefore decided to move on from measuring Aβ in the form of fibrils but instead focus on measuring the monomeric form of Aβ.

Silicon nanowires has been heralded as a great prospect for biosensor applications. Recently interest have gathered around conductive polymer nanowires as low cost and environmental friendlier alternatives. In this project a method for fabricating PEDOT:TsO thin films down to 40 nm was developed. This is a great base for producing nanowires as one dimension is already defined. It was also shown that it was possible to fabricate PEDOT:TsO ribbons using the agarose stamping technique. Smaller structures however were limited by the aspect ratio of the agarose and over oxidation of the PEDOT:TsO. During this a novel a novel low cost and rapid (entire process could be conducted in approximately 5 hours) fabrication of PEDOT:TsO nanowires based on peptide lithography has been demonstrated. The potential use of theses nanowires as highly sensitive biosensors was demonstrated partly through backgating experiments indicating that the nanowires responds to induced charges and through very sensitive temperature sensing (changes of temperature down to 0.05° C was measured).

The PEDOT:TsO nanowire also proved to have potential for being used in single cell

measurements. It was shown that it was possible to measure the attachment of a single cell on the surface of the nanowire.

This PhD project also presents a different biosensor system. The coulter counter combined with a sorting channel based on an antibody double assay. It was showed that the bead coulter counter was able to detect single beads flowing by the electrodes. By counting the number of beads passing the electrodes and correlating it with their velocity and the parameters of the channel it was accomplished to measure the bead concentration with 97% accuracy. If the double assay of the coulter counter results in a good separation/selection of Aβ coated beads and un-coated beads this could lead to a low cost and very fast method for measuring Aβ concentrations in solution.

Finally this thesis has presented a very thorough study of the physical and chemical properties of Boc-Phe-Phe-OH peptide spheres. Previous literature had presented the peptide spheres as the hardest biological material in the world with an incredible stiffness and a Young's modulus of 160 GPa. These results is amongst other based on an assumption that the peptide spheres are hollow entities. The studies presented in this thesis prove that the peptide spheres are in fact solid and have a Young's modulus of $\approx 20 - 25$ MPa.

10.1 Outlook

The studies carried out through the last three years investigates a wide variety of methods for assisting in measuring the concentration of Aβ_{42} in CSF. Recently conductive polymer nanowires have received a lot of attention across as an alternative to silicon nanowires. It has recently been shown that PEDOT nanowires can be used as biosensors for both DNA and proteins. This thesis presented a novel, low cost and rapid fabrication method for producing PEDOT:TsO nanowires. It was also shown that it was sensitive to large biological samples. The next step is to measure on Aβ to investigate the possibility of utilizing the nanowires as sensors for early detection of Alzheimer's disease.
To increase the specificity of the biosensor it would be preferable to use a double assay. It would hence be very interesting to possible detect not only one interaction with the nanowire (Aβ) but also a second adding a second biorecognition molecule.

Traditional biosensors most often use antibodies as biorecognition molecules the sensitivity of a nanowire is however dependent on the Debye screening length Aptamers are much smaller than antibodies, which is why it would make an enthralling study to see if there could be measured a difference between using aptamers or antibodies as biorecognition molecules.

The experiment on the Double Assay Analyzer showed that it is possible to measure the bead concentration in a fluid by counting the number of beads passing a three electrode system. The work on sorting the target coated beads from the un-coated were however inconclusive mainly due to the time constraints on this part of the work. It would allow for

an interesting project to look deeper into this. Investigation to whether it would function better with antibodies or aptamers could also be carried out.

Bibliography

[1] R. A. Stelzma, H. N. Schnitzlein, and F. R. Murllagh, "An English translation of Alzheimer's 1907 Paper, " ûjber eine eigenartige Erlranliung der Hirnrinde"," *Clinical Anatomy*, vol. 1, pp. 429–431, 1995.

[2] G. G. Glenner and C. W. Wong, "Alzheimer's disease: Initial report of the purification and characterization of a novel cerebrovascular amyloid protein," *Biochemical and Biophysical Research Communications*, vol. 120, pp. 885–890, May 1984.

[3] M. Goedert, C. M. Wischik, R. a. Crowther, J. E. Walker, and A. Klug, "Cloning and sequencing of the cDNA encoding a core protein of the paired helical filament of Alzheimer disease: identification as the microtubule-associated protein tau.," *Proceedings of the National Academy of Sciences of the United States of America*, vol. 85, pp. 4051–5, June 1988.

[4] F. M. LaFerla, K. N. Green, and S. Oddo, "Intracellular amyloid-beta in Alzheimer's disease.," *Nature reviews. Neuroscience*, vol. 8, pp. 499–509, July 2007.

[5] Alzheimer's Association, "http://www.alz.org," 2011.

[6] R. Warner and J. Butler, "Alzheimer's Disease," *Clinical Evidence*, vol. 3, 2000.

[7] R. Brookmeyer, E. Johnson, K. Ziegler-Graham, and H. M. Arrighi, "Forecasting the global burden of Alzheimer's disease.," *Alzheimer's & dementia : the journal of the Alzheimer's Association*, vol. 3, pp. 186–91, July 2007.

[8] Alzheimer's Foreningen, "http://www.alzheimer.dk/," 2013.

[9] R. Craig-Schapiro, A. M. Fagan, and D. M. Holtzman, "Biomarkers of Alzheimer's disease.," *Neurobiology of disease*, vol. 35, pp. 128–40, Aug. 2009.

[10] H. Hampel, S. J. Teipel, T. Fuchsberger, N. Andreasen, J. Wiltfang, M. Otto, Y. Shen, R. Dodel, Y. Du, M. Farlow, H.-J. Möller, K. Blennow, and K. Buerger, "Value of CSF Beta-amyloid1-42 and tau as predictors of Alzheimer's disease in patients with mild cognitive impairment," *Molecular Psychiatry*, pp. 705–710, Dec. 2003.

[11] N. Andreasen, "Cerebrospinal Fluid β-Amyloid(1-42) in Alzheimer Disease: Differences Between Early- and Late-Onset Alzheimer Disease and Stability During the Course of Disease.," *Archives of Neurology*, vol. 56, p. 673, June 1999.

[12] N. Andreasen, L. Minthon, P. Davidsson, E. Vanmechelen, H. Vanderstichele, B. Winblad, and K. Blennow, "Evaluation of CSF-tau and CSF-Abeta42 as diagnostic markers for Alzheimer disease in clinical practice.," *Archives of neurology*, vol. 58, pp. 373–9, Mar. 2001.

[13] C. M. Clark, S. Xie, J. Chittams, D. Ewbank, E. Peskind, D. Galasko, J. C. Morris, D. W. McKeel, M. Farlow, S. L. Weitlauf, J. Quinn, J. Kaye, D. Knopman, H. Arai, R. S. Doody, C. DeCarli, S. Leight, V. M.-Y. Lee, and J. Q. Trojanowski, "Cerebrospinal fluid tau and beta-amyloid: how well do these biomarkers reflect autopsy-confirmed dementia diagnoses?," *Archives of neurology*, vol. 60, pp. 1696–702, Dec. 2003.

[14] A. M. Fagan, C. M. Roe, C. Xiong, M. a. Mintun, J. C. Morris, and D. M. Holtzman, "Cerebrospinal fluid tau/beta-amyloid(42) ratio as a prediction of cognitive decline in nondemented older adults.," *Archives of neurology*, vol. 64, pp. 343–9, Mar. 2007.

[15] D. Galasko, L. Chang, R. Motter, C. M. Clark, J. Kaye, D. Knopman, R. Thomas, D. Kholodenko, D. Schenk, I. Lieberburg, B. Miller, R. Green, R. Basherad, L. Kertiles, M. a. Boss, and P. Seubert, "High cerebrospinal fluid tau and low amyloid beta42 levels in the clinical diagnosis of Alzheimer disease and relation to apolipoprotein E genotype.," *Archives of neurology*, vol. 55, pp. 937–45, July 1998.

[16] H. a. Pearson and C. Peers, "Physiological roles for amyloid beta peptides.," *The Journal of physiology*, vol. 575, pp. 5–10, Aug. 2006.

[17] S. Kumar and J. Udgaonkar, "Mechanisms of amyloid fibril formation by proteins," *Curr. Sci*, vol. 98, no. 5, pp. 639–656, 2010.

[18] A. K. Paravastu, I. Qahwash, R. D. Leapman, S. C. Meredith, and R. Tycko, "Seeded growth of beta-amyloid fibrils from Alzheimer's brain-derived fibrils produces a distinct fibril structure.," *Proceedings of the National Academy of Sciences of the United States of America*, vol. 106, pp. 7443–8, May 2009.

[19] B. O'Nuallain, A. D. Williams, P. Westermark, and R. Wetzel, "Seeding specificity in amyloid growth induced by heterologous fibrils.," *The Journal of biological chemistry*, vol. 279, pp. 17490–9, Apr. 2004.

[20] W. P. Esler, E. R. Stimson, J. R. Ghilardi, H. V. Vinters, J. P. Lee, P. W. Mantyh, and J. E. Maggio, "In vitro growth of Alzheimer's disease beta-amyloid plaques displays first-order kinetics.," *Biochemistry*, vol. 35, pp. 749–57, Jan. 1996.

[21] K. C. Evans, E. P. Berger, C. G. Cho, K. H. Weisgraber, and P. T. Lansbury, "Apolipoprotein E is a kinetic but not a thermodynamic inhibitor of amyloid formation: implications for the pathogenesis and treatment of Alzheimer disease.,"

Proceedings of the National Academy of Sciences of the United States of America, vol. 92, pp. 763–7, Jan. 1995.

[22] A. Jan, D. M. Hartley, and H. a. Lashuel, "Preparation and characterization of toxic Abeta aggregates for structural and functional studies in Alzheimer's disease research.," *Nature protocols*, vol. 5, pp. 1186–209, Jan. 2010.

[23] S. Terry, J. Jerman, and J. Angell, "A Gas Chromatographic Air Analyzer Fabricated on a Silicon Wafer," *IEEE Transactions on Electron Devices*, no. 12, pp. 1880–1886, 1979.

[24] J. W. Hong and S. R. Quake, "Integrated nanoliter systems.," *Nature biotechnology*, vol. 21, pp. 1179–83, Oct. 2003.

[25] D. Janasek, J. Franzke, and A. Manz, "Scaling and the design of miniaturized chemical-analysis systems.," *Nature*, vol. 442, pp. 374–80, July 2006.

[26] G. M. Whitesides, "The origins and the future of microfluidics.," *Nature*, vol. 442, pp. 368–73, July 2006.

[27] a. Manz, N. Graber, and H. Widmer, "Miniaturized total chemical analysis systems: A novel concept for chemical sensing," *Sensors and Actuators B: Chemical*, vol. 1, pp. 244–248, Jan. 1990.

[28] C. D. Chin, V. Linder, and S. K. Sia, "Commercialization of microfluidic point-of-care diagnostic devices.," *Lab on a chip*, vol. 12, pp. 2118–34, June 2012.

[29] M. Reches and E. Gazit, "Molecular Self-Assembly of Peptide Nanostructures: Mechanism of Association and Potential Uses," *Current Nanoscience*, vol. 2, pp. 105–111, May 2006.

[30] M. Reches and E. Gazit, "Formation of Closed-Cage Nanostructures by Self-Assembly of Aromatic Dipeptides," *Nano Letters*, vol. 4, pp. 581–585, Apr. 2004.

[31] L. Adler-Abramovich and E. Gazit, "Controlled patterning of peptide nanotubes and nanospheres using inkjet printing technology.," *Journal of peptide science : an official publication of the European Peptide Society*, vol. 14, pp. 217–23, Feb. 2008.

[32] S. Song, L. Wang, J. Li, C. Fan, and J. Zhao, "Aptamer-based biosensors," *TrAC Trends in Analytical Chemistry*, vol. 27, pp. 108–117, Feb. 2008.

[33] S. Mohanty and E. Kougianos, "Biosensors: a tutorial review," *IEEE Potentials*, vol. 25, pp. 35–40, Mar. 2006.

[34] J. Wang, "Glucose Biosensors: 40 Years of Advances and Challenges," *Electroanalysis*, vol. 13, pp. 983–988, Aug. 2001.

[35] T. Vo-Dinh and B. Cullum, "Biosensors and biochips: advances in biological and medical diagnostics.," *Fresenius' journal of analytical chemistry*, vol. 366, no. 6-7, pp. 540–51, 2000.

[36] S. Kienle, S. Lingler, W. Kraas, a. Offenhäusser, W. Knoll, and G. Jung, "Electropolymerization of a phenol-modified peptide for use in receptor-ligand interactions studied by surface plasmon resonance.," *Biosensors & bioelectronics*, vol. 12, pp. 779–86, Jan. 1997.

[37] S. S. Pathak and H. F. Savelkoul, "Biosensors in immunology: the story so far.," *Immunology today*, vol. 18, pp. 464–7, Oct. 1997.

[38] V. Regnault, J. Arvieux, L. Vallar, and T. Lecompte, "Both kinetic data and epitope mapping provide clues for understanding the anti-coagulant effect of five murine monoclonal antibodies to human beta2-glycoprotein I.," *Immunology*, vol. 97, pp. 400–7, July 1999.

[39] M. H. Van Regenmortel, D. Altschuh, J. Chatellier, L. Christensen, N. Rauffer-Bruyère, P. Richalet-Secordel, J. Witz, and G. Zeder-Lutz, "Measurement of antigen-antibody interactions with biosensors.," *Journal of molecular recognition : JMR*, vol. 11, pp. 163–7, Jan. 1998.

[40] R. Batey, R. Rambo, and J. Doudna, "Tertiary Motifs in RNA Structure and Folding.," *Angewandte Chemie (International ed. in English)*, vol. 38, pp. 2326–2343, Aug. 1999.

[41] R. Monosik, M. Streansky, and E. Sturdik, "Biosensors - classification, characterization and new trends," *Acta Chimica Slovaca*, vol. 5, pp. 109–120, Jan. 2012.

[42] J.-O. Lee, H.-M. So, E.-K. Jeon, H. Chang, K. Won, and Y. H. Kim, "Aptamers as molecular recognition elements for electrical nanobiosensors.," *Analytical and bioanalytical chemistry*, vol. 390, pp. 1023–32, Feb. 2008.

[43] a. Bonanni and M. del Valle, "Use of nanomaterials for impedimetric DNA sensors: a review.," *Analytica chimica acta*, vol. 678, pp. 7–17, Sept. 2010.

[44] J. MacDonald, "Impedance Spectroscopy," *Annals of Biomedical Engineering*, vol. 20, pp. 289–305, 1992.

[45] J. S. Daniels and N. Pourmand, "Label-Free Impedance Biosensors: Opportunities and Challenges.," *Electroanalysis*, vol. 19, pp. 1239–1257, May 2007.

[46] K. Besteman, J. Lee, and F. Wiertz, "Enzyme-coated carbon nanotubes as single-molecule biosensors," *Nano letters*, vol. 3, no. 6, pp. 727–730, 2003.

[47] L. De Vico, M. H. Sø rensen, L. Iversen, D. M. Rogers, B. S. Sø rensen, M. Brandbyge, J. Nygå rd, K. L. Martinez, and J. H. Jensen, "Quantifying signal changes in nano-wire based biosensors.," *Nanoscale*, vol. 3, pp. 706–17, Mar. 2011.

[48] T. S. Hansen, K. West, O. Hassager, and N. B. Larsen, "Integration of conducting polymer network in non-conductive polymer substrates," *Synthetic Metals*, vol. 156, pp. 1203–1207, Nov. 2006.

[49] B. r. Winther-Jensen, J. Chen, K. West, and G. Wallace, "Vapor Phase Polymerization of Pyrrole and Thiophene Using Iron(III) Sulfonates as Oxidizing Agents," *Macromolecules*, vol. 37, pp. 5930–5935, Aug. 2004.

[50] B. r. Winther-Jensen and K. West, "Vapor-Phase Polymerization of 3,4-Ethylenedioxythiophene: A Route to Highly Conducting Polymer Surface Layers," *Macromolecules*, vol. 37, pp. 4538–4543, June 2004.

[51] B. r. Winther-Jensen and K. West, "Stability of highly conductive poly-3,4-ethylenedioxythiophene," *Reactive and Functional Polymers*, vol. 66, pp. 479–483, May 2006.

[52] J. U. Lind, C. Acikgöz, A. E. Daugaard, T. L. Andresen, S. r. Hvilsted, M. Textor, and N. B. Larsen, "Micropatterning of functional conductive polymers with multiple surface chemistries in register.," *Langmuir : the ACS journal of surfaces and colloids*, vol. 28, pp. 6502–11, Apr. 2012.

[53] J. Dapra, L. Holm, A. Toftgaard, N. Rozlosnik, and J. Dapr, "Biosensors and Bioelectronics Comparative study on aptamers as recognition elements for antibiotics in a label-free all-polymer biosensor," *Biosensors & bioelectronics*, vol. 43, pp. 315–320, 2013.

[54] L. Groenendaal, G. Zotti, P.-H. Aubert, S. Waybright, and J. Reynolds, "Electrochemistry of Poly(3,4-alkylenedioxythiophene) Derivatives," *Advanced Materials*, vol. 15, pp. 855–879, June 2003.

[55] J. Dapra, *All-Polymer Biosensor for Label-Free Point of Care Diagnostics*. Phd., Technical University of Denmark, 2013.

[56] N. Rozlosnik, "New directions in medical biosensors employing poly(3,4-ethylenedioxy thiophene) derivative-based electrodes.," *Analytical and bioanalytical chemistry*, vol. 395, pp. 637–45, Oct. 2009.

[57] S. Timpanaro, M. Kemerink, F. Touwslager, M. De Kok, and S. Schrader, "Morphology and conductivity of PEDOT/PSS films studied by scanning-tunneling microscopy," *Chemical Physics Letters*, vol. 394, pp. 339–343, Aug. 2004.

[58] J. Ding, W. E. Price, S. F. Ralph, and G. G. Wallace, "Synthesis and properties of a mechanically strong poly(bithiophene) composite polymer containing a polyelectrolyte dopant," *Synthetic Metals*, vol. 110, no. 2, pp. 123–132, 2000.

[59] B. L. Groenendaal, F. Jonas, D. Freitag, H. Pielartzik, and J. R. Reynolds, "Its Derivatives : Past , Present , and Future **," *Advanced Materials*, vol. 12, no. 7, pp. 481–494, 2000.

[60] K. Aasmundtveit, E. Samuelsen, O. Inganäs, L. Pettersson, T. Johansson, and S. Ferrer, "Structural aspects of electrochemical doping and dedoping of poly(3,4-ethylenedioxythiophene)," *Synthetic Metals*, vol. 113, pp. 93–97, June 2000.

[61] V. Foderà, F. Librizzi, M. Groenning, M. van de Weert, and M. Leone, "Secondary nucleation and accessible surface in insulin amyloid fibril formation.," *The journal of physical chemistry. B*, vol. 112, pp. 3853–8, Mar. 2008.

[62] R. Khurana, C. Coleman, C. Ionescu-Zanetti, S. a. Carter, V. Krishna, R. K. Grover, R. Roy, and S. Singh, "Mechanism of thioflavin T binding to amyloid fibrils.," *Journal of structural biology*, vol. 151, pp. 229–38, Sept. 2005.

[63] S. a. Hudson, H. Ecroyd, T. W. Kee, and J. a. Carver, "The thioflavin T fluorescence assay for amyloid fibril detection can be biased by the presence of exogenous compounds.," *The FEBS journal*, vol. 276, pp. 5960–72, Oct. 2009.

[64] H. Räder and W. Schrepp, "MALDI-TOF mass spectrometry in the analysis of synthetic polymers," *Acta Polymerica*, vol. 49, pp. 272–293, June 1998.

[65] H. Ohno, J. Blackwell, a. M. Jamieson, D. a. Carrino, and a. I. Caplan, "Calibration of the relative molecular mass of proteoglycan subunit by column chromatography on Sepharose CL-2B.," *The Biochemical journal*, vol. 235, pp. 553–7, Apr. 1986.

[66] V. Gelfanova, R. E. Higgs, R. a. Dean, D. M. Holtzman, M. R. Farlow, E. R. Siemers, A. Boodhoo, Y.-W. Qian, X. He, Z. Jin, D. L. Fisher, K. L. Cox, and J. E. Hale, "Quantitative analysis of amyloid-beta peptides in cerebrospinal fluid using immunoprecipitation and MALDI-Tof mass spectrometry.," *Briefings in functional genomics & proteomics*, vol. 6, pp. 149–58, June 2007.

[67] D. M. Walsh, "Amyloid beta -Protein Fibrillogenesis. STRUCTURE AND BIOLOGICAL ACTIVITY OF PROTOFIBRILLAR INTERMEDIATES," *Journal of Biological Chemistry*, vol. 274, pp. 25945–25952, Sept. 1999.

[68] A. Jan, O. Gokce, R. Luthi-Carter, and H. a. Lashuel, "The ratio of monomeric to aggregated forms of Abeta40 and Abeta42 is an important determinant of amyloid-beta aggregation, fibrillogenesis, and toxicity.," *The Journal of biological chemistry*, vol. 283, pp. 28176–89, Oct. 2008.

[69] J. D. Harper and P. T. Lansbury, "Models of amyloid seeding in Alzheimer's disease and scrapie: mechanistic truths and physiological consequences of the time-dependent solubility of amyloid proteins.," *Annual review of biochemistry*, vol. 66, pp. 385–407, Jan. 1997.

[70] R. Kodali and R. Wetzel, "Polymorphism in the intermediates and products of amyloid assembly.," *Current opinion in structural biology*, vol. 17, pp. 48–57, Mar. 2007.

[71] K. B. Andersen, J. Castillo-Leon, M. Hedström, and W. E. Svendsen, "Stability of diphenylalanine peptide nanotubes in solution.," *Nanoscale*, vol. 3, pp. 994–8, Mar. 2011.

[72] K. B. Andersen, J. Castillo-León, T. Bakmand, and W. E. Svendsen, "Alignment and Use of Self-Assembled Peptide Nanotubes as Dry-Etching Mask," *Japanese Journal of Applied Physics*, vol. 51, p. 06FF13, June 2012.

[73] L. Adler-Abramovich, M. Reches, V. L. Sedman, S. Allen, S. J. B. Tendler, and E. Gazit, "Thermal and chemical stability of diphenylalanine peptide nanotubes: implications for nanotechnological applications.," *Langmuir : the ACS journal of surfaces and colloids*, vol. 22, pp. 1313–20, Jan. 2006.

[74] X. Hou and L. Jiang, "Learning from nature: building bio-inspired smart nanochannels.," *ACS nano*, vol. 3, pp. 3339–42, Nov. 2009.

[75] A. Lakshmanan, S. Zhang, and C. a. E. Hauser, "Short self-assembling peptides as building blocks for modern nanodevices.," *Trends in biotechnology*, vol. 30, pp. 155–65, Mar. 2012.

[76] J. Castillo-Leon, R. Rodriguez-Trujillo, S. Gauthier, A. C. Jensen, and W. E. Svendsen, "Micro-factory for self-assembled peptide nanostructures," *Microelectronic Engineering*, vol. 88, pp. 1685–1688, Aug. 2011.

[77] S. Scanlon and A. Aggeli, "Self-assembling peptide nanotubes," *Nano Today*, vol. 3, pp. 22–30, June 2008.

[78] L. Adler-Abramovich, N. Kol, I. Yanai, D. Barlam, R. Z. Shneck, E. Gazit, and I. Rousso, "Self-Assembled Organic Nanostructures with Metallic-Like Stiffness.," *Angewandte Chemie (International ed. in English)*, vol. 49, pp. 9939–42, Dec. 2010.

[79] J. Castillo, S. Tanzi, M. Dimaki, and W. Svendsen, "Manipulation of self-assembly amyloid peptide nanotubes by dielectrophoresis.," *Electrophoresis*, vol. 29, pp. 5026–32, Dec. 2008.

[80] C. H. Clausen, M. Dimaki, S. P. Panagos, E. Kasotakis, A. Mitraki, W. E. Svendsen, and J. Castillo-León, "Electrostatic force microscopy of self-assembled peptide structures.," *Scanning*, vol. 33, no. 4, pp. 201–7, 2011.

[81] C. H. Clausen, J. Jensen, J. Castillo, M. Dimaki, and W. E. Svendsen, "Qualitative mapping of structurally different dipeptide nanotubes.," *Nano letters*, vol. 8, pp. 4066–9, Nov. 2008.

[82] X. Yan, P. Zhu, and J. Li, "Self-assembly and application of diphenylalanine-based nanostructures.," *Chemical Society reviews*, vol. 39, pp. 1877–90, June 2010.

[83] M. Reches and E. Gazit, "Biological and Chemical Decoration of Peptide Nanostructures via Biotin-Avidin Interactions," *Journal of Nanoscience and Nanotechnology*, vol. 7, pp. 2239–2245, July 2007.

[84] K. B. Andersen, N. O. Christiansen, J. Castillo-León, N. Rozlosnik, and W. E. Svendsen, "Fabrication and characterization of PEDOT nanowires based on self-assembled peptide nanotube lithography," *Organic Electronics*, vol. 14, pp. 1370–1375, May 2013.

[85] J. J. Castillo, W. E. Svendsen, N. Rozlosnik, P. Escobar, F. Martínez, and J. Castillo-León, "Detection of cancer cells using a peptide nanotube-folic acid modified graphene electrode.," *The Analyst*, vol. 138, pp. 1026–31, Feb. 2013.

[86] M. B. Larsen, K. B. Andersen, W. E. Svendsen, and J. Castillo-León, "Self-Assembled Peptide Nanotubes as an Etching Material for the Rapid Fabrication of Silicon Wires," *BioNanoScience*, vol. 1, pp. 31–37, Apr. 2011.

[87] S. Pavan and F. Berti, "Short peptides as biosensor transducers.," *Analytical and bioanalytical chemistry*, vol. 402, pp. 3055–70, Apr. 2012.

[88] L. Sasso, I. Vedarethinam, J. Emnéus, W. E. Svendsen, and J. Castillo-Leóon, "Self-Assembled Diphenylalanine Nanowires for Cellular Studies and Sensor Applications," *Journal of Nanoscience and Nanotechnology*, vol. 12, pp. 3077–3083, Apr. 2012.

[89] M. B. Taskin, L. Sasso, M. Dimaki, W. E. Svendsen, and J. Castillo-León, "Combined cell culture-biosensing platform using vertically aligned patterned peptide nanofibers for cellular studies.," *ACS applied materials & interfaces*, vol. 5, pp. 3323–8, Apr. 2013.

[90] Extance A, "Peptide balls prove stiffer than stan steel," 2010.

[91] A. Boccaccio, M. C. Frassanito, L. Lamberti, R. Brunelli, G. Maulucci, M. Monaci, M. Papi, C. Pappalettere, T. Parasassi, L. Sylla, F. Ursini, and M. De Spirito, "Nanoscale characterization of the biomechanical hardening of bovine zona pellucida.," *Journal of the Royal Society, Interface / the Royal Society*, vol. 9, pp. 2871–82, Nov. 2012.

[92] H. Brochu and P. Vermette, "Young's moduli of surface-bound liposomes by atomic force microscopy force measurements.," *Langmuir : the ACS journal of surfaces and colloids*, vol. 24, pp. 2009–14, Mar. 2008.

[93] J. F. Graveland-Bikker, I. a. T. Schaap, C. F. Schmidt, and C. G. de Kruif, "Structural and mechanical study of a self-assembling protein nanotube.," *Nano letters*, vol. 6, pp. 616–21, Apr. 2006.

[94] J. a. Last, S. M. Thomasy, C. R. Croasdale, P. Russell, and C. J. Murphy, "Compliance profile of the human cornea as measured by atomic force microscopy.," *Micron (Oxford, England : 1993)*, vol. 43, pp. 1293–8, Dec. 2012.

[95] J. L. Maciaszek, B. Andemariam, and G. Lykotrafitis, "Microelasticity of red blood cells in sickle cell disease," *The Journal of Strain Analysis for Engineering Design*, vol. 46, pp. 368–379, June 2011.

[96] I. Obataya, C. Nakamura, S. Han, N. Nakamura, and J. Miyake, "Nanoscale operation of a living cell using an atomic force microscope with a nanoneedle.," *Nano letters*, vol. 5, pp. 27–30, Jan. 2005.

[97] A. Parra, E. Casero, E. Lorenzo, F. Pariente, and L. Vázquez, "Nanomechanical properties of globular proteins: lactate oxidase.," *Langmuir : the ACS journal of surfaces and colloids*, vol. 23, pp. 2747–54, Feb. 2007.

[98] C. Rotsch, F. Braet, E. Wisse, and M. Radmacher, "AFM imaging and elasticity measurements on living rat liver macrophages.," *Cell biology international*, vol. 21, pp. 685–96, Nov. 1997.

[99] P. Paik, K. Kar, D. Deva, and A. Sharma, "Measurement of mechanical properties of polymer nanospheres by atomic force microscopy: effects of particle size," *Micro & Nano Letters*, vol. 2, no. 3, p. 72, 2007.

[100] A. Pakzad, J. Simonsen, P. a. Heiden, and R. S. Yassar, "Size effects on the nanomechanical properties of cellulose I nanocrystals," *Journal of Materials Research*, vol. 27, pp. 528–536, Sept. 2011.

[101] A. Solmaz, T. Aytun, J. K. Deuschle, and C. W. Ow-Yang, "Nanoscale elastic modulus variation in loaded polymeric micelle reactors.," *Langmuir : the ACS journal of surfaces and colloids*, vol. 28, pp. 10592–6, July 2012.

[102] W. Zhang, J. Hughes, and Y. Chen, "Impacts of hematite nanoparticle exposure on biomechanical, adhesive, and surface electrical properties of Escherichia coli cells.," *Applied and environmental microbiology*, vol. 78, pp. 3905–15, June 2012.

[103] Y. Zhao, Z. Ge, and J. Fang, "Elastic modulus of viral nanotubes," *Physical Review E*, vol. 78, p. 031914, Sept. 2008.

[104] L. Han, L. Wang, J. Song, M. C. Boyce, and C. Ortiz, "Direct quantification of the mechanical anisotropy and fracture of an individual exoskeleton layer via uniaxial compression of micropillars.," *Nano letters*, vol. 11, pp. 3868–74, Sept. 2011.

[105] M. Lombardo, G. Lombardo, G. Carbone, M. P. De Santo, R. Barberi, and S. Serrao, "Biomechanics of the anterior human corneal tissue investigated with atomic force microscopy.," *Investigative ophthalmology & visual science*, vol. 53, pp. 1050–7, Feb. 2012.

[106] S. Sen, S. Subramanian, and D. E. Discher, "Indentation and adhesive probing of a cell membrane with AFM: theoretical model and experiments.," *Biophysical journal*, vol. 89, pp. 3203–13, Nov. 2005.

[107] N. M. Ziebarth, E. Arrieta, W. J. Feuer, V. T. Moy, F. Manns, and J.-M. Parel, "Primate lens capsule elasticity assessed using Atomic Force Microscopy.," *Experimental eye research*, vol. 92, pp. 490–4, June 2011.

[108] B.-W. Park, R. Zheng, K.-A. Ko, B. D. Cameron, D.-Y. Yoon, and D.-S. Kim, "A novel glucose biosensor using bi-enzyme incorporated with peptide nanotubes.," *Biosensors & bioelectronics*, vol. 38, no. 1, pp. 295–301, 2012.

[109] B. Viguier, K. Zór, E. Kasotakis, A. Mitraki, C. H. Clausen, W. E. Svendsen, and J. Castillo-León, "Development of an electrochemical metal-ion biosensor using self-assembled peptide nanofibrils.," *ACS applied materials & interfaces*, vol. 3, pp. 1594–600, May 2011.

[110] I. Lee, X. Luo, X. T. Cui, and M. Yun, "Highly sensitive single polyaniline nanowire biosensor for the detection of immunoglobulin G and myoglobin.," *Biosensors & bioelectronics*, vol. 26, pp. 3297–302, Mar. 2011.

[111] J. Castillo, M. Dimaki, and W. E. Svendsen, "Manipulation of biological samples using micro and nano techniques.," *Integrative biology : quantitative biosciences from nano to macro*, vol. 1, pp. 30–42, Jan. 2009.

[112] R. de la Rica, E. Mendoza, L. M. Lechuga, and H. Matsui, "Label-free pathogen detection with sensor chips assembled from Peptide nanotubes.," *Angewandte Chemie (International ed. in English)*, vol. 47, pp. 9752–5, Jan. 2008.

[113] J. Ryu and C. B. Park, "High stability of self-assembled peptide nanowires against thermal, chemical, and proteolytic attacks.," *Biotechnology and bioengineering*, vol. 105, pp. 221–30, Feb. 2010.

[114] E.-j. Choi, D. Kim, and K.-s. Yun, "A Study on the Electrical Circuit Model for Impedance-based Microfluidic Sensor," *IPCBEE*, vol. 2, pp. 85–89, 2011.

[115] H. Morgan, M. P. Hughes, and N. G. Green, "Separation of submicron bioparticles by dielectrophoresis.," *Biophysical journal*, vol. 77, pp. 516–25, July 1999.

[116] M. S. Williams, K. J. Longmuir, and P. Yager, "A practical guide to the staggered herringbone mixer.," *Lab on a chip*, vol. 8, pp. 1121–9, July 2008.

[117] A. D. Stroock, S. K. W. Dertinger, A. Ajdari, I. Mezic, H. a. Stone, and G. M. Whitesides, "Chaotic mixer for microchannels.," *Science (New York, N.Y.)*, vol. 295, pp. 647–51, Jan. 2002.

[118] W. a. Hendrickson, a. Pähler, J. L. Smith, Y. Satow, E. a. Merritt, and R. P. Phizackerley, "Crystal structure of core streptavidin determined from multiwavelength anomalous diffraction of synchrotron radiation.," *Proceedings of the National Academy of Sciences of the United States of America*, vol. 86, pp. 2190–4, Apr. 1989.

[119] E. K. r. U. Larsen and N. B. Larsen, "One-step polymer surface modification for minimizing drug, protein, and DNA adsorption in microanalytical systems.," *Lab on a chip*, vol. 13, pp. 669–75, Feb. 2013.

[120] Y. Cui, Q. Wei, H. Park, and C. M. Lieber, "Nanowire nanosensors for highly sensitive and selective detection of biological and chemical species.," *Science (New York, N.Y.)*, vol. 293, pp. 1289–92, Aug. 2001.

[121] C.-Y. Hsiao, C.-H. Lin, C.-H. Hung, C.-J. Su, Y.-R. Lo, C.-C. Lee, H.-C. Lin, F.-H. Ko, T.-Y. Huang, and Y.-S. Yang, "Novel poly-silicon nanowire field effect transistor for biosensing application.," *Biosensors & bioelectronics*, vol. 24, pp. 1223–9, Jan. 2009.

[122] W. E. Svendsen, M. Jø rgensen, L. Andresen, K. Andersen, M. Larsen, S. Skov, and M. Dimaki, "Silicon Nanowire as Virus Sensor in a Total Analysis System," *Procedia Engineering*, vol. 25, pp. 288–291, Jan. 2011.

[123] G.-J. Zhang, L. Zhang, M. J. Huang, Z. H. H. Luo, G. K. I. Tay, E.-J. A. Lim, T. G. Kang, and Y. Chen, "Silicon nanowire biosensor for highly sensitive and rapid detection of Dengue virus," *Sensors and Actuators B: Chemical*, vol. 146, pp. 138–144, Apr. 2010.

[124] G. Zheng, F. Patolsky, Y. Cui, W. U. Wang, and C. M. Lieber, "Multiplexed electrical detection of cancer markers with nanowire sensor arrays.," *Nature biotechnology*, vol. 23, pp. 1294–301, Oct. 2005.

[125] F. Patolsky, G. Zheng, and C. M. Lieber, "Fabrication of silicon nanowire devices for ultrasensitive, label-free, real-time detection of biological and chemical species.," *Nature protocols*, vol. 1, pp. 1711–24, Jan. 2006.

[126] P. S. Waggoner and H. G. Craighead, "Micro- and nanomechanical sensors for environmental, chemical, and biological detection.," *Lab on a chip*, vol. 7, pp. 1238–55, Oct. 2007.

[127] W. U. Wang, C. Chen, K.-h. Lin, Y. Fang, and C. M. Lieber, "Label-free detection of small-molecule-protein interactions by using nanowire nanosensors.," *Proceedings of the National Academy of Sciences of the United States of America*, vol. 102, pp. 3208–12, Mar. 2005.

[128] J. a. Arter, D. K. Taggart, T. M. McIntire, R. M. Penner, and G. a. Weiss, "Virus-PEDOT Nanowires for Biosensing.," *Nano letters*, pp. 4858–4862, Nov. 2010.

[129] J.-i. Hahm and C. M. Lieber, "Direct Ultrasensitive Electrical Detection of DNA and DNA Sequence Variations Using Nanowire Nanosensors," *Nano Letters*, vol. 4, pp. 51–54, Jan. 2004.

[130] K. Balasubramanian, "Challenges in the use of 1D nanostructures for on-chip biosensing and diagnostics: a review.," *Biosensors & bioelectronics*, vol. 26, pp. 1195–204, Dec. 2010.

[131] Y. Wang, K. K. Coti, J. Wang, M. M. Alam, J.-J. Shyue, W. Lu, N. P. Padture, and H.-R. Tseng, "Individually addressable crystalline conducting polymer nanowires in a microelectrode sensor array.," *Nanotechnology*, vol. 18, p. 424021, Oct. 2007.

[132] a. Das, C. Lei, M. Elliott, J. Macdonald, and M. Turner, "Non-lithographic fabrication of PEDOT nano-wires between fixed Au electrodes," *Organic Electronics*, vol. 7, pp. 181–187, Aug. 2006.

[133] B. Kannan, D. E. Williams, C. Laslau, and J. Travas-Sejdic, "A highly sensitive, label-free gene sensor based on a single conducting polymer nanowire.," *Biosensors & bioelectronics*, vol. 35, pp. 258–64, May 2012.

[134] B. Kannan, D. E. Williams, K. Khoshmanesh, G. a. Bowmaker, and J. Travas-Sejdic, "The electrochemical growth of conducting polymer nanowires," *Journal of Electroanalytical Chemistry*, vol. 669, pp. 82–89, Mar. 2012.

[135] Y. Long, J. Duvail, M. Li, C. Gu, Z. Liu, and S. P. Ringer, "Electrical conductivity studies on individual conjugated polymer nanowires: two-probe and four-probe results.," *Nanoscale research letters*, vol. 5, pp. 237–42, Jan. 2009.

[136] T. Carstens, A. Prowald, S. Zein El Abedin, and F. Endres, "Electrochemical synthesis of PEDOT and PPP macroporous films and nanowire architectures from ionic liquids," *Journal of Solid State Electrochemistry*, vol. 16, pp. 3479–3485, July 2012.

[137] C. M. Hangarter, M. Bangar, S. C. Hernandez, W. Chen, M. a. Deshusses, A. Mulchandani, and N. V. Myung, "Maskless electrodeposited contact for conducting polymer nanowires," *Applied Physics Letters*, vol. 92, no. 7, p. 073104, 2008.

[138] C. M. Hangarter, S. C. Hernandez, X. He, N. Chartuprayoon, Y. H. Choa, and N. V. Myung, "Tuning the gas sensing performance of single PEDOT nanowire devices.," *The Analyst*, vol. 136, pp. 2350–8, June 2011.

[139] J. a. Arter, J. E. Diaz, K. C. Donavan, T. Yuan, R. M. Penner, and G. a. Weiss, "Virus-polymer hybrid nanowires tailored to detect prostate-specific membrane antigen.," *Analytical chemistry*, vol. 84, pp. 2776–83, Mar. 2012.

[140] D. K. Taggart, Y. Yang, S.-C. Kung, T. M. McIntire, and R. M. Penner, "Enhanced thermoelectric metrics in ultra-long electrodeposited PEDOT nanowires.," *Nano letters*, vol. 11, pp. 125–31, Jan. 2011.

[141] Y. Z. Long, J. L. Duvail, Z. J. Chen, a. Z. Jin, and C. Z. Gu, "Electrical properties of isolated poly(3,4-ethylenedioxythiophene) nanowires prepared by template synthesis," *Polymers for Advanced Technologies*, vol. 20, pp. 541–544, June 2009.

[142] J. L. Duvail, Y. Long, S. Cuenot, Z. Chen, and C. Gu, "Tuning electrical properties of conjugated polymer nanowires with the diameter," *Applied Physics Letters*, vol. 90, no. 10, p. 102114, 2007.

[143] J. L. Duvail, Y. Long, P. Rétho, G. Louarn, L. Dauginet De Pra, and S. Demoustier-Champagne, "Enhanced Electroactivity and Electrochromism in PEDOT Nanowires," *Molecular Crystals and Liquid Crystals*, vol. 485, pp. 835–842, Apr. 2008.

[144] J. Duvail, P. Rétho, S. Garreau, G. Louarn, C. Godon, and S. Demoustier-Champagne, "Transport and vibrational properties of poly(3,4-ethylenedioxythiophene) nanofibers," *Synthetic Metals*, vol. 131, pp. 123–128, Nov. 2002.

[145] M. Bangar, C. Hangarter, B. Yoo, Y. Rheem, W. Chen, A. Mulchandani, and N. Myung, "Magnetically Assembled Multisegmented Nanowires and Their Applications," *Electroanalysis*, vol. 21, pp. 61–67, Jan. 2009.

[146] a. Bensimon, a. Simon, a. Chiffaudel, V. Croquette, F. Heslot, and D. Bensimon, "Alignment and sensitive detection of DNA by a moving interface.," *Science (New York, N.Y.)*, vol. 265, pp. 2096–8, Sept. 1994.

[147] R. Lebofsky and A. Bensimon, "Single DNA molecule analysis: applications of molecular combing.," *Briefings in functional genomics & proteomics*, vol. 1, pp. 385–96, Jan. 2003.

[148] S. Samitsu, T. Iida, M. Fujimori, S. Heike, T. Hashizume, T. Shimomura, and K. Ito, "Conductivity measurements of PEDOT nanowires on nanoelectrodes," *Synthetic Metals*, vol. 152, pp. 497–500, Sept. 2005.

[149] M. Hamedi, A. Elfwing, R. Gabrielsson, and O. Inganäs, "Electronic polymers and DNA self-assembled in nanowire transistors.," *Small (Weinheim an der Bergstrasse, Germany)*, vol. 9, pp. 363–8, Feb. 2013.

[150] R. H. Karlsson, A. Herland, M. Hamedi, J. A. Wigenius, A. Å slund, X. Liu, M. Fahlman, O. Inganas, and P. Konradsson, "Iron-Catalyzed Polymerization of Alkoxysulfonate-Functionalized 3,4-Ethylenedioxythiophene Gives Water-Soluble Poly(3,4-ethylenedioxythiophene) of High Conductivity," *Chemistry of Materials*, vol. 21, pp. 1815–1821, May 2009.

[151] M. Hamedi, A. Herland, R. H. Karlsson, and O. Inganäs, "Electrochemical devices made from conducting nanowire networks self-assembled from amyloid fibrils and alkoxysulfonate PEDOT.," *Nano letters*, vol. 8, pp. 1736–40, June 2008.

[152] D. S. Ginger, H. Zhang, and C. a. Mirkin, "The evolution of dip-pen nanolithography.," *Angewandte Chemie (International ed. in English)*, vol. 43, pp. 30–45, Jan. 2004.

[153] H.-H. Lu, C.-Y. Lin, T.-C. Hsiao, Y.-Y. Fang, K.-C. Ho, D. Yang, C.-K. Lee, S.-M. Hsu, and C.-W. Lin, "Electrical properties of single and multiple poly(3,4-ethylenedioxythiophene) nanowires for sensing nitric oxide gas.," *Analytica chimica acta*, vol. 640, pp. 68–74, Apr. 2009.

[154] D. E. Bornside, C. W. Macosko, and L. E. Scriven, "Spin coating: One-dimensional model," *Journal of Applied Physics*, vol. 66, no. 11, p. 5185, 1989.

[155] T. Hansen, K. West, O. Hassager, and N. Larsen, "Direct Fast Patterning of Conductive Polymers Using Agarose Stamping," *Advanced Materials*, vol. 19, pp. 3261–3265, Sept. 2007.

[156] J. Ouyang, Q. Xu, C.-W. Chu, Y. Yang, G. Li, and J. Shinar, "On the mechanism of conductivity enhancement in poly(3,4-ethylenedioxythiophene):poly(styrene sulfonate) film through solvent treatment," *Polymer*, vol. 45, pp. 8443–8450, Nov. 2004.

[157] I. Lee, X. Luo, J. Huang, X. T. Cui, and M. Yun, "Detection of Cardiac Biomarkers Using Single Polyaniline Nanowire-Based Conductometric Biosensors," *Biosensors*, vol. 2, pp. 205–220, May 2012.

[158] X. Luo, I. Lee, J. Huang, M. Yun, and X. T. Cui, "Ultrasensitive protein detection using an aptamer-functionalized single polyaniline nanowire.," *Chemical communications (Cambridge, England)*, vol. 47, pp. 6368–70, June 2011.

[159] L. Yun-Ze, D. Jean-Luc, C. Zhao-Jia, J. Ai-Zi, and G. Chang-Zhi, "Electrical Conductivity and Current-Voltage Characteristics of Individual Conducting Polymer PEDOT Nanowires," *Chinese Physics Letters*, vol. 25, pp. 3474–3477, Sept. 2008.

[160] Y. Chen and Y. Luo, "Precisely Defined Heterogeneous Conducting Polymer Nanowire Arrays - Fabrication and Chemical Sensing Applications," *Advanced Materials*, vol. 21, pp. 2040–2044, May 2009.

[161] R. H. Farahi, a. Passian, L. Tetard, and T. Thundat, "Critical issues in sensor science to aid food and water safety.," *ACS nano*, vol. 6, pp. 4548–56, June 2012.

[162] H. Kang, D. Kim, and M. Song, "¡title¿Sensitivity enhancement of FBG temperature sensor¡/title¿," vol. 8439, pp. 84392C–84392C–6, Apr. 2012.

[163] T. Larsen, S. Schmid, L. Gronberg, a. O. Niskanen, J. Hassel, S. Dohn, and A. Boisen, "Ultrasensitive string-based temperature sensors," *Applied Physics Letters*, vol. 98, no. 12, p. 121901, 2011.

[164] A. K. Pandey, O. Gottlieb, O. Shtempluck, and E. Buks, "Performance of an AuPd micromechanical resonator as a temperature sensor," *Applied Physics Letters*, vol. 96, no. 20, p. 203105, 2010.

[165] A. Menzel, K. Subannajui, F. Güder, D. Moser, O. Paul, and M. Zacharias, "Multifunctional ZnO-Nanowire-Based Sensor," *Advanced Functional Materials*, vol. 21, pp. 4342–4348, Nov. 2011.

[166] C.-p. Wang, C.-W. Liu, and C. Gau, "Silicon nanowire temperature sensor and its characteristic," in *2011 6th IEEE International Conference on Nano/Micro Engineered and Molecular Systems*, pp. 630–633, IEEE, Feb. 2011.

[167] A. M. Zaitsev, A. M. Levine, and S. H. Zaidi, "Carbon nanowire-based temperature sensor," *Physica Status Solidi (a)*, vol. 204, pp. 3574–3579, Oct. 2007.

[168] L. R. Arias, C. a. Perry, and L. Yang, "Real-time electrical impedance detection of cellular activities of oral cancer cells.," *Biosensors & bioelectronics*, vol. 25, pp. 2225–31, June 2010.

[169] T. Ona and J. Shibata, "Advanced dynamic monitoring of cellular status using label-free and non-invasive cell-based sensing technology for the prediction of anticancer drug efficacy.," *Analytical and bioanalytical chemistry*, vol. 398, pp. 2505–33, Nov. 2010.

[170] K. Cheung, S. Gawad, and P. Renaud, "Impedance spectroscopy flow cytometry: on-chip label-free cell differentiation.," *Cytometry. Part A : the journal of the International Society for Analytical Cytology*, vol. 65, pp. 124–32, June 2005.

[171] M. H. McCoy and E. Wang, "Use of electric cell-substrate impedance sensing as a tool for quantifying cytopathic effect in influenza A virus infected MDCK cells in real-time.," *Journal of virological methods*, vol. 130, pp. 157–61, Dec. 2005.

[172] C. E. Campbell, M. M. Laane, E. Haugarvoll, and I. Giaever, "Monitoring viral-induced cell death using electric cell-substrate impedance sensing.," *Biosensors & bioelectronics*, vol. 23, pp. 536–42, Nov. 2007.

[173] K. Kiilerich-Pedersen, J. Daprà, S. Cherré, and N. Rozlosnik, "High sensitivity point-of-care device for direct virus diagnostics.," *Biosensors & bioelectronics*, vol. 49, pp. 374–9, Nov. 2013.

[174] K. Fujita and N. I. Smith, "Label-free molecular imaging of living cells.," *Molecules and cells*, vol. 26, pp. 530–5, Dec. 2008.

[175] K. Kiilerich-Pedersen, C. R. Poulsen, T. Jain, and N. Rozlosnik, "Polymer based biosensor for rapid electrochemical detection of virus infection of human cells.," *Biosensors & bioelectronics*, vol. 28, pp. 386–92, Oct. 2011.

Appendix A

Fabrication of Double Assay Analyzer

A detailed process flow for fabricating the silicon masters used for hot embossing fluidic channels used in the Double Assay Analyzer is shown below. As well as the process flow for fabricating the platinum electrodes for the bead coulter counter.

Si stamp wafers				Revision 2.2
DTU Danchip National Center for Micro- and Nanofabrication	Contact email s103332@student.dtu.dk		Contact person Alexander Neergaard	Contact phone 29840968
	Labmanager group Customer support	Batch name	Date of creation 18-Jun-13	Date of revision 18-Jun-13

Objective

This document covers the fabrication of the 1st generation stamp wafers. These are used to optimize the etching process to reach a desired height of 10 µm.

Substrates

Substrate	Orient.	Size	Doping/type	Polish	thickness	Box	Purpose	#	Sample ID
Silicon	<100>	4”	n (Phos.)	SSP	525±25µm		Stamp wafers	4	

Step	Heading	Equipment	Procedure	Comments
1	Lithography – 1.5µm standard			**All wafers**
1.1	Surface treatment	Wet bench	Place wafers in BHF for 30 s., then rinse in DI water for 5 min.	
1.2	Clean spinner	SSE spinner	Clean spinner nozzle and run the dummy wafers Recipe: 1.5 4inch	1-3 dummies
1.3	Coat wafers	SSE spinner	Coat the device wafers 1.5 µm AZ5214e Novolac resist Softbake on hotplate Recipe: 1.5 4inch (Temp: 90°C, time:60 sec)	Resist thickness not checked
1.4	Exposure	KS Aligner	Align to flat. Hard contact Lamp: Cl2, intensity 7 Exposure time: 8 s. Mask: Channel mask, courtesy of Romén Trujillo	
1.5	Develop	Developer bench	Develop in 351B for 70 s.	
1.6	Rinse/dry	Wet bench/ Spin dryer	Rinse in DI water for 5 min. Spin dry	
2	Si Etching			**All wafers**
2.1	Dry etch	DRIE-Pegasus	Process D. Time: 28, 42, 56 and 70 cycles.	1st wafer, 28 cycles, 2nd wafer 42 cycles, 3rd wafer 56 cycles and 4th wafer 70 cycles.
2.2	Inspection	Dektak	Check etch depth	Target is 10 µm. Depth is checked at three different locations on each wafer. Data is then used to optimize process.

Si stamp wafers

Revision: **2.2**

DTU Danchip
National Center for Micro- and Nanofabrication

Contact email	Contact person	Contact phone
s103332@student.dtu.dk	Alexander Neergaard	29840968

Date of creation	Date of revision
18-Jun-13	18-Jun-13

Objective

Batch name: **Error! Reference source not found.**

Process flow covers fabrication of Si stamp to be used in future hot embossing process.

Substrates

Substrate	Orient.	Size	Doping/type	Polish	thickness	Box	Purpose	#	Sample ID
Silicon	<100>	4”	n (Phos.)	SSP	525±25µm		Stamp wafers	4	

Step	Heading	Equipment	Procedure	Comments
1	**Lithography – 1.5µm standard**			**All wafers**
1.1	Surface treatment	Wet bench	Place wafers in BHF for 30 s., then rinse in DI water for 5 min.	
1.2	Clean spinner	SSE spinner	Clean spinner nozzle and run the dummy wafers Recipe: 1.5 4inch	1-3 dummies
1.3	Coat wafers	SSE spinner	Coat the device wafers 1.5 µm AZ5214e Novolac resist Softbake on hotplate Recipe: 1.5 4inch (Temp: 90°C, time:60 sec)	Resist thickness not checked
1.4	Exposure	KS Aligner	Align to flat. Hard contact Lamp: Cl2, intensity 7 Exposure time: 8 s. Mask: Channel mask, courtesy of Romén Trujillo	
1.5	Develop	Developer bench	Develop in 351B for 70 s.	
1.6	Rinse/dry	Wet bench/ Spin dryer	Rinse in DI water for 5 min. Spin dry	
2	**Si Etching**			**All wafers**
2.1	Dry etch	DRIE-Pegasus	Process D. Time: 35 cycles.	No. of cycles determined from optimizing process.
2.2	Inspection	Dektak	Check etch depth	Target is 10 µm. Depth is checked at three different locations on each wafer.

Si stamp wafers

Revision: **2.2**

DTU Danchip
National Center for Micro- and Nanofabrication

Contact email	Contact person	Contact phone
s103332@student.dtu.dk	Alexander Neergaard	29840968

Date of creation	Date of revision
18-Jun-13	18-Jun-13

Objective

Batch name: **Error! Reference source not found.**

Process flow covers fabrication of Si stamp to be used in future hot embossing process.

Substrates

Substrate	Orient.	Size	Doping/type	Polish	thickness	Box	Purpose	#	Sample ID
Silicon	<100>	4”	n (Phos.)	SSP	525±25µm		Stamp wafers	4	

Step	Heading	Equipment	Procedure	Comments
1	**Lithography – 1.5µm standard**			**All wafers**
1.1	Surface treatment	Wet bench	Place wafers in BHF for 30 s., then rinse in DI water for 5 min.	
1.2	Clean spinner	SSE spinner	Clean spinner nozzle and run the dummy wafers Recipe: 1.5 4inch	1-3 dummies
1.3	Coat wafers	SSE spinner	Coat the device wafers 1.5 µm AZ5214e Novolac resist Softbake on hotplate Recipe: 1.5 4inch (Temp: 90°C, time:60 sec)	Resist thickness not checked
1.4	Exposure	KS Aligner	Align to flat. Hard contact Lamp: Cl2, intensity 7 Exposure time: 8 s. Mask: Channel mask, courtesy of Romén Trujillo	
1.5	Develop	Developer bench	Develop in 351B for 70 s.	
1.6	Rinse/dry	Wet bench/ Spin dryer	Rinse in DI water for 5 min. Spin dry	
2	**Si Etching**			**All wafers**
2.1	Dry etch	DRIE-Pegasus	Process D. Time: 56 cycles.	No. of cycles determined from optimizing process.
2.2	Inspection	Dektak	Check etch depth	Target is 15 µm. Depth is checked at three different locations on each wafer.
3	**Resist stripping**			**All wafers**
3.1	Strip	Acetone bench	1st bath for 5 min, then 2nd bath w/ ultrasound for 3 min. Rinse in running water for 4-5 min.	2nd bath ended up with 2x10 min.

Pt electrodes TOPAS

Revision
2.2

DTU Danchip
National Center for Micro- and Nanofabrication

Contact email	Contact person	Contact phone
S103332@student.dtu.dk	Alexander Neergaard	29840968

Date of creation	Date of revision
18-Jun-13	18-Jun-13

Objective

Batch name: **Error! Reference source not found.**

This process flow covers the fabrication of 6 TOPAS wafers intended for electrode usage.

Substrates

Substrate	Orient.	Size	Doping/type	Polish	thickness	Box	Purpose	#	Sample ID
TOPAS	<100>	4”	N/A	N/A	???		Electrodes	6	

Step	Heading	Equipment	Procedure	Comments
1	**Preparation**			**All wafers**
1.1	Wafer cleaning		Rinse wafers in DI water, 10 min.	
2	**Lithography – 2.2 µm standard**			**All wafers**
2.1	Clean spinner	SSE spinner	Clean spinner nozzle and run the dummy wafers Recipe: 2.2 4inch	1-3 dummies
2.2	Coat wafers	SSE spinner	Coat the topas wafers. 2.2 µm AZ5214e Novolac resist Softbake on hotplate Recipe: 2.2 4inch (Temp: 90°C, time:60 sec)	Resist thickness not checked One wafer broke during loading.
2.3	Exposure	KS Aligner	Align to flat. Hard contact Lamp: Cl2, intensity 7 Exposure time: 9 s. Mask: Electrode mask, courtesy of Romén Trujillo.	
2.4	Develop	Developer bench	Develop in 351B for 70 s.	
2.5	Rinse/dry	Wet bench/ Spin dryer	Rinse in DI water for 5 min. Spin dry	
2.6	Inspection	Optical microscope	Check pattern and alignment marks	
3	**Metal deposition**			**All wafers**
3.1	Ti/Pt deposition	Wordentech	Metal: Ti/Pt Thickness: 10/90 nm	10 nm Ti used as adhesion layer.
3.2	Lift-off	Lift-off bench	Leave wafers in acetone with sonic for 20-30 min. Rotate two-three times during lift-off.	Fill the bench with Acetone until carrier is covered.
3.3	Rinse/dry	Wet bench/ Spin dryer	Rinse in DI water for 5 min. Spin dry	
3.4	Inspection	Optical microscope	Check for completeness	

Appendix B

List of Publications

B.1 Journals

1 Andersen, K. B.; **Christiansen, N. O.**; Castillo-Leon, J.; Rozlosnik, N.; Svendsen, W. E.
Fabrication and characterization of PEDOT nanowires based on self-assembled peptide nanotube lithography
Organic Electronic 2013, 14, 1370-1375
Authors contributed equally

2 **Christiansen, N. O.**; Clausen C. H.; Hedstrom, M.; Rozlosnik, N.; Fletcher, D. A.; Svendsen, W.E. and Castillo-Leon; J.
Structural characterization of self-assembled Boc-diphenylalanine nanoparticles
Manuscript in preparation

B.2 Proceedings

1 **Christiansen, N. O.**; Andersen, K. B.; Castillo-Leon, J.; Rozlosnik, N.; Svendsen, W. E.
Novel fabrication method of conductive polymer nanowires for sensor applications
Technical Proceedings of the 2013 NSTI Nanotechnology Conference and Expo, pages: 458-461, 2013, Nano Science and Technology Institute - NSTI

2 ; Castillo-Leon, J.; Andersen, K. B.; **Christiansen, N. O.** Dimaki, M.; Svendsen, W. E.
Peptide self-assembled nanostructures: advances and challenges for their use in nanobiotechnology applications
3rd International Conference on Advanced Nano Materials, 2010

B.3 Book Chapter

1 Kiilerich-Pedersen, K; Poulsen, C R; Dapra, J; **Christiansen, N. O.**; Rozlosnik, N.
Polymer Based Biosensors for Pathogen Diagnostics
part of: Environmental Biosensors (ISBN: 978-953-307-486-3), 2011, InTech

B.4 Conference Contributions

1 2013 NSTI Nanotechnology Conference and Expo, Washington, DC
Christiansen, N. O.; Andersen, K. B.; Castillo-Leon, J.; Rozlosnik, N.; Svendsen, W. E.
Presentation: Novel fabrication method of conductive polymer nanowires for sensor applications

2 2012, 2nd Nano Today conference, Hawaii
Christiansen, N. O.; Rozlosnik, N
Poster: Detection of Aß-42 in CSF for early diagnostics of Alzheimer's disease

3 2012, 2nd Nano Today conference, Hawaii
Christiansen, N. O.; Clausen C. H.; Hedstrom, M.; Rozlosnik, N.; Fletcher, D. A.; Svendsen, W.E. and Castillo-Leon; J.
Presentation: Self-assembled peptide nanoparticles: Stiffer than steel?

4 2010, 3rd International Conference on Advanced Nano Materials, Agadir
Clausen, C. H.; Castillo, J.; **Christiansen, N. O.**; Svendsen, W. E.
Poster: Scanning probe microscopy characterization of peptide structures

5 2010, Lab-on-a-chip World Congres, San Diego, USA
Christiansen, N. O.; Ajine, M. A.; Castillo, J.; Svendsen, W. E.
Poster: Controlled synthesis and manipulation of self-assembled peptide nano spheres by microfluidic dielectrophoresis (DEP)